PARTICLE COLLISION RATE AND SMALL-SCALE STRUCTURE OF PARTICLE CONCENTRATION IN TURBULENT FLOWS

by

Kevin Cunkuo Hu

A DISSERTATION PRESENTED TO THE GRADUATE SCHOOL OF
THE UNIVERSITY OF FLORIDA IN PARTIAL FULFILLMENT OF
THE REQUIREMENTS FOR THE DEGREE OF DOCTOR OF
PHILOSOPHY

UNIVERSITY OF FLORIDA

1998

ACKNOWLEDGMENTS

I would like to take this opportunity to express my sincere thanks to my advisor, Professor Renwei Mei, for his patience, encouragement, and help. This work would be impossible without his guidance and insights. I appreciate my advisory committee members, Professor James F. Klausner, Professor Corin Segal, Professor Ulrich H. Kurzweg, and Professor Roger Tran-Son-Tay, for their suggestions and help. I also express gratitude to Professor Michael W. Reeks (in England), Professor Ibrahim K. Ebcioglu, Professor Otis Walton and Professor Nicolae D. Cristescu for their help.

Thanks to Dr. Guobao Guo and my fellow graduate students Xueliang Zhang, Hong Shang , and others for their helpful discussions and friendship.

I acknowledge the financial support of the Engineering Research Center (ERC) for Particle Science & Technology at the University of Florida, the National Science Foundation (EEC-9402989), industrial partners of the ERC, and the ALCOA Foundation Award.

I am deeply indebted to my wife, Rui, for her love, patience, and encouragement during my thesis work, which were more than I could ever have asked.

TABLE OF CONTENTS

Page

ACKNOWLEDGMENTS ii

LIST OF TABLES vi

LIST OF FIGURES vii

ABSTRACT xii

CHAPTER 1 INTRODUCTION 1

- 1.1 Smoluchowski's Prediction in Laminar Shear Flow 4
- 1.2 Various Theories for Collision Rate in Turbulence 5
- 1.3 Recent Development in Computer Simulation on Particle Collision Rate 7
- 1.4 Recent Development in Particle Concentration Non-uniformity 8
- 1.5 Scope of Present Study 11

CHAPTER 2 TURBULENCE AND PARTICLE COLLISION DETECTION 13

- 2.1 Turbulence Representation 13
  - 2.1.1 Isotropic, Gaussian Turbulence 13
  - 2.1.2 Rapidly Sheared Homogeneous Turbulence 16
  - 2.1.3 Isotropic Turbulence Generation in a Periodic Box 17
- 2.2 Numerical Integration of Particle Motion and Error Analysis 19
- 2.3 Particle Collision Treatment 21
  - 2.3.1 Collision Detection Scheme 21
  - 2.3.2 Post-Collision Treatment 24
- 2.4 Computer Simulation 25
  - 2.4.1 Time Step 25
  - 2.4.2 Turbulence Realization 27
  - 2.4.3 Validation of the Collision Detection Scheme 27

CHAPTER 3 A NEW THEORETICAL FRAMEWORK FOR PREDICTING COLLISION RATE OF SMALL PARTICLES IN GENERAL TURBULENT FLOWS....33

3.1 Introduction....33
3.2 Analysis....37
3.3 Numerical Simulation....43
3.4 Results and Discussions....44
3.4.1 Comparison with Simulation Results in a Laminar Shear Flow....44
3.4.2 Collision Rate and Velocity in a Gaussian, Isotropic Turbulence....47
3.4.3 Collision in a Rapidly Sheared Homogeneous Turbulence....52
3.5 Summary and Conclusions....55

CHAPTER 4 EFFECT OF INERTIA ON THE PARTICLE COLLISION VELOCITY AND COLLISION ANGLE IN GAUSSIAN TURBULENCE....59

4.1 Introduction....59
4.2 Saffman & Turner's Analysis....62
4.3 Present Analysis....65
4.3.1 Asymptotic Analysis....65
4.3.2 PDF-Based Method....68
4.4 Results and Discussions....69
4.5 Summary and Conclusions....76

CHAPTER 5 QUANTIFICATION OF PARTICLE CONCENTRATION NON-UNIFORMITY IN TURBULENCE....77

5.1 Introduction....78
5.2 Quantification Method....79
5.2.1 Inherent Noise of the Concentration Non-uniformity....79
5.2.2 Concentration Non-uniformity Parameter....82
5.3 Results and Discussions....89
5.4 Summary and Conclusions....96

CHAPTER 6 COLLISION RATE AT FINITE PARTICLE INERTIA AND SIZE IN GAUSSIAN TURBULENCE....97

6.1 Introduction....98
6.2 Correction of Smoluchowski's Theory....100

6.3 An Analysis on the Effect of Particle Inertia on the Collision Rate 106
6.3.1 Saffman & Turner 's Analysis 106
6.3.2 Effect of Small Inertia on the Collision Kernel..107
6.3.3 A Proposed Expression on Collision Kernel...110
6.4 Comparison of the Analysis with Simulation Results 111
6.4.1 Effect of Particle Inertia 111
6.4.2 Effect of Particle Size...113
6.4.3 Effect of Particle Mean Concentration..114
6.4.4 Effect of Particle Gravitational Settling 114
6.5 Collision Rate in Polydisperse Suspension...115
6.5.1 Particle Size Spectrum..122
6.5.2 Effect of Particle Inertia 124
6.5.3 Effect of Particle Gravitational Settling 125
6.6 Collision Rate in Hard Sphere Suspension and Assessment of Collision Models 127
6.7 Summary and Conclusions..129

CHAPTER 7 SUMMARY AND CONCLUSIONS...137

REFERENCES..140

BIOGRAPHICAL SKETCH 146

LIST OF TABLES

Table 3.1 Comparison of the collision velocity among monosized particles between prediction and direct numerical simulation in laminar shear flow....................45

Table 3.2 Comparison of the collision velocity among monosized particles between prediction and direct numerical simulation in Gaussian, isotropic turbulence.................... 50

LIST OF FIGURES

Figure 2.1 The effect of time step on the cumulative average of the normalized collision kernel α^*_{11} for inertialess particles in turbulence. D=0.05........................26

Figure 2.2 Turbulence dissipation rate ε against turbulence realization. (a) Variation of ensemble average. (b) Cumulative average. 29

Figure 2.3 Turbulence small eddy shear rate $(\varepsilon / \nu)^{1/2}$ against turbulence realization. (a) Variation of ensemble average. (b) Cumulative average........................30

Figure 2.4 Inverse of total number of monodisperse particles against time in laminar shear flow. Γ=1.0, D=0.02........................31

Figure 2.5 Multiple collisions of HARD SPHERE particles in laminar shear flow...... 32

Figure 3.1 Sketch of particle collision velocity. The separation distance is $x_2-x_1 = \pm R_{ij} = \pm(r_i+r_j)$. 35

Figure 3.2 Variations of $\mathcal{H}(\zeta)$, $\mathcal{G}(\zeta)$, $\mathcal{K}(\zeta)$ with ζ where $f_1=\frac{3}{8}\mathcal{H}(\zeta)$, $f_2=\frac{\mathcal{G}(\zeta)}{\mathcal{H}(\zeta)}$ and $f_3=\frac{\mathcal{K}(\zeta)}{\mathcal{H}(\zeta)}$........................36

Figure 3.3 Local coordinates for collision in laminar shear flow. 42

Figure 3.4 Comparison of the pdf's for the collision angles θ_c between the theory and the simulation in laminar shear flow. 47

Figure 3.5 Convergence of α^*_{12} as $N_k \to \infty$........................50

Figure 3.6 Particle collision kernel α^*_{11} from direct numerical simulation in isotropic turbulence. (a) Variation of the ensemble average. (b) Cumulative time average....... 51

Figure 3.7 (a) Normalized particle collision kernel in a highly sheared homogeneous turbulence without contribution from the mean shear rate...56

Figure 3.7 (b) Collision kernel in a rapidly sheared homogeneous turbulence. ε_0 denotes the dissipation rate of the isotropic state at t=0....... 57

Figure 3.8 Collision velocity in a rapidly sheared homogeneous turbulence. ε_0 denotes the dissipation rate of the isotropic state at t=0. 58

Figure 4.1 Sketch of particle collision scheme. 63

Figure 4.2 Sketch of particle collision velocity and collision angles (θ_{12} & θ_c). The separation distance is $x_2 - x_1 = \pm R = \pm(r_1 + r_2)$....... 63

Figure 4.3 Comparison for the increased collision velocity due to the particle inertia between numerical simulation and theoretical prediction, D/η=0.957. 70

Figure 4.4 Effect of particle inertia on the probability density function of the particle collision velocity w_r. (a) D/η=0.957. (b) D/η=2.522...... 71

Figure 4.5 Effect of particle inertia on the probability density function of the particle collision angle θ_{12}. (a) D/η=0.957. (b) D/η=2.522..73

Figure 4.5 (c) Effect of particle inertia on the probability density function of the particle collision angle θ_c, D/η=0.957. 74

Figure 4.6 Effect of particle inertia on the mean collision angle $\bar{\theta}_{12}$ in isotropic, Gaussian turbulence. 74

Figure 4.7 Effect of particle inertia on the standard deviation of collision angle θ_{12} in isotropic, Gaussian turbulence. 75

Figure 4.8 Effects of particle inertia and size on the probability density function of the particle collision angle θ_{12}, $\beta\tau_k$=1.023. 75

Figure 5.1 The normalized variance of the concentration as function of cell size for inertialess particles in isotropic turbulence. $\beta\tau_k$=1.023. 83

Figure 5.2 The expressions (5.17) & (5.18) of the concentration non-uniformity as function of cell size for inertialess particles in uniform shear flow. β/Γ=∞...... 84

Figure 5.3 The expressions (5.17) & (5.18) of the concentration non-uniformity as function of cell size for inertialess particles in isotropic turbulence. $\beta\tau_k=\infty$................86

Figure 5.4 The concentration non-uniformity parameter Δ_β as function of cell size in uniform shear flow. $\Gamma=1.0$, $\beta/\Gamma=1.0$. 87

Figure 5.5 The concentration non-uniformity as function of cell size for small inertia particles in isotropic turbulence. 88

Figure 5.6 The concentration non-uniformity as function of cell size for various particle number densities at a given inertia in isotropic turbulence. $\beta\tau_k=1.023$. 89

Figure 5.7 The concentration non-uniformity of sizeless particles as function of cell size for various inertia in isotropic turbulence. 91

Figure 5.8 The concentration non-uniformity parameter Δ_β of finite-size particles as function of cell size for various inertia in isotropic turbulence. (a) $D/\eta=0.957$. (b) $D/\eta=2.52$..93

Figure 5.9 The maximum concentration non-uniformity parameter Δ_β of finite-size particles as function of particle inertia in isotropic turbulence. 94

Figure 5.10 The concentration non-uniformity parameter Δ_β as function of $\Delta x/\eta$ for small-size and zero-size particles in isotropic turbulence. $\beta\tau_k=1.023$. 94

Figure 5.11 The concentration non-uniformity of particles at a given inertia as function of $\Delta x/D$ cell size for various sizes in isotropic turbulence. (a) Log scale in x-axis. (b) in normal scale in x-axis. 95

Figure 6.1 Collision kernel α_{ii} against time in laminar shear flow. $\Gamma=1.0$, $D=0.04$. (a) Variation of ensemble average. (b) Cumulative average...... 105

Figure 6.2 The effect of particle inertia on the increased collision kernel $\Delta\alpha^*_{11}$ for monodisperse particles for (a) $D/\eta=0.957$. (b) $D/\eta=2.52$. 116

Figure 6.3 The effect of particle size on the collision kernel α^*_{11} for monodisperse particles at a very dilute system. $\beta\tau_k=\infty$ 117

Figure 6.4 The effect of particle size on the collision kernel α^*_{11} for monodisperse particles at 'not' very dilute system. $\beta\tau_k=\infty$ 117

Figure 6.5 Variation of the collision kernel α^*_{11} against particle number concentration for monodisperse particles. $\beta\tau_k = \infty$, D/η=0.435......118

Figure 6.6 The effect of gravitational settling on the collision kernel α^*_{11} for monodisperse particles. $\beta\tau_k$=1.023, D/η=2.52......118

Figure 6.7 The effect of gravitational settling for monodisperse particles. D/η=2.52, $\beta\tau_k$=1.023. (a) on the collision velocity. (b) on the concentration non-uniformity...119

Figure 6.8 Collision kernel α^*_{11} of polydisperse particles against time. $\beta\tau_k = \infty$, D/η=0.957. (a) Variation of the collision kernel. (b) Cumulative average......120

Figure 6.9 Collision kernel α^*_{11} of polydisperse particles with various inertia against turbulence realization. D/η=0.957. (a) Variation of the collision kernel. (b) Cumulative average of the collision kernel......121

Figure 6.10 Inverse of total number of particles against time for polydisperse particles. D/η=0.957. (a) primary size (v_0) particles. (b) secondary size (2 v_0) particles.........122

Figure 6.11 The evolution of particle size distribution at various instants for polydisperse particles. D/η=2.17, $\beta\tau_k$=1.023......123

Figure 6.12 The effect of particle inertia on the increased collision kernel $\Delta\alpha^*_{11}$ for polydisperse particles for (a) D/η=0.957. (b) D/η=2.52. 126

Figure 6.13 The effect of gravitational settling on the collision kernel α^*_{11} for polydisperse particles. $\beta\tau_k$=1.023, D/η=2.52......127

Figure 6.14 The effect of gravitational settling for polydisperse particles. D/η=2.52, $\beta\tau_k$=1.023. (a) on the collision velocity. (b) on the concentration non-uniformity.... 128

Figure 6.15 Collision kernel α^*_{11} of hard sphere particles with various inertia against time in laminar shear flow. D=0.04. (a) Variation of the collision kernel. (b) Cumulative average......130

Figure 6.16 The effects of the collision schemes on the collision kernel α^*_{11} against time in laminar shear flow. Γ=1.0, D=0.04. (a) Variation of the collision kernel. (b) Cumulative average of the collision kernel......131

Figure 6.17 The effects of the inertia on the collision kernel α_{11}^{*} against time for hard sphere particles in Gaussian turbulence. $D/\eta=0.957$. (a) Variation of the collision kernel. (b) Cumulative average of the collision kernel...... 132

Figure 6.18 The effects of the collision schemes on the collision kernel α_{11}^{*} against time in Gaussian turbulence. $D/\eta=2.174$, $\beta\tau_k=1.023$. (a) Variation of the collision kernel. (b) Cumulative average of the collision kernel..... 133

Figure 6.19 The effects of the collision schemes on the collision kernel α_{11}^{*} of hard sphere particles in Gaussian turbulence. $D/\eta=0.957$, $\beta\tau_k=0.292$. (a) Variation of the collision kernel. (b) Cumulative average of the collision kernel...... 134

Abstract of Dissertation Presented to the Graduate School of the University
of Florida in Partial Fulfillment of the Requirements for the Degree of Doctor
of Philosophy

PARTICLE COLLISION RATE AND SMALL-SCALE STRUCTURE OF PARTICLE CONCENTRATION IN TURBULENT FLOWS

by

Kevin Cunkuo Hu

May, 1998

Chairman: Renwei Mei
Major Department: Aerospace Engineering, Mechanics and Engineering Science

A study of particle collision and concentration non-uniformity in turbulent flows is carried out. A correction to the classical result of Smoluchowski for the collision rate of monodisperse particles in a laminar shear flow has been made. A theoretical framework has been developed to evaluate the collision rate and collision velocity of very small particles in *general* turbulent flows. The present approach differs significantly from the classical approach of Saffman & Turner in that the ensemble average is taken after the collision rate for a given flow realization is calculated. This avoids the assumption of isotropy, as needed in the classical approach, and allows for the evaluation of the collision rate in general turbulent flows.

Direct numerical simulations and analytical studies on particle collisions in an isotropic, Gaussian turbulence have been carried out. Several different collision models (or post-collision treatments) are implemented in the simulations and the difference among various collision models is examined. The effects of particle inertia, size, gravity, and mean-concentration on the collision rate, collision velocity, and collision angle are investigated. Asymptotic analyses have been developed to predict the effects of small inertia on the increases in collision rate and collision velocity. Asymptotic prediction for the increased collision velocity agrees well with the results of both numerical simulation and PDF-based method. The increased collision velocity is found to contain terms of both $O((\beta\tau_k)^{-1})$ and $O((\beta\tau_k)^{-2})$, where β^{-1} is the particle response time and τ_k is the kolmogorov time scale. The increases in particle size, gravitational acceleration, and mean-concentration in general reduce the normalized particle collision rate in isotropic turbulence for monosized particles as opposed to very small particles in the very dilute limit.

A new method has been developed to quantify the concentration non-uniformity of particles in turbulent flows. The effects of particle size and inertia on the concentration non-uniformity are examined and elucidated. The concentration non-uniformity can be greatly overestimated if the effect of finite particle size is neglected.

CHAPTER 1
INTRODUCTION

Particles and turbulence are around us everywhere and greatly impact our daily life. Dusts, sand, rain drops, fine powders, glass beads, viruses and bacteria are all 'particles.' Most of the fluid flows occurring in nature such as air current and water flows in rivers and seas are turbulent flows. The particles in the atmosphere remain airborne for long periods, lowering visibility. The brown haze that is often seen over large cities in autumn, winter and spring is due mainly to the interactions between particles and the air.

The improvement of particulate-fluid systems requires a better understanding of the fundamental physics of the particle-particle and particle-fluid interactions. The behavior of particulate-fluid mixtures may vary widely depending upon the conditions under which the particle-fluid system functions. Particle-particle interactions involve the collisions among particles which depend on inter-particle forces, particle size distribution, and the concentration distribution. Particle-fluid interactions include the hydrodynamic forces acting on particles by fluid and the feedback to fluid from particles, etc. Particle collision, coagulation, and aggregation are the examples of most important scenarios of those interactions that are determined by particle properties and flow structures. The fact that collisions do occur among the particles of size ranging from a few Angstroms to a few millimeters explains the vast amount of scientific and industrial applications of the collision process. For example, molecular collisions help explain the physical properties such as viscosity, diffusivity, and conductivity in gases and liquids. Numerous industrial applications can be cited: design of fine spray combustion nozzles, control of industrial emissions (Presser & Gupta 1993, Tu et al. 1996) and the understanding of the collision process among suspended particles in pneumatic transport systems or in gas cleaning chambers (Abrahamson 1975, William & Crane 1983), and in sewage disposal devices (Hunt 1982), where particle size distribution and concentration non-uniformity are important characteristics that depend on particle collision and coagulation. Most of previous studies on particulate removal have focused on the filters, with little attention to the particle-particle interactions and particle-fluid interactions. Despite many years of research and development in particulate removal technologies, the collection of small particles with size less than 1 μm is still a rather difficult task. It is extremely difficult to remove fine organic active particles (<0.03 μm) from a waste stream because the particles are much smaller than the pores in existing filters. Typical collection efficiencies of the filtration devices decrease rapidly with the decrease of particle size in the range 0.2-30μm (Davies 1953). A good alternative is to aggregate fine particles which can be removed using conventional technologies. For the coagulation and aggregation to occur, particles have to collide with each other and adhere. It is very desirable that one can predict how the small particles are driven to collide with each other so they aggregate or grow in size and become large enough to be captured by the filters. Obviously, the efficiency of particle removal mainly depends on the control of particle collisions and concentration non-uniformity in filtration systems (Fathikalajahi et al. 1996). It is evident that particle collision is one of the most important interactions for understanding the fundamentals of particle-fluid systems.

Particle collision kernel and collision rate are critical quantities in the development of collision theories. The rate of flow induced particle collisions affects directly the particle size distribution in particle production. Examples of turbulence induced particle collision can be seen in the formation of rain drops in clouds, pulverized coal combustion, agglomeration of fine powders in gas flows, air filtration equipment, sewage disposal devices, fast fluidized beds, dust and spray burners, and so on. Particle collisions can take place through a variety of collision mechanisms. Particle collisions may be induced by centrifugal and gravitational forces, thermal forces in Brownian motion, and van der Waal forces. In an actual system, the scenario after every contact between particles may be different from one to another, depending on the underlying physics of the system. The collisions among raindrops enhance the growth of droplets in the air, since the contact between droplets may most likely result in the coalescence of two droplets. The growth of bubbles in a liquid flow is another example of particle coagulation upon collisions. The contacts between two solid particles may behave in various different ways. When two solid particles are brought together the colliding pair may stick or separate after collision upon contact. Many theoretical efforts were made to predict the collision kernel and rate. To validate a theoretical analysis, direct numerical simulations were carried out to obtain statistical average of the collision rate in a particle-fluid system. Different interpretations of the immediate consequence after the contact between a pair of particles have resulted in different collision models or so-called "post-collision treatment" schemes. To quantify the post-collision treatment, a statistical parameter called *collision efficiency* has been introduced. The collision efficiency is one if particles coagulate to form a larger one. Usually, it is less than one since some of the colliding particles may bounce back. Although many theoretical and experimental studies have been devoted to estimates of the collision efficiency for water droplets settling through still air (Klett & Davis 1973, Lin & Lee 1975, Beard & Ochs 1983) and droplets settling down through laminar shear flow (Jonas & Goldsmith 1972), even an approximate estimate of the collision efficiency in a complicated situation can be very difficult to obtain. At this stage, it is still not possible to obtain an accurate solution for the evaluation of collision efficiency in complex systems. To better focus on the issues of our interests, the collision rate, the collision efficiency is assumed to be either one or zero in this study. Although a unity collision efficiency will overestimate the size growth, however, theoretical and numerical exploration on the governing physics may still hold its significance for a better understanding of the interactions in particle-fluid systems.

Population balance equations are often used for predicting the evolution of particle size distribution in particle production systems or in studying particle coagulation. They are typically given in the form of

$$\frac{dn_1}{dt} = -\alpha_{11}n_1n_1 - \alpha_{12}n_1n_2 - \alpha_{13}n_1n_3 - \dots$$

$$\frac{dn_2}{dt} = \frac{1}{2}\,\alpha_{11}n_1n_1 - \alpha_{12}n_1n_2 - \alpha_{22}n_2n_2 - \alpha_{23}n_2n_3 - \dots \tag{1.1}$$

$$\frac{dn_3}{dt} = \alpha_{12}n_1n_2 - \alpha_{13}n_1n_3 - \alpha_{23}n_2n_3 - \alpha_{33}n_3n_3 - \dots$$

$$\frac{dn_4}{dt} = \alpha_{13}n_1n_3 + \frac{1}{2}\,\alpha_{22}n_2n_2 - \alpha_{14}n_1n_4 - \alpha_{24}n_2n_4 - \dots$$

$$\dots$$

In the above, n_i is the number concentration of the *i*th particle size group. For primary particles, i=1, with a volume v_1, the particle in the *i*th group has a volume of iv_1. The quantity $\alpha_{ij}n_in_j$, denoted as $\dot{n}_{c_{ij}}$ in this thesis,

$$\dot{n}_{c_{ij}} = \alpha_{ij}n_in_j \tag{1.2}$$

is called *collision rate* which represents the number of collisions among *i*th particle with *j*th particle per unit volume and per unit time. The coefficient α_{ij} is called the *collision kernel* or *collision function*, it depends on particle size, particle inertia and flow structure, and must be evaluated separately. The collision rate or collision kernel is a measure of the ability of particles to collide, coagulate, and aggregate. It is essential to determine the instantaneous particle size distribution and momentum transfer among particles in a particulate system. Over past 80 years, many efforts have been devoted to developing the particle collision theories for predicting the particle collision rate in fluid flows. A brief review is given below.

1.1 Smoluchowski's Prediction in Laminar Shear Flow

A geometrical collision occurs when two particles reach a separation distance less than $R=r_i+r_j$, in which r_i and r_j are the respective radii of two particle groups and R is the radius of the colliding surface. Theoretical analysis of geometrical collisions in a uniform shear flow was first carried out by Smoluchowski (1917). At a given instant the particle number concentrations per unit volume are n_i and n_j for each size group. Taking any particle of the *i*th-group as a target particle, the volume flow rate of the *j*th-group particles reaching the colliding surface of radius R of the given target particle is $n_j \int_{w_r \le 0} w_r dS$ in which **w** is the relative velocity between *i*th-group and *j*th-group particles and w_r is the radial component of **w**. Thus the number of collisions occurring among *i*th-group and *j*th-group particles per unit time per unit volume is given by

$$\dot{n}_{C_{ij}} = n_i n_j \int_{w_r \le 0} w_r dS = n_i n_j \frac{4}{3} \Gamma (r_i + r_j)^3 = \alpha_{ij} \; n_i n_j \tag{1.3}$$

where Γ is the shear rate and

$$\alpha_{ij} = \frac{4}{3} \Gamma (r_i + r_j)^3 \tag{1.4}$$

is often called the collision kernel. For like particles, the number of collisions per unit time and per unit volume was often simply taken as

$$\dot{n}_{C_{ii}} = \frac{1}{2} n_i n_i \frac{4}{3} \Gamma (2r_i)^3 \,. \tag{1.5}$$

The factor $\frac{1}{2}$ was introduced to avoid double counting of the collisions among the like particles. When the above results are used in the population balance equations, for example, the rate of the "destruction" of *i*th-group particles due to collisions is $-2\dot{n}_{C_{ii}} + \sum_{j \ne i} \dot{n}_{C_{ij}} = - n_i n_i \frac{4}{3} \Gamma (2r_i)^3 - \sum_{j \ne i} n_i n_j \frac{4}{3} \Gamma (r_i + r_j)^3$ since each collision among the like particles results in the loss of two particles of that size group. Equation (1.5) has been extensively used in the literature in calculating the particle collision rate and particle size evolution.

In addition to Smoluchowski's work, Hocking & Jonas (1970) also calculated the collision rate for the sedimenting particles in a uniform shear flow using Stokesian theory. They studied the collision efficiency by which the particle coagulation was assumed if the surface distance between two neighboring particles was less than a prescribed fraction of particle diameter.

1.2 Various Theories for Collision Rate in Turbulence

When particles collide in complex flows, such as turbulent flows, or when more than one collision mechanism are involved in the particulate system, it is quite difficult to derive an exact expression for collision rate. Numerous efforts have been made to estimate the collision rate by means of evaluating the collision velocity in turbulence during past decades. Camp and Stein (1943) employed the concept of mean velocity gradient related to the turbulent energy dissipation rate ε and kinematics viscosity ν and obtained the collision kernel for turbulence shear-induced collision rate based on Smoluchowski work (1917) in laminar shear flow.

$$\alpha_{ij} = \frac{4}{3} R^3 \left(\frac{\varepsilon}{\nu}\right)^{1/2}. \tag{1.6}$$

Saffman and Turner (1956) gave two predictions of particle collision kernel in an isotropic, Gaussian turbulence. In the first prediction, it was assumed that particles are inertialess so that they follow the fluid completely and particle size is small compared with the Kolmogorov length scale of the turbulence. The collision kernel was given

$$\alpha_{ij} = 1.294 \ R^3 \left(\frac{\varepsilon}{\nu}\right)^{1/2}. \tag{1.7}$$

Their second prediction was for the particles with small inertia and gravity.

$$\alpha_{ij} = 2(2\pi)^{1/2} R^2 \Big[\left(1 - \frac{\rho}{\rho_0}\right)^2 (\tau_1 - \tau_2)^2 \overline{\left(\frac{Du}{Dt}\right)^2} + \frac{1}{3}\left(1 - \frac{\rho}{\rho_0}\right)^2 (\tau_1 - \tau_2)^2 g^2 + \frac{1}{9} R^2 \frac{\varepsilon}{\nu} \Big]^{1/2}. \tag{1.8}$$

However, collision kernel for like particles or the particles with same inertia is reduced to

$$\alpha_{ii} = 1.67 \ R^3 \left(\frac{\varepsilon}{\nu}\right)^{1/2}. \tag{1.9}$$

Thus the effect of particle inertia and gravity disappeared in the monodisperse case, which is not physically sound. In addition, the result of their second analysis was inconsistent with the first one, as easily seen from (1.7) and (1.9).

Abrahamson (1975) extended the concept of kinetic theory of gases for the collisions among large particles in a high Reynolds number turbulence. It was assumed that the velocities of colliding particles are uncorrelated, normally distributed in the absence of gravitational settling. The variance of particle velocity v was estimated by

$$< \mathbf{v}^2 > = \frac{\mathbf{u}^2}{1 + 1.5\ \tau_p\ \varepsilon / \mathbf{u}^2} \tag{1.10}$$

where $\mathbf{u}^2$ is the mean-squared fluctuating velocity of the fluid and τ_p is the particle response time. The collision kernel, without gravitational settling, was given by

$$\alpha_{ij} = 5.0\ R^2\ (\ < v_1^2 > + < v_2^2 >\ )^{1/2}. \tag{1.11}$$

Balachandar (1988) performed an analysis on the collision kernel by assuming that the probability distribution function (PDF) of the velocity gradient in turbulence follows a log-normal PDF distribution. He found a correction to Saffman & Turner's prediction for collision kernel in isotropic turbulence. Williams & Crane (1983) and Kruis & Kusters (1996) performed stochastic analysis to obtain the collision kernel with inclusion of the combined effects of local shear and particle inertia. Zhou et al. (1997) carried out a similar analysis and modified the Kruis & Kusters' result in turbulence. Those analyses on the collision kernels were obtained on the basis of two-point velocity correlations without tracking the trajectories of individual particles in the turbulent flow (hereinafter referred as Eulerian method). However, we have found that the collection of the relative velocities (or collision velocities) upon collisions based on tracking the trajectories of individual particles in turbulent flow is a biased average in favor of those regions where the collision velocity is high. Hereinafter, this method based on particle tracking is referred as Lagrangian method. The detailed discussions on the difference between the results of Eulerian and Lagrangian methods on collision velocity will be presented in chapter IV.

1.3 Recent Development in Computer Simulation on Particle Collision Rate

Recent developments of direct numerical simulations (DNS) in turbulence have greatly enhanced the understanding of the turbulence-induced particle collisions. Balachandar (1988) also carried out DNS of particle collision in an isotropic turbulence. It was found that the probability distribution function of the velocity gradient follows a log-normal distribution instead of Gaussian distribution. The collision kernel was obtained in a frozen turbulence with a maximum of 500 particles in the flow field. Artificially large particles were used in order to increase the collision events within a reasonable computational time. It was concluded that the particle inertia does not affect the average collision kernel for large, monosize particles. Large discrepancy in the collision rate for monosize inertialess particles between his numerical results and Saffman & Turner's prediction was reported. However it is not clear whether this discrepancy is due to the difference in the small scale turbulence structure or not.

Chen et al. (1995) carried out DNS results for the aerosols in a turbulent channel flow. They mainly focused on the possible effects of collisions on the deposition rate of the droplets on the channel walls. They found that the particle concentration in the wall region can be significant while the bulk concentration is small. The collision kernel and rate were found to peak in the wall region, and particle depositions can be enhanced by the formation of larger particles.

Wang et al. (1997) also carried out DNS to investigate the collision kernel in homogeneous turbulence. They allowed particles in the system to overlap in space which is unphysical. The effects of finite inertia on collision kernel were also reported in their DNS results (Zhou, Wexler & Wang 1997). Zhou et al. (1997) developed an analysis showing that the increases in particle collision velocity, the non-uniformity of particle concentration and the compressibility of particle velocity in the continuum sense are three possible mechanisms to affect the overall collision kernel for particles with finite inertia. However, they did not quantify these terms separately in their work. Thus how the collision velocity and the concentration non-uniformity play in enhancing the overall collision kernel remains unknown at this stage.

1.4 Recent Development in Particle Concentration Non-uniformity

Recent studies have shown that the particle concentration in turbulence may be highly nonuniform. Heavy particles with finite inertia tend to accumulate in the regions of high strain rate and to move away from the vortex cores. The occurrence of particle accumulations is referred as concentration non-uniformity or preferential concentration. The coherent vortical structures are the mechanisms that cause the nonuniform distribution of particles. The coherent vortices and concentration non-uniformity have been observed by many numerical simulations and experimental visualizations. The numerical simulations for demonstration of the concentration non-uniformity were carried out in plane mixing layers (Crowe et al. 1988, Chien & Chung 1987, Wen et al. 1992, Tang et al. 1992, Wang 1992), in wake flows (Chien & Chung 1988, Tang et al. 1992), in jet flows (Chung & Trout 1988, Hansell 1992), in wall-bounded flows (Kallio & Reeks 1989, McLaughlin 1989, Yonemura et al. 1993, Rouson & Eaton 1994, Tanaka et al. 1996), in homogeneous flows (Maxey & Corrsin 1986, Hunt et al. 1987, Fung & Perkins 1989, Squires & Eaton 1991, Wang & Maxey 1993, Fessler et al. 1993). The non-uniform distribution of particles has also been found by the experiments in plane mixing layers (Kobayashi et al. 1988, Kamalu et al. 1988, Lazaro & Lasheras 1992, Ishima et al. 1993), in wake flows (Tang et al. 1992, Yang et al. 1993, Bachalo 1993), in jet flows (Longmire & Eaton 1992), in wall-bounded flows (Rashidi et al. 1990, Young & Hanratty 1991). Wang & Maxey (1993) have, through direct numerical simulations (DNS) in isotropic turbulence, shown that the preferential concentration achieves maximum at $\beta\tau_k = 1$ in which β is the reciprocal particle response time and τ_k is the Kolmogorov time scale of the turbulence. One of the consequences of the preferential concentration is the enhancement of the settling velocity of heavy particles in the Stokes drag range (Maxey 1987, Mei 1994). One of the related industrial applications is that the particulate removal efficiency of the venturi type scrubber was affected by the nonuniform concentration distribution of droplets (Fathikalajahi et al. 1996).

Particle trajectories, therefore individual particle positions, can be obtained accurately only in Lagrangian frame by solving the equations of particle motions. Particles have finite response times in general but they do not have an intrinsic diffusivity or viscosity associated with the motion of individual particles. Turbulence particle diffusivity is the consequence of ensemble averaging over many realizations and it is used for predicting the variation of average concentration field on a large scale. It cannot be used to describe the small-scale spatial variation of the particle concentration. From the computational point of view, a DNS using 128^3 grid resolution for an isotropic turbulence becomes routine and DNS using 256^3 or even 512^3 have been carried out. For a reasonable contour representation of particle concentration, it is desirable to have at least, say, 10 particles in each cell so that the statistical noise does not become overwhelming. This requires 1.7×10^8 particles with a 256^3 grid resolution. Due to the preferential concentration, there will be regions and cells that do not contain any particle or only one or two particles at a given instant. Thus, an accurate, three-dimensional contour representation of instantaneous particle concentration with such high resolution will still be heavily contaminated by the inherent statistical noise. No such three-dimensional concentration contour has been reported to date. Due to the computer power limitation, previous numerical simulations involved anywhere from 10^4 to 10^6 particles, which is far below the level of reaching a reasonable statistics.

It has been difficult to quantify the extent/degree of particle concentration non-uniformity induced by the small-scale turbulence structure. Squires & Eaton (1991) and Wang & Maxey (1993) showed in their DNS the similarity between the instantaneous particle concentration contours with the contours of the vorticity magnitude (or enstrophy) in the same plane at the same instant. To quantify the deviation of the particle concentration field from a statistically uniform distribution, Wang & Maxey (1993) used a statistical quantity $\sum(P(k) - P_b(k))^2$ averaged over space, where P(k) is the probability of finding k particles in a given cell and $P_b(k)$ follows the Bernoulli distribution for a random distribution of the particles. While this quantity shows that the preferential concentration maximizes near $\beta\tau_k = 1$ (Wang & Maxey 1993), it varies with total number of particles in each of their simulations. The particle-particle interactions are neglected in their simulation and no systematic investigation on its dependence on the cell size was carried out. Hence, its usefulness is limited. Although numerous experimental studies have clearly shown the non-uniform particle distribution in turbulent flows, it is quite difficult to measure the 3D non-uniformity so as to isolate the effects of flow shear, particle inertia and gravity.

Obviously, the local accumulation will affect the encounters among the particles and thus the overall collision rate is expected to be modified accordingly. However, the effect of the preferential concentration on the collision kernel has never been estimated or separated from other factors such as the increased particle collision velocity due to small particle inertia.

1.5 Scope of Present Study

Particle collisions are extremely difficult to observe experimentally, even with today's sophisticated laser instrumentations. Direct numerical simulation, however, has its advantages of providing detailed information on particle trajectories, flow structures and is ideally suited for parametrical investigations of particle and fluid flow properties. Numerical implementation of particle interactions in a simulation, while posing a considerable numerical challenge, introduces no fundamental difficulties. In this work, extensive data obtained by numerical simulations on the collision velocity, collision angle, collision kernel and collision rate are vital to understanding of the fundamental physics in the particle-fluid interactions. One of the major objectives of this thesis is to develop analytical and numerical methods for predicting the particle collision rate and concentration non-uniformity with respect to the effects of turbulent shear, particle inertia and gravity in particle-fluid systems.

As mentioned in §1.2, previous theories on the collision rate were restricted on assumed turbulent flow. In Chapter III, we have developed a new theoretical framework for prediction of the collision rate and collision velocity of small particles at zero inertia in *general* turbulent flows. The collision velocity is a critical variable related to the collision rate. However, the effects of particle inertia on the collision velocity and collision angle have never been predicted using Lagrangian tracking method. In Chapter IV, we carried out an asymptotic analysis to predict the effects of small particle inertia on the collision velocity and presented the effect of the inertia on collision angle in isotropic Gaussian turbulence. As pointed out in §1.4, no realiable method exists for quantifying the concentration non-uniformity and the effect of the preferential concentration on the collision rate has never been estimated. In Chapter V, a new quantification method has been developed to reliably quantify the concentration non-uniformity of particles in turbulent flows, and the effect of the preferential concentration on the collision rate is predicted in isotropic Gaussian turbulence. The first result of Chapter VI is our correction to the classical result of Smoluchowski for the collision rate of monodisperse particles in a laminar shear flow. The combined effects of both the increased collision velocity and increased concentration non-uniformity on the collision rate due to the inertia are then examined. The effects of particle size, gravity and mean-concentration on the collision rate are investigated through direct numerical simulations in Chapter VI. The effects of the collision models on the collision rate are also presented in Chapter VI.

CHAPTER 2
TURBULENCE AND PARTICLE COLLISION DETECTION

2.1 Turbulence Representation

2.1.1 Isotropic, Gaussian Turbulence

The following model for the energy spectrum developed in Mei & Adrian (1995) is assumed for turbulence,

$$E(k) = \frac{3}{2}\ u_0^2\ \psi \frac{k^4}{k_0^5} \frac{1}{[1+(k/k_0)^2]^{17/6}}\ \exp(-\eta_0^2\ k^2) \tag{2.1}$$

where u_0 is the root-mean-squared turbulent velocity, k_0 is a typical wave number and the dimensionless parameter $\bar{\eta}_0 = \eta_0 k_0$ is related to the turbulent Reynolds number Re_λ. Large Re_λ correspond to small $\bar{\eta}_0$ and *vice versa*. The normalizing coefficient ψ in E(k) is determined from (2.1) by satisfying the total energy requirement,

$$\psi^{-1} = \int_0^\infty \frac{\bar{k}^4}{(1+\bar{k}^2)^{17/6}}\ \exp(-\bar{\eta}_0^2\, \bar{k}^2)\, d\bar{k}\ . \tag{2.2}$$

For small $\bar{\eta}_0$, $E(k) \sim k^4$ when $\bar{k} = k/k_0 \ll 1$ and $E(k) \sim k^{-5/3}$, which is the scaling law in the inertial subrange, when $1 \ll \bar{k} \ll 1/\bar{\eta}_0$. For large $\bar{\eta}_0$, the above energy spectrum recovers that of Kraichnan (1970). The relationship between the Eulerian integral length $L_{11}k_0$ and $\bar{\eta}_0$ (or Re_λ) is given in Mei & Adrian (1994).

A turbulent eddy loses its identity as it is convected and dissipated; this behavior is described by the eddy-self decay function $D(\tau)$ which has an integral time scale T_0.

The Fourier transformation of $D(\tau)$ gives the power spectrum $\tilde{D}(\omega)$. A composite form for the power spectrum $\tilde{D}(\omega)$ was constructed in Mei & Adrian (1995) as

$$\tilde{D}(\omega) = \tilde{A}\frac{\exp(-\eta_1^2\omega^2)}{1+(T\omega)^2} \tag{2.3}$$

where η_1 is intended for the viscous dissipation time scale if the turbulent Reynolds number is high, and T is close to T_0 if $\eta_1/T \ll 1$. The coefficient $\tilde{A}$ is determined as

$$\tilde{A} = \frac{T}{\pi}\frac{\exp(-\eta_1^2/T^2)}{1-\mathrm{erf}(\eta_1/T)} \tag{2.4}$$

by satisfying $\int_{-\infty}^{\infty}\tilde{D}(\omega)\,d\omega = 1$. The integral time scale T_0 is related to T as $T_0 = \pi\tilde{D}(0) = \pi\tilde{A}$.

The relationship between L_{11} and T_0 is not known in general; it can be taken to have the form

$$T_0 = c^E(Re_\lambda)L_{11}/u_0, \tag{2.5}$$

where $c^E(Re_\lambda)$ was determined approximately in Mei & Adrian (1995) based on the experimental data of Sato & Yamamotto (1988) for the fluid dispersion and the value of high Reynolds number turbulent Prandtl number.

Using random Fourier modes representation, an isotropic, Gaussian, pseudo turbulence

$$u_i(\mathbf{x}, t) = \sum_{m=1}^{N}[b_i^{(m)}\cos(\mathbf{k}^{(m)}\cdot\mathbf{x} + \omega^{(m)}\cdot t) + c_i^{(m)}\sin(\mathbf{k}^{(m)}\cdot\mathbf{x} + \omega^{(m)}\cdot t)] \tag{2.6}$$

is constructed to simulate the turbulent flow with a specified energy spectrum. In the above N_k is the number of the random Fourier modes in one fluid realization, $\mathbf{k}^{(m)}$ and $\omega^{(m)}$ are the wavenumber and frequency of the m-th mode. The random coefficients $b_i^{(m)}$ and $c_i^{(m)}$ are chosen as follows,

$$b_i^{(m)} = \tilde{b}_j^{(m)}(\delta_{ij} - k_i^{(m)} k_j^{(m)} / k^{(m)^2})\ f(k^{(m)}, \omega^{(m)}) \tag{2.7}$$

where $\tilde{b}_j^{(m)}$ follows a normal distribution with

$$<\tilde{b}_j^{(m)}> = 0 \ \& \ <\tilde{b}_i^{(m)} \tilde{b}_j^{(m)}> = \delta_{ij}. \tag{2.8}$$

The factor $(\delta_{ij} - k_i^{(m)} k_j^{(m)} / k^{(m)^2})$ in Eq (2.26) ensures the incompressibility $\nabla \cdot \mathbf{u} = 0$ for every Fourier mode. The scale factor $f(\mathbf{k}, \omega)$ depends on the energy spectrum and the probability density functions (pdf), $p_1(\mathbf{k})$ and $p_2(\omega)$, of $\mathbf{k}$ and ω,

$$f^2(k, \omega) = \frac{E(k)\, \tilde{D}(\omega)}{4\pi N_k^2 p_1(\mathbf{k}) p_2(\omega)}. \tag{2.9}$$

Since E(k) decays as $k^{-5/3}$ in the inertia subrange, a Gaussian distribution for **k** would lead to a very slow statistical convergence for $u_i(\mathbf{x}, t)$. To achieve convergence of the statistics involving the derivatives such as $\frac{\partial u_i}{\partial x_j}$, the following algebraic pdf

$$p_{1i}(k_i) = \frac{\mu - 1}{2} (1 + |k_i|)^{-\mu} \quad \text{for } i = 1, 2 \ \& \ 3 \tag{2.10a}$$

and

$$P_1(\mathbf{k}) = P_{11}(k_1) P_{12}(k_2) P_{13}(k_3) \tag{2.10b}$$

is used to sample k_i for $k_0 = 1$. The frequency $\omega^{(m)}$ is generated with the following pdf,

$$p_2(\omega) = \frac{1}{\pi} \frac{1}{1 + (\omega / u_0 k_0)^2}. \tag{2.11}$$

The scale factor is finally set to be

$$f^2(k, \omega) = \frac{E(k) \tilde{D}(\omega)}{4\pi N_k k^2 p_{11}(k_1) p_{12}(k_2) p_{13}(k_3) p_2(\omega)}. \tag{2.12}$$

It is noted that in the present studies on particle collisions, the collision rate is dictated by the spatial structure and the eddy-self decay has no effect on the collision rate. In the direct numerical simulation of particle collision in isotropic turbulence, however, the eddy self-decay can be easily incorporated. Hence, the dependence of $b_i^{(m)}$ and $c_i^{(m)}$ on ω is still included.

2.1.2 Rapidly Sheared Homogeneous Turbulence

For an initially isotropic turbulence under rapid shear, $\Gamma=\frac{\partial U}{\partial y}$, the variation of $b_i^{(m)}$ with time was given in Townsend (1976) based on rapid distortion theory (RDT). Hunt & Carruthers (1990) gave an overview on the use of RDT for representing various types of homogeneous turbulence. Denoting the total shear S as

$$S = \Gamma t \tag{2.13}$$

the new wavenumber vector $\chi^{(m)}$ after the shearing is given by

$$\begin{aligned} \chi_1^{(m)} &= k_1^{(m)} \\ \chi_2^{(m)} &= k_2^{(m)} - S k_1^{(m)} \\ \chi_3^{(m)} &= k_3^{(m)} \end{aligned} \tag{2.14}$$

where $k^{(m)}$ is the wavenumber vector of the m-th mode before the mean shear is applied. The amplitude of each Fourier mode becomes

$$\begin{aligned} b_1^{(m)}(S) &= b_1^{(m)}(0) + a_1 b_2^{(m)}(0) \\ b_2^{(m)}(S) &= a_2\, b_2^{(m)}(0) \\ b_3^{(m)}(S) &= b_3^{(m)}(0) + a_3 b_2^{(m)}(0) \end{aligned} \tag{2.15}$$

where $b_i^{(m)}(0)$ is the corresponding amplitude of the m-th mode before the rapid distortion. Dropping the superscript m for convenience, the coefficient a_i for each mode m is given as

$$a_1 = \frac{S k_1^2}{k_1^2 + k_3^2} \frac{k^2 - 2k_2^2 + S k_1 k_2}{\chi^2}$$

$$-\frac{k^2k_3^2}{(k_1^2+k_3^2)^{3/2}k_1}\left[\tan^{-1}\left(\frac{k_2}{\sqrt{k_1^2+k_3^2}}\right)-\tan^{-1}\left(\frac{k_2-Sk_1}{\sqrt{k_1^2+k_3^2}}\right)\right]$$

$$a_2 = k^2/\chi^2 \tag{2.16}$$

$$a_3 = \frac{Sk_1k_3}{k_1^2+k_3^2}\,\frac{k^2-2k_2^2+Sk_1k_2}{\chi^2}$$

$$-\frac{k^2k_3}{(k_1^2+k_3^2)^{3/2}}\left[\tan^{-1}\left(\frac{k_2}{\sqrt{k_1^2+k_3^2}}\right)-\tan^{-1}\left(\frac{k_2-Sk_1}{\sqrt{k_1^2+k_3^2}}\right)\right]$$

where $k=\sqrt{k_1^2+k_2^2+k_3^2}$ and $\chi=\sqrt{\chi_1^2+\chi_2^2+\chi_3^2}$. The coefficient $c_i^{(m)}$ is similarly obtained. It is clear from the above that the amplitude of each mode is entirely determined by the total shear $S=\Gamma t$. The dissipation rate $\varepsilon(S)$ can be evaluated as

$$\varepsilon(S)/\nu = \frac{1}{2} < \sum_{m=1}^{N} \{\chi^{(m)2} \sum_{i=1}^{3} [b_i^{(m)2}(S) + c_i^{(m)2}(S)]\} >. \tag{2.17}$$

Finally, the total velocity field is

$$u_i(\underline{x}, t) = \sum_{m=1}^{N} [\, b_i^{(m)}(S)\ \cos(\chi^{(m)}\cdot\underline{x} + \omega^{(m)}t)$$

$$+ c_i^{(m)}(S)\ \sin(\chi^{(m)}\cdot\underline{x} + \omega^{(m)}t)]$$

$$+ \Gamma x_2\, \delta_{i1}. \tag{2.18}$$

Since the shear rate is high, the term $\omega^{(m)}t$ in the above acts merely as a random phase.

2.1.3 Isotropic Turbulence Generation in a Periodic Box

For the direct numerical simulations of particle collisions in this work, the velocity field of an isotropic and Gaussian turbulence is generated by a random Fourier modes representation (2.6). To effectively conduct a computational study on particle collision, a region of finite size in which a large number of collisions occur should be used with periodic boundary conditions. To render the turbulence represented by random

Fourier modes periodic in a box of volume π^3, the random wave numbers, $k_i^{(m)}$, are rounded to the nearest even integers while all other quantities are held fixed so that the flow is periodic within the box of volume π^3. The periodic box of volume π^3 yields virtually the same collision statistics when the volume is increased to $(2\pi)^3$. Hence π^3 is used throughout this study. The corresponding statistics (turbulence rms velocity u_0, Reynolds number Re_λ, Taylor micro length scale λ, Kolmogorove length scale η, and Kolmogorov time scale τ_k) are computed based on the modified wavenumbers. As will be demonstrated using the present analysis outlined in §2.1.1, the collision statistics, when normalized using $R^3(\varepsilon/\nu)^{1/2}$ for α_{11} and $<-w_r>$, the results are the same using the turbulence generated in an unbounded domain and in a periodic box.

Unless specifically mentioned, most of the isotropic turbulence used in the numerical simulations throughout this study is within the periodic box of length π and have the following characteristics: root-mean-squared turbulence velocity $u_0=1.0$, integral length scale $L_{11}=0.594$, Taylor micro length scale $\lambda=0.277$, Kolmogorov length scale $\eta=0.023$, Kolmogorov time scale $\tau_k = (\nu/\varepsilon)^{1/2}=0.073$, and $Re_\lambda=40.1$. The turbulence is imposed on a box π^3 with periodic boundary conditions in three perpendicular directions. The periodic treatment of boundary conditions allows the simulation results by a finite volume to be extended to an infinite homogeneous system.

Initially, a given number of monosize particles are randomly introduced in the flow field of volume π^3. The periodic boundary conditions are also applied to the motions of the particles. The particles are advanced using $u_i(\underline{x}, t)$ given by (2.6) with a time step Δt. A semi-implicit finite difference scheme is implemented to integrate the equation of particle motion and to detect collision. The scheme has an accuracy of second order. The detailed error analysis of the semi-implicit finite difference scheme will be given in next section.

2.2 Numerical Integration of Particle Motion and Error Analysis

Major concerns in numerical simulation are the accuracy and robustness of the numerical scheme. Since the collision detection in the present simulation is based on the calculation of particle trajectories, the collision kernel/rate/velocity/angle are affected by the accuracy of the finite difference scheme. In this study, both tracking particles and detecting collision are carried out in a Lagrangian frame. A semi-implicit finite difference scheme is implemented to integrate the equation of particle motion and to detect collision. This scheme is unconditionally stable. With consistent treatment for both particle velocity and turbulence, The truncation error in the semi-implicit scheme is $O((\Delta t)^2)$ and independent of β. The accuracy analysis of the scheme is given as follows.

The particle dynamic equation in the absence of (or weak) gravity is

$$\frac{d\mathbf{v}}{dt} = \beta(\mathbf{u} - \mathbf{v}). \tag{2.19}$$

The semi-implicit finite difference scheme for the particle dynamic equation (2.19) is

$$\begin{aligned}\frac{\mathbf{v}^{n+1} - \mathbf{v}^n}{\Delta t} &= \frac{1}{2}\beta[(\mathbf{u} - \mathbf{v})^{n+1} + (\mathbf{u} - \mathbf{v})^n] \\ &= \frac{1}{2}\beta[(\mathbf{u}^{n+1} + \mathbf{u}^n - (\mathbf{v}^{n+1} + \mathbf{v}^n)].\end{aligned} \tag{2.20}$$

Taylor series expansions for $\mathbf{u}^{n+1}$ and $\mathbf{v}^{n+1}$ give

$$\mathbf{v}^{n+1} = \mathbf{v}^n + \Delta t\frac{d\mathbf{v}^n}{dt} + \frac{1}{2}(\Delta t)^2\frac{d^2\mathbf{v}^n}{dt^2} + \frac{1}{6}(\Delta t)^3\frac{d^3\mathbf{v}^n}{dt^3} + \ldots \tag{2.21}$$

$$\mathbf{u}^{n+1} = \mathbf{u}^n + \Delta t\frac{d\mathbf{u}^n}{dt} + \frac{1}{2}(\Delta t)^2\frac{d^2\mathbf{u}^n}{dt^2} + \frac{1}{6}(\Delta t)^3\frac{d^3\mathbf{u}^n}{dt^3} + \ldots \tag{2.22}$$

Each side of equation (2.20) can be evaluated as

$$\text{LHS}=\frac{d\mathbf{v}^n}{dt} + \frac{1}{2}(\Delta t)\frac{d^2\mathbf{v}^n}{dt^2} + \frac{1}{6}(\Delta t)^2\frac{d^3\mathbf{v}^n}{dt^3} + O(\Delta t)^3 \tag{2.23}$$

$$\text{RHS}=\beta(\mathbf{u}^n - \mathbf{v}^n) + \frac{1}{2}\beta\Delta t(\frac{d\mathbf{u}^n}{dt} - \frac{d\mathbf{v}^n}{dt}) + \frac{1}{4}\beta(\Delta t)^2(\frac{d^2\mathbf{u}^n}{dt^2} - \frac{d^2\mathbf{v}^n}{dt^2}) + O(\Delta t)^3. \tag{2.24}$$

Then equation (2.20) can be rewritten as

$$
\begin{aligned}
0 &= \frac{\mathbf{v}^{n+1}-\mathbf{v}^{n}}{\Delta t} - \frac{1}{2}\beta[(\mathbf{u}-\mathbf{v})^{n+1} + (\mathbf{u}-\mathbf{v})^{n}] \\
&= \frac{d\mathbf{v}^{n}}{dt} + \frac{1}{2}(\Delta t)\frac{d^2\mathbf{v}^{n}}{dt^2} + \frac{1}{6}(\Delta t)^2\frac{d^3\mathbf{v}^{n}}{dt^3} + \ldots \\
&\quad - \beta(\mathbf{u}^{n}-\mathbf{v}^{n}) - \frac{1}{2}\beta\Delta t(\frac{d\mathbf{u}^{n}}{dt} - \frac{d\mathbf{v}^{n}}{dt}) - \frac{1}{4}\beta(\Delta t)^2(\frac{d^2\mathbf{u}^{n}}{dt^2} - \frac{d^2\mathbf{v}^{n}}{dt^2}) + \ldots
\end{aligned} \tag{2.25}
$$

Thus, equation (2.20) is equivalent to

$$
\begin{aligned}
\frac{d\mathbf{v}^{n}}{dt} - \beta(\mathbf{u}^{n}-\mathbf{v}^{n}) &= -\frac{1}{2}(\Delta t)\frac{d^2\mathbf{v}^{n}}{dt^2} - \frac{1}{6}(\Delta t)^2\frac{d^3\mathbf{v}^{n}}{dt^3} \\
&\quad + \frac{1}{2}\beta\Delta t(\frac{d\mathbf{u}^{n}}{dt} - \frac{d\mathbf{v}^{n}}{dt}) + \frac{1}{4}\beta(\Delta t)^2(\frac{d^2\mathbf{u}^{n}}{dt^2} - \frac{d^2\mathbf{v}^{n}}{dt^2}) + \ldots \\
&= -\frac{1}{2}\Delta t[\frac{d^2\mathbf{v}^{n}}{dt^2} - \beta(\frac{d\mathbf{u}^{n}}{dt} - \frac{d\mathbf{v}^{n}}{dt})] - \frac{1}{6}(\Delta t)^2\frac{d^3\mathbf{v}^{n}}{dt^3} \\
&\quad + \frac{1}{4}\beta(\Delta t)^2(\frac{d^2\mathbf{u}^{n}}{dt^2} - \frac{d^2\mathbf{v}^{n}}{dt^2}).
\end{aligned} \tag{2.26}
$$

Taking derivative with t repeatedly, we get

$$
\begin{aligned}
\frac{d^2\mathbf{v}^{n}}{dt^2} - \beta(\frac{d\mathbf{u}^{n}}{dt} - \frac{d\mathbf{v}^{n}}{dt}) &= -\frac{1}{2}\Delta t[\frac{d^3\mathbf{v}^{n}}{dt^3} - \beta(\frac{d^2\mathbf{u}^{n}}{dt^2} - \frac{d^2\mathbf{v}^{n}}{dt^2})] \\
&\quad - \frac{1}{6}(\Delta t)^2\frac{d^4\mathbf{v}^{n}}{dt^4} + \frac{1}{4}\beta(\Delta t)^2(\frac{d^3\mathbf{u}^{n}}{dt^3} - \frac{d^3\mathbf{v}^{n}}{dt^3})
\end{aligned} \tag{2.27}
$$

and

$$
\begin{aligned}
\frac{d^3\mathbf{v}^{n}}{dt^3} - \beta(\frac{d^2\mathbf{u}^{n}}{dt^2} - \frac{d^2\mathbf{v}^{n}}{dt^2}) &= -\frac{1}{2}\Delta t[\frac{d^4\mathbf{v}^{n}}{dt^4} - \beta(\frac{d^3\mathbf{u}^{n}}{dt^3} - \frac{d^3\mathbf{v}^{n}}{dt^3})] \\
&\quad - \frac{1}{6}(\Delta t)^2\frac{d^5\mathbf{v}^{n}}{dt^5} + \frac{1}{4}\beta(\Delta t)^2(\frac{d^4\mathbf{v}^{n}}{dt^4} - \frac{d^4\mathbf{v}^{n}}{dt^4}).
\end{aligned} \tag{2.28}
$$

Repeatedly substituting above equations into the RHS of (2.26) results in

$$
\frac{d\mathbf{v}^{n}}{dt} - \beta(\mathbf{u}^{n}-\mathbf{v}^{n}) = -\frac{1}{6}(\Delta t)^2\frac{d^3\mathbf{v}^{n}}{dt^3} + \frac{1}{4}(\Delta t)^2\frac{d^3\mathbf{v}^{n}}{dt^3} + O((\Delta t)^3)
$$

$$=\frac{1}{12}(\Delta t)^2\frac{d^3\mathbf{v}^n}{dt^3}+\ O((\Delta t)^3)\,. \tag{2.29}$$

It is noted that the truncation error in equation (2.29) is independent of β. Thus motions of particles with very large β can be simulated without loss of accuracy.

2.3 Particle Collision Treatment

2.3.1 Collision Detection Scheme

Collision detection between any pairing particles is given as follows (Chen et al. 1995). At *n*th time step t_0, these two particles are initially located at $\mathbf{r}_{10}=(x_{10},\ y_{10},\ z_{10})$ and $\mathbf{r}_{20}=(x_{20},\ y_{20},\ z_{20})$. After a small time advancement Δt, at (*n+1*)th time step t_1, new positions of these two particles are $\mathbf{r}_{11}=(x_{11},\ y_{11},\ z_{11})$ and $\mathbf{r}_{21}=(x_{21},\ y_{21},\ z_{21})$. The particle position vectors at time t, which is between t_0 and t_1, can be expressed as

$$\mathbf{r}_1(t)=\{x_{10}+v_{x1}(t-t_0),\ y_{10}+v_{y1}(t-t_0),\ z_{10}+v_{z1}(t-t_0)\} \tag{2.30}$$

$$\mathbf{r}_2(t)=\{x_{20}+v_{x2}(t-t_0),\ y_{20}+v_{y2}(t-t_0),\ z_{20}+v_{z2}(t-t_0)\}\,. \tag{2.31}$$

The distance between two particles, s(t), is

$$s(t)=\ |\mathbf{r}_2(t)-\mathbf{r}_1(t)|. \tag{2.32}$$

These two particles will collide if the condition $s(t)\le R$ is satisfied. It is noted that the relative distance s(t) varies with time t, and it is not a monotonic function of t. The minimum relative distance occuring at time t_m is determined by

$$\frac{\partial s}{\partial t}\Big|_{t=t_m}=0\,. \tag{2.33}$$

Combining (2.30)-(2.33) gives

$$t_m=t_0-\frac{D_1}{D_2} \tag{2.34}$$

where

$$D_1 = (x_{10} - x_{20})(v_{x1} - v_{x2}) + (y_{10} - y_{20})(v_{y1} - v_{y2}) + (z_{10} - z_{20})(v_{z1} - v_{z2}) \qquad (2.35)$$

and

$$D_2 = (v_{x1} - v_{x2})^2 + (v_{y1} - v_{y2})^2 + (v_{z1} - v_{z2})^2. \qquad (2.36)$$

Equation (2.33) does not guarantee that the moment, when the above mentioned minimum distance occurs, has to be within the time interval t_0 and $t_0 + \Delta t$. Three cases need to be considered for calculating the minimum distance within a time step.

(i) if $t_m < t_0$, then the minimum distance is at the initial time t_0.

$$s_{min} = s(t_0) \qquad (2.37)$$

i.e.

$$s_{min} = \{(x_{10} - x_{20})^2 + (y_{10} - y_{20})^2 + (z_{10} - z_{20})^2\}^{1/2}. \qquad (2.38)$$

(ii) if $t_m > t_0 + \Delta t$, the minimum distance must occur at the time $t_0 + \Delta t$.

$$s_{min} = s(t_0 + \Delta t) \qquad (2.39)$$

i.e.

$$s_{min} = (s_x^2 + s_y^2 + s_z^2)^{1/2} \qquad (2.40)$$

where

$$s_x = x_{10} - x_{20} + \Delta t(v_{x1} - v_{x2})$$
$$s_y = y_{10} - y_{20} + \Delta t(v_{y1} - v_{y2})$$
$$s_z = z_{10} - z_{20} + \Delta t(v_{z1} - v_{z2}).$$

(iii) if $t_0 \le t_m \le t_0 + \Delta t$, the minimum distance occurs during the time interval t_0 and $t_0 + \Delta t$. In this case, we have

$$s_{min} = s(t_m) \qquad (2.41)$$

i.e.

$$s_{min} = (s_{mx}^2 + s_{my}^2 + s_{mz}^2)^{1/2} \qquad (2.42)$$

where

$$s_{mx} = x_{10} - x_{20} + (t_m - t_0)(v_{x1} - v_{x2})$$
$$s_{my} = y_{10} - y_{20} + (t_m - t_0)(v_{y1} - v_{y2})$$
$$s_{mz} = z_{10} - z_{20} + (t_m - t_0)(v_{z1} - v_{z2}).$$

After s_{min} is evaluated within the time step, the examination of collision events is still needed because s_{min} can be either larger or smaller than R. Collision occurs if

$$s_{min} \le R \tag{2.43}$$

At the collision instant t_c,

$$s(t_c) = R \tag{2.44}$$

and

$$s(t_c) = |\mathbf{r}_2(t_c) - \mathbf{r}_1(t_c)| . \tag{2.45}$$

Hence the collision instant t_c can be obtained solving (2.44) and (2.45)

$$t_c = t_0 + \frac{-b - \sqrt{b^2 - 4(s_0^2 - R^2)w^2}}{2w^2} \tag{2.46}$$

where

$$\begin{aligned} b = 2[&(x_{10} - x_{20})(v_{x1} - v_{x2}) + (y_{10} - y_{20})(v_{y1} - v_{y2}) \\ &\qquad (z_{10} - z_{20})(v_{z1} - v_{z2})] \\ s_0 &= \{(x_{10} - x_{20})^2 + (y_{10} - y_{20})^2 + (z_{10} - z_{20})^2\}^{1/2} \\ w &= \{(v_{x1} - v_{x2})^2 + (v_{y1} - v_{y2})^2 + (v_{z1} - v_{z2})^2\}^{1/2} . \end{aligned}$$

With perfect sticking collision model, any collision can produce a new born particle (daughter particle). The daughter particle will inherit all possessions of parent particles, i.e., conservation of mass and momentum. Let the daughter particle be numbered 3, then the conservation law gives the size of daughter particle as

$$d_3 = (d_1^3 + d_2^3)^{1/3} \tag{2.47}$$

where d_i (i=1, 2, 3) are particle radii. The velocity components of daughter particle are

$$v_{x3} = \frac{v_{x1}d_1^3 + v_{x2}d_2^3}{d_3^3} \tag{2.48}$$

$$v_{y3} = \frac{v_{y1}d_1^3 + v_{y2}d_2^3}{d_3^3} \tag{2.49}$$

$$v_{z3} = \frac{v_{z1}d_1^3 + v_{z2}d_2^3}{d_3^3} \tag{2.50}$$

and the position components at the end of time step

$$x_3 = \{[x_{10} + v_{x1}(t_c - t_0)]d_1^3 + [x_{20} + v_{x2}(t_c - t_0)]d_2^3\} / d_3^3 + v_{x3}(t_0 - t_c + \Delta t) \qquad (2.51)$$

$$y_3 = \{[y_{10} + v_{y1}(t_c - t_0)]d_1^3 + [y_{20} + v_{y2}(t_c - t_0)]d_2^3\} / d_3^3 + v_{y3}(t_0 - t_c + \Delta t) \qquad (2.52)$$

$$z_3 = \{[z_{10} + v_{z1}(t_c - t_0)]d_1^3 + [z_{20} + v_{z2}(t_c - t_0)]d_2^3\} / d_3^3 + v_{z3}(t_0 - t_c + \Delta t) \qquad (2.53)$$

In general, the collision detection takes a lot of computer time since a large number of particles are considered. The primitive collision detection scheme searches the collision candidates by going through all particles N, so that the computing time is proportional to N^2. The collision detection method in Chen et al. (1995) is an efficient scheme, and it is also implemented in this thesis. By dividing the computational domain into a number of small cells, the potential collision partners for a given particle in one cell are then searched within this cell and neighboring twenty-six cells during one time step. This search only involves a small number of particles. The total computing time with this scheme can be reduced dramatically. Only binary collision is considered by assuming a negligible probability of multiple collisions in a small time step in a dilute condition. For any particle moving out of the computational box, it is re-introduced into the box by invoking periodicity. The collision rate or kernel can be determined, in principle, by counting the number of collisions per time step. Initially, a given number of particles are randomly distributed into the computational domain. The particles are evolved with turbulence for a period of time before collision detection turned on. The collision events are not counted until all particles with finite inertia have reached dynamical equilibrium in turbulence.

2.3.2 Post-Collision Treatment

The collision event is counted when two particles are brought into contact, as stated above. The collision among particles and its subsequent treatment are expected to disturb the original system and permanently impact the subconsequent collision evaluation. For the droplets in gas turbulence, the collision may, most likely, result in coalesce of two droplets and a larger droplet is then formed by the colliding droplets. Similar phenomena may be found in a system consisting of bubbles and fluids. The collision between two solid particles may behave in different ways. Two solid particles may stick together upon contact or the colliding solid particles will separate after collision. In summary, the issue dealing with immediate consequence of those contacts is referred as post-collision treatment. Several models with regard to post-collision treatment have been developed during past decades.

In Chen et al. (1995) every collision results in the collision partners disappearing from their respective size groups to produce a larger particle. Mass and momentum conservation laws were applied for the birth of the new particle. This scheme is considered to be a physically realistic model assuming a unity collision efficiency. It is hereinafter referred as 'KEEP ALL' model. Balachandar (1988) used a different post-collision scheme. Starting with monosize particles in system, after each collision, the resulting larger particle was discarded in the computation so that it does not contribute to future collisions. This post-collision treatment is hereinafter referred as the 'THROW AWAY' scheme. Sundaram & Collins (1997) employed a 'HARD SPHERE' collision model in which the particles were assumed to be rigid spheres and forced to bounce back after the contact. Momentum conservation is applied to the particles after collision. In contrast to the 'KEEP ALL' and 'THROW AWAY' schemes, the 'HARD SPHERE' model allows a particle to have multiple collisions with other particles in a system. Wang et al. (1997) tested three different schemes and presented one of their own. In their scheme, collision does not disturb the system. The colliding particles are allowed to overlap in space (hereinafter referred as 'OVERLAPPING' scheme), but no larger particles are formed after the collision. Two colliding particles can separate after their trajectories satisfy $|\mathbf{r}_2(t) - \mathbf{r}_1(t)| \geq R$. Thus, a particle can have multiple collisions with other particles. These four different post-collision treatments will, in principle, result in different collision rate/kernel.

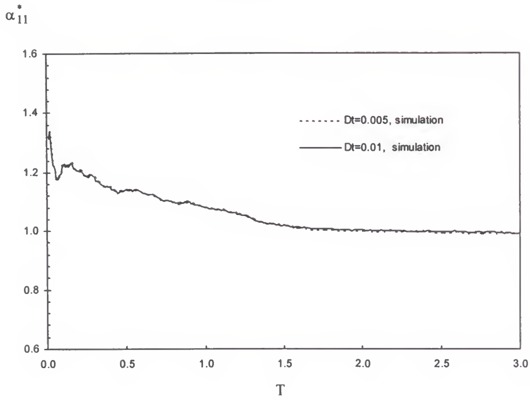

Figure 2.1 The effect of time step on the cumulative average of the normalized collision kernel α^*_{11} for inertialess particles in turbulence. Particle size D=0.05.

2.4 Computer Simulation

2.4.1 Time Step

Three collision models: "THROW AWAY," "KEEP ALL" and "HARD SPHERE" are employed in this work. For the following simulations with "THROW AWAY" and "KEEP ALL" collision models, the time step $\Delta t=0.01$ is used to advance the motions of particles. Figure 2.1 shows the effect of time step on the collision kernel α^*_{11} using "KEEP ALL" collision model. It can be seen that there is almost no difference between the results of $\Delta t=0.01$ and $\Delta t=0.005$. Similar results are obtained by "THROW AWAY" scheme. The volume concentration of suspended particles is usually quite low in many natural systems such as spray burners and air scrubbers, which is within the interest of this work. In such dilute systems, the multiple collisions during a small time step may be negligible, thus binary collision mechanism is considered solely in this study.

2.4.2 Turbulence Realization

The averages of statistical quantities are evaluated in two directions: average over all time steps and turbulence ensemble average over all turbulence realizations. The total time steps mainly depend on the particle response time and the number of collision pairs during whole time period. We start counting the time steps for collision detection after the motions of particles have been evolved for three times the particle response time. Ideally, to form the turbulence ensemble average, the numerical simulation should be repeated an infinite number of realizations with different initial particle distributions. An infinite number of turbulence realizations is impractical due to limited computer capacity and may be unnecessary from the viewpoint of the accuracy of numerical scheme. Figures 2.2 (a) & (b) show the turbulence dissipation rate against turbulence realizations. While the ensemble averaged turbulence dissipation rate varies with the realization by a large amplitude shown in figure 2.2 (a), the cumulative average of turbulence dissipation rate approaches a constant for the number of turbulence realizations greater than 30, as seen from figure 2.2 (b). Figures 2.3 (a) & (b) show the small eddy shear rate against turbulence realizations. It can also be seen that, although the ensemble averaged small eddy shear rate randomly varies with the turbulence realization in figure 2.3 (a), the cumulative average of small eddy shear rate is close to a constant by the 40th realization seen in figure 2.3 (b). Therefore, in this study forty turbulence realizations are used for turbulence ensemble average.

2.4.3 Validation of the Collision Detection Scheme

Starting with monosize particles in system and using the "THROW AWAY" collision model for post-collision treatment. The evolution of the particle number $n_1(t)$

follows the simple population balance equation:

$$dn_1/dt = -\alpha_{11}n_1^2 \qquad \text{with} \qquad n_1(t=0) = n_0 . \tag{2.54}$$

The solution is

$$n_0 / n_1(t) = 1 + \alpha_{11}n_0 t . \tag{2.55}$$

It should be mentioned that the collision rate of monosize particles (2.54) is only accurate for large number of particles in a system. For small number of particles, however, the collision rate (2.54) must be corrected. The detailed discussions on this issue will be given in §6.2. Since the statistics for the number of the remaining particles $n_1(t)$ is much more accurate, the average slope of the curve $1/n_1(t)$ gives the collision kernel, so it can be used to check the accuracy of the collision kernel obtained by simulation in laminar shear flow.

To validate the collision detection, particle collision in a uniform shear flow of velocity gradient Γ=1.0 is first considered. For large number of particles the theoretical prediction of the collision kernel α_{ij} of Smoluchowski is accurate and is given by $\alpha_{ij} = 4R_{ij}^3\Gamma / 3$. For a small number of monosized particles the theoretical prediction of the collision rate of Smoluchowski has to be corrected, as mentioned above. Ten thousand particles of radius 0.075 are introduced into a box of volume 2x2x2. The time step is Dt=0.01 and a total of 800 time steps is used. The number of shear flow realizations is 80. Since no periodic condition may be imposed along vertical direction in uniform shear flow, periodic boundary conditions are employed in the streamwise and spanwise directions only. In such a case, a boundary correction of the collision rate has to be imposed (Wang et al. 1997). Another correction on the collision rate is also applied due to the inaccurate expression of the collision rate (§6.2) Figure 2.4 shows the particle number evolution. The collision kernel α_{11} can be obtained from the average slope of the curve. Very good agreement can be observed between simulation result and Smoluchowski's prediction. Hence, the collision detection scheme and the numerical implementation are validated.

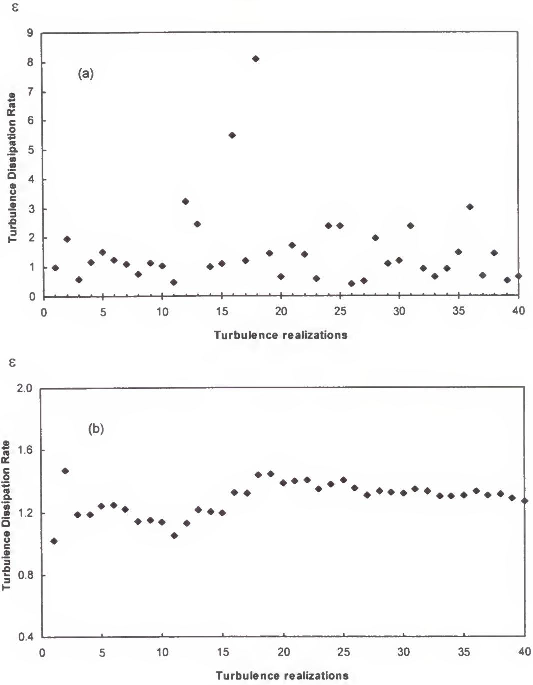

Figure 2.2 Turbulence dissipation rate ε against turbulence realization. (a) Variation of ensemble average. (b) Cumulative average.

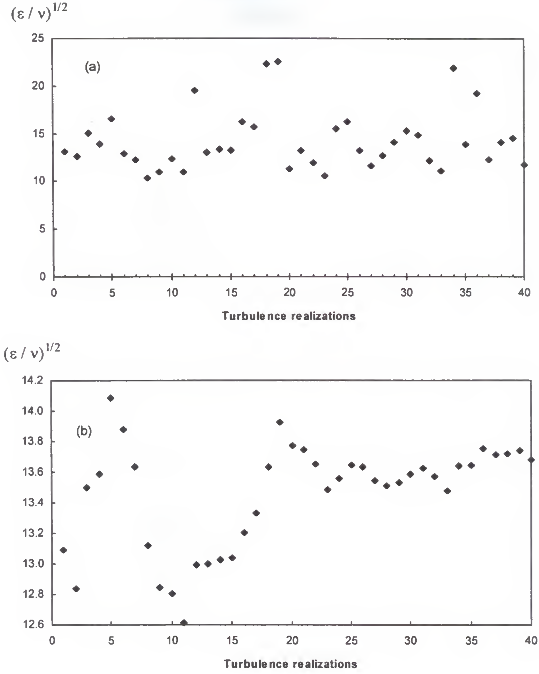

Figure 2.3 Turbulence small eddy shear rate $(\varepsilon / \nu)^{1/2}$ against turbulence realization. (a) Variation of ensemble average. (b) Cumulative average.

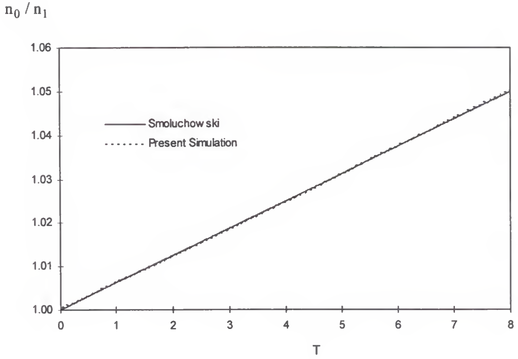

Figure 2.4 Inverse of total number of monodisperse particles against time in laminar shear flow. Γ=1.0, D=0.015.

For "HARD SPHERE" particles, the time step for advancing the motions of particles is much less than 0.01. It is found that Δt=0.001 may generate almost same result as Δt=0.0005 for large inertia particles. For small inertia or zero inertia particles, the collision kernel strongly depends on time step due to multiple collision mechanism, which is shown in figures 2.5 for uniform shear flow. A pair of particles can have tens or hundreds of collisions depending on the size of time step before they completely separate. Similar multiple collisions have been found for particles in turbulence. Due to this technical difficulty, the "HARD SPHERE" collision model is limited to particles with large inertia.

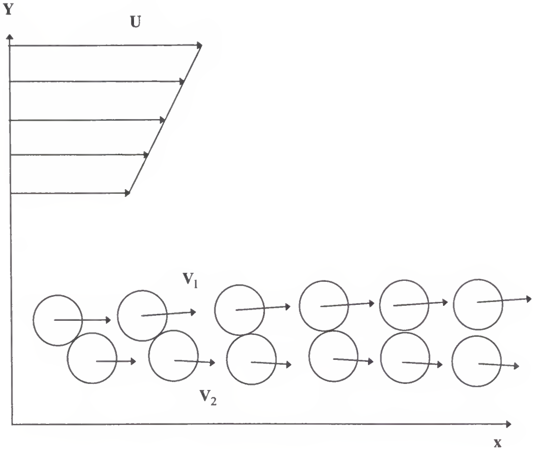

Figure 2.5 Multiple collisions of HARD SPHERE particles in laminar shear flow.

CHAPTER 3
A NEW THEORETICAL FRAMEWORK FOR PREDICTING COLLISION RATE OF SMALL PARTICLES IN GENERAL TURBULENT FLOWS

A new theoretical framework is developed to predict the collision rate and collision velocity of small, inertialess particles in *general* turbulent flows. The present approach evaluates the collision rate for small particles in a given instantaneous flow field based on the local eigen-values of the rate of strain tensor. An ensemble average is applied to the instantaneous collision rate to obtain average collision rate. The collision kernels predicted by Smoluchowski (1917) for laminar shear flow and by Saffman & Turner (1956) for isotropic turbulence are recovered. The collision velocities presently predicted in both laminar shear flow and isotropic turbulence agree well with the results form direct numerical simulation for particle collision in both flows. The present theory for evaluating the collision rate and collision velocity is also applied to a rapidly sheared homogeneous turbulence. Using the mean turbulent shear rate $(\varepsilon/\nu)^{1/2}$ as the characteristic shear rate to normalize the collision rate, the effect of the turbulence structure on the collision rate and velocity can be reasonably described. The combined effects of the mean flow shear and the turbulence shear on the collision rate and collision velocity are elucidated.

3.1 Introduction

Smoluchowski (1917) considered collision rate among spherical particles in a laminar shear flow, $(u_x, u_y, u_z) = (\Gamma y, 0, 0)$ with a constant gradient Γ. For a target particle of radius r_i centered at an arbitrary position $\mathbf{x}_i$, any particle with a radius r_j moving toward the target particle will cause a collision if

$$|\mathbf{x}_i - \mathbf{x}_j| \leq R_{ij} = r_i + r_j \tag{3.1}$$

is satisfied. The collision rate can be evaluated as

$$\dot{n}_{cij} = n_i n_j \int_{w_r<0} -w_r dA \tag{3.2}$$

where w_r is the radial component of the relative fluid velocity between $\mathbf{x}_i$ and $\mathbf{x}_j$, $w_r<0$ indicates an impending collision, $-n_1 n_2 w_r$ is the particle flux moving inward to the target particle, and A is a spherical surface with radius $R_{ij}=r_i+r_j$. Using standard spherical coordinates (R, θ, ϕ) centered at particle i (see figure 3.1), w_r on the spherical surface of $R=R_{ij}$ can be written as $w_r = \Gamma y \cos\theta = R_{ij} \sin\theta \cos\theta \cos\phi$. With $dA= R_{ij}^2 \sin\theta \, d\theta d\phi$, it is easily seen that

$$\dot{n}_{cij} = n_i n_j \frac{4}{3} \Gamma R_{ij}^3 \tag{3.3}$$

or

$$\alpha_{ij} = \frac{4}{3} \Gamma R_{ij}^3 . \tag{3.4}$$

Saffman & Turner (1956, hereinafter referred as ST) presented a classical theory for the collision rate of small droplets in Gaussian, isotropic turbulence. The collision rate among particle size group i and j is

$$\dot{n}_{cij} = n_i n_j < \int_{w_r<0} -w_r dA >. \tag{3.5}$$

The ensemble average, denoted by < >, is necessary since turbulence is random. Because of the continuity of the fluid flow, the volume influx entering the spherical surface of radius R_{ij} is equal to the efflux so that

$$\dot{n}_{cij} = \frac{1}{2} n_i n_j < \int_{\text{entire sphere}} |w_r| \, dA >. \tag{3.6}$$

ST further interchanged the integration with the ensemble average so that $\dot{n}_{cij}$ can be evaluated in isotropic turbulence,

$$\dot{n}_{c_{ij}} \approx \frac{1}{2}\, n_i n_j \int_{\text{entire sphere}} <|w_r|>\, dA. \tag{3.7}$$

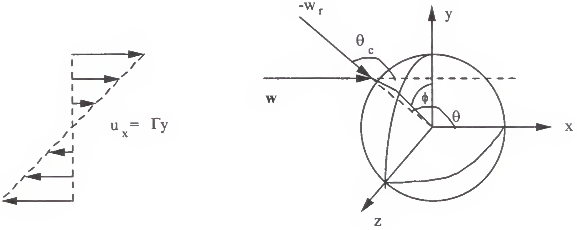

Figure 3.1 Local coordinates for collision rate calculation in laminar shear flow.

For isotropic turbulence, the above becomes

$$\dot{n}_{c_{ij}} = n_i n_j\, 2\pi R_{ij}^2\; <|w_x|> \tag{3.8}$$

where x is the local coordinate parallel to the line connecting the centers of the colliding particles as shown in figure 3.2. For particle size smaller than Kolmogorove length scale η, the relative velocity upon the collision was evaluated using the standard results of small-scale turbulence theory as

$$<|w_x|> = <|u_{ix} - u_{jx}|> \approx R_{ij} < \frac{\partial u}{\partial x} > = R_{ij} \left(\frac{2}{15\pi} \frac{\varepsilon}{\nu}\right)^{1/2} \tag{3.9}$$

where ε is the dissipation rate of turbulence and ν is fluid kinematic viscosity. This gives

$$\dot{n}_{c_{ij}} = n_i n_j R_{ij}^3 \left[\frac{8\pi}{15} \frac{\varepsilon}{\nu}\right]^{1/2} = 1.2944 n_i n_j R_{ij}^3 \left(\frac{\varepsilon}{\nu}\right)^{1/2} \tag{3.10}$$

or

$$\alpha_{ij} = 1.2944 R_{ij}^3 \left(\frac{\varepsilon}{\nu}\right)^{1/2} \tag{3.11}$$

or

$$\alpha_{ij}^* = \frac{\alpha_{ij}}{R_{ij}^3 \left(\frac{\varepsilon}{\nu}\right)^{1/2}} = 1.2944 \tag{3.12}$$

where α_{ij}^{*} is normalized collision kernel.

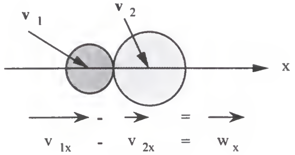

Figure 3.2 Sketch of particle collision velocity. The separation distance is $x_2\text{-}x_1 = \pm R_{ij} = \pm(r_i+r_j)$.

It needs pointed out that from equation (3.6) to equation (3.7), the interchange between the integration with the ensemble average is only an approximation even in a Gaussian, isotropic turbulence. Furthermore, the interchange between these two operations severely limits the extension of ST's result and approach to other turbulent flows such as the near wall region where the mean flow gradient contributes to $<|w_r|>$. Of course, in the theory of Smoluchowski for laminar shear flow, this issue does not arise since the ensemble average is not needed. In a typical industrial facility where particle collision leads to the desirable growth of particles, the inhomogeneity of the turbulent flow structure is common. Due to the effects such as turbopheresis, particles tend to be driven toward wall regions to cause a further inhomogeneity in the particle concentration distribution. It was not clear how one can predict the collision rate of small particles in the presence of both strong mean flow shear and high turbulence intensity (Kontamaris, 1995).

In this chapter, a new theoretical framework is presented for the collision rate of inertialess particles, whose sizes are smaller than the Kolmogorove length scale, in general turbulent flows. The present analysis starts from equation (3.5). Using the leading order term, $(\mathbf{x}_i\text{-}\mathbf{x}_j)\cdot\nabla\mathbf{u}$, in the Taylor series expansion to approximate the relative fluid velocity, **w**, at the collision instant, the collision rate for an arbitrarily given $\nabla\mathbf{u}$ is evaluated first. The ensemble average is then carried out in a Gaussian, isotropic turbulence to obtain the collision rate and collision velocity. Direct numerical simulations are also performed to obtain the collision rate and collision velocity in a Gaussian, isotropic turbulence. Good agreement is obtained between the present prediction and the simulation for the collision kernel α_{ij}^{*}. Excellent agreement is obtained for the average collision velocity between the prediction and the simulation. While the present result for the collision rate agrees with the prediction of ST, the present theory predicts an average collision velocity $<-w_r>$ that is 1.58 times the value given by ST. The difference is caused by the bias of the collision toward higher values of collision velocity which was not considered in previous studies on flow induced particle collisions. Using the rapid distortion theory (RDT) for a rapidly sheared homogeneous turbulence and the random Fourier modes representation, the dependence of particle collision kernel α_{ij} on the mean flow shear rate and the turbulence structure in homogeneous shear flow is studied under the present theoretical framework. It is found that the collision kernel, after normalized by particle volume and the turbulence mean shear rate characterized by the dissipation rate, mainly depends on the ratio of the mean flow shear rate to the turbulence mean shear rate.

3.2 Analysis

The relative fluid velocity, $\mathbf{w} = \mathbf{u}_1 - \mathbf{u}_2$, between target particle centered at $\mathbf{x}_1$ and the colliding particle centered at $\mathbf{x}_2$ in space with $|\mathbf{x}_1 - \mathbf{x}_2| = |\mathbf{r}_{12}| = R$ less than the Kolmogorove length scale η can be expressed using Taylor series expansion as

$$\mathbf{w} = \mathbf{u}_2 - \mathbf{u}_1 \approx \mathbf{r}_{12}\cdot\nabla\mathbf{u} + \ldots \tag{3.13}$$

$$\mathbf{r}_{12} = \mathbf{x}_2 - \mathbf{x}_1 \tag{3.14}$$

to the leading order. The collision rate, $\dot{n}_{c12}$, for a given $\nabla\mathbf{u}$ at a given instant is thus

$$n_{c12} = n_1 n_2 \int_{w_r<0} -\mathbf{w}\cdot\mathbf{n}dA \tag{3.15}$$

where **n** is the outward normal of the surface given by $|\mathbf{x}_2 - \mathbf{x}_1| = R_{ij} = R$ and $w_r = \mathbf{w}\cdot\mathbf{n}$. For a spherical surface, $\mathbf{n} = \mathbf{r}_{12}/R$ so that

$$\int_{w_r<0} -\mathbf{w}\cdot\mathbf{n}dA = \frac{1}{R}\int_{w_r<0} -\mathbf{w}\cdot\mathbf{r}_{12}\, dA$$

$$\approx \frac{1}{R}\int_{w_r<0} -\mathbf{r}_{12}\cdot\nabla\mathbf{u}\cdot\mathbf{r}_{12}\, dA. \tag{3.16}$$

Representing $\nabla\mathbf{u}$ as the sum of a symmetrical part (rate-of-strain tensor) and an anti-symmetrical part (vorticity tensor), it can be easily seen that the antisymmetrical part of $\nabla\mathbf{u}$ does not contribute to w_r. Physically, it is simply because a rigid body rotation does not contribute to normal velocity. For a symmetric tensor $\mathbf{E} = \frac{1}{2}(\nabla\mathbf{u} + (\nabla\mathbf{u})^T)$, or a symmetric matrix E_{ij}, a linear transformation, which is a rotation of the coordinate system from (x, y, z) to $(\tilde{x}, \tilde{y}, \tilde{z})$, can be easily found to reduce E_{ij} to a diagonal form as

$$\tilde{\mathbf{E}} = \begin{bmatrix} e_{\tilde{x}} & 0 & 0 \\ 0 & e_{\tilde{y}} & 0 \\ 0 & 0 & e_{\tilde{z}} \end{bmatrix} \tag{3.17}$$

where $(e_{\tilde{x}}, e_{\tilde{y}}, e_{\tilde{z}})$ are the eigen-values of E and are the principal values of the rate-of-strain tensor. Due to incompressibility, $e_{\tilde{x}} + e_{\tilde{y}} + e_{\tilde{z}} = 0$ so that there are only two independent parameters (say $e_{\tilde{x}}$ and $e_{\tilde{y}}$) in $\tilde{\mathbf{E}}$ in order to evaluate the integral in (3.16). Arranging the eigenvalues in the order of

$$e_{\tilde{z}} = -(e_{\tilde{x}} + e_{\tilde{y}}) \le e_{\tilde{y}} \le e_{\tilde{x}}, \tag{3.18}$$

and defining

$$\zeta = \frac{e_{\tilde{y}}}{e_{\tilde{x}}} \qquad \text{with} \quad -0.5 \le \zeta \le 1 \tag{3.19}$$

the integrand in (3.16) can be expressed as

$$-\mathbf{r}_{12}\cdot\nabla\mathbf{u}\cdot\mathbf{r}_{12} = -(e_{\tilde{x}}\tilde{x}^2 + e_{\tilde{y}}\tilde{y}^2 + e_{\tilde{z}}\tilde{z}^2)$$

$$= -e_{\tilde{x}}\,[\tilde{x}^2 + \zeta\tilde{y}^2 - (1+\zeta)\,\tilde{z}^2]$$

$$= - e_{\tilde{x}}\ R^2[\cos^2\theta + \zeta\sin^2\theta\cos^2\phi - (1+\zeta)\sin^2\theta\sin^2\phi] \qquad (3.20)$$

where a local spherical coordinate system ($\tilde{x}$ =Rcosθ, $\tilde{y}$ =Rsinθcosϕ, $\tilde{z}$ =Rsinθsinϕ) has been introduced. Hence

$$\int_{w_r<0} -\mathbf{w}\cdot\mathbf{n}dA = -R^3 e_{\tilde{x}} \int_0^{2\pi}\int_0^{\pi}{}_{w_r<0}[\cos^2\theta + \zeta\sin^2\theta\cos^2\phi - (1+\zeta)\sin^2\theta\sin^2\phi]\sin\theta\, d\theta\, d\phi$$

$$= R^3 e_{\tilde{x}}\ \mathcal{H}(\zeta). \qquad (3.21)$$

Again, $w_r<0$ in the integration limit implies that only the non-positive values inside the square bracket are evaluated in the integration. While an analytical expression for $\mathcal{H}(\zeta)$ is difficult to obtain due to the dependence of the integration limits on arbitrary ζ, accurate numerical integration for $\mathcal{H}(\zeta)$ can be easily carried out (using Simpson's rule). The following interpolation is then constructed for $\mathcal{H}(\zeta)$ based on numerical integration results,

$$\mathcal{H}(\zeta) \approx \frac{8}{3}\ [0.90725 + 0.2875(0.5+\zeta)^2 + 0.333(0.5+\zeta)^4] \qquad \zeta<0$$

$$\approx \frac{8}{3}\ [1 + 0.55\zeta + 0.724071\zeta^2 - 0.96874\zeta^3$$

$$+ 0.73924\zeta^4 - 0.23035\zeta^5]. \qquad \zeta\geq 0 \qquad (3.22)$$

Consider the laminar shear flow for example. In this case, ζ=0, $e_{\tilde{x}} = \frac{\Gamma}{2}$, $\mathcal{H}(0) = \frac{8}{3}$, so that $\dot{n}_{c12} = n_1 n_2 \frac{1}{2}\Gamma R^3 \frac{8}{3} = n_1 n_2 \frac{4}{3}\Gamma R^3$ which is the same as given by Smoluchowski (1917). Equation (3.22) is valid for $-1\leq\zeta\leq-0.5$ as well since it is based on (3.21). The restriction for $\zeta\geq-0.5$ results only from equation (3.18) when the eigenvalues are arranged in such a manner. For $-1\leq\zeta\leq0$, $\mathcal{H}(\zeta)$ is symmetrical with respect to ζ =-0.5. For example, ζ=0 corresponds to a 2-D stagnation flow in ($\tilde{x}$, $\tilde{z}$) plane and ζ=-1 corresponds to a 2-D stagnation flow in ($\tilde{x}$, $\tilde{y}$) plane so that the collision rates are completely equivalent. It is also interesting to note that ζ=-0.5 is equivalent to ζ=1 since both correspond to an axisymmetric stagnation flow with ζ=-0.5 for an axisymmetric contraction and ζ=1 for an axisymmetric expansion; the only difference is the scale $e_{\tilde{x}}$. With these examples in mind, a simple analysis for the flow field quickly shows that $\mathcal{H}(\zeta\leq 0)$ can be obtained from $\mathcal{H}(\zeta\geq 0)$ as

$$\mathcal{H}(-\frac{1}{1+\zeta}) = \mathcal{H}(\frac{1}{1+\zeta} -1) = \frac{1}{1+\zeta}\ \mathcal{H}(\zeta) \qquad \text{for} \quad \zeta\geq 0. \tag{3.23}$$

Finally, the collision rate for small inertialess particles in a turbulent flow is simply

$$\dot{n}_{c12} = n_1 n_2 R^3 < e_{\tilde{x}}\ \mathcal{H}(\zeta) > \tag{3.24}$$

where the ensemble average is taken over all possible values of the rate-of-strain tensor. It is emphasized that this result is applicable to general turbulent flow. Needless to say, the isotropy assumption is not needed in the present framework. When the detailed knowledge of $\nabla\mathbf{u}$ is available, such as from DNS or random Fourier modes representation (Kraichnan, 1970) of turbulence, the ensemble average in (3.24) can be carried out.

The foregoing analysis can also be extended to evaluate the average of the normal (or radial) component of the collision velocity $<-w_r>$. For a given position with arbitrary $e_{\tilde{x}}$ and ζ at any given instant, the instantaneous average of the normal collision velocity can be calculated by integrating over the spherical surface of radius R as

$$< w_r|e_{\tilde{x}}\ , \zeta>^{\mathcal{A}} = \frac{\int_{w_r<0} w_r(-w_r)dA}{\int_{w_r<0} (-w_r)dA}\ . \tag{3.25}$$

In the above, the superscript $\mathcal{A}$ on the left hand side denotes the area-average, $(-w_r)dA$ in the numerator can be interpreted as proportional to the probability of a particle striking the target surface at a position (θ, ϕ) over an area dA and w_r in the numerator is the relative radial velocity of the collision at (θ, ϕ) on the target surface. The denominator is the normalizing factor for the probability. The product, $w_r(-w_r)$, clearly indicates that $<w_r|e_{\tilde{x}}\ , \zeta>^{\mathcal{A}}$ is a biased average in favor of these regions in (θ, ϕ) where $(-w_r)$ is high. Suppose that N_R realizations of turbulence be taken in a turbulent flow, the total number of collisions will be

$$N_c = N_R n_1 n_2 <\int_{w_r<0} (-w_r)dA>$$

per unit time using equation (3.5). The chance of a particle striking the target surface over an area dA at (θ, ϕ) relative to the axis of the principal direction $\tilde{x}$ of the instantaneous rate-of-strain tensor in a given realization is then $n_1 n_2(-w_r)dA|_{w_r<0}/N_c$. Integrating over the target surface and summing over N_R realizations, the ensemble average, $<w_r>$, is obtained,

$$< w_r > = N_R < \int_{w_r<0} w_r \frac{n_1 n_2(-w_r)}{N_c}\, dA > = \frac{<\int_{w_r<0} (-w_r) w_r dA>}{<\int_{w_r<0} (-w_r) dA>} . \qquad (3.26)$$

The above can be simplified as

$$< w_r > = -R \frac{< e_{\tilde{x}}^2\, \mathcal{G}(\zeta) >}{< e_{\tilde{x}}\, \mathcal{H}(\zeta) >} \qquad (3.27)$$

where

$$\mathcal{G}(\zeta) = \int_0^{2\pi} \int_0^{\pi} \left[\cos^2\theta + \zeta \sin^2\theta \cos^2\phi - (1+\zeta) \sin^2\theta \sin^2\phi\right]^2_{w_r<0} \sin\theta\, d\theta\, d\phi. \qquad (3.28)$$

The integration can again be evaluated numerically and represented in the following piecewise interpolations

$$\frac{\mathcal{G}(\zeta)}{\mathcal{H}(\zeta)} = 0.4 + 1.0777(0.5+\zeta)^2 - 0.64767(0.5+\zeta)^4 \qquad \text{for} \qquad \zeta<0$$

$$= 0.62831 + 0.68495\zeta - 0.091083\zeta^2$$

$$+ 0.090301\zeta^3 - 0.034658\zeta^4 \qquad \text{for} \qquad \zeta \geq 0. \qquad (3.29)$$

Similarly, the mean square value of the radial component velocity $< w_r^2 >$ can be evaluated as

$$< w_r^2 > = R \frac{< e_{\tilde{x}}^3\, \mathcal{K}(\zeta) >}{< e_{\tilde{x}}\, \mathcal{H}(\zeta) >} \qquad (3.30)$$

with

$$\frac{\mathcal{K}(\zeta)}{\mathcal{H}(\zeta)} = 0.17114 + 1.2643(0.5+\zeta)^2 - 0.48123(0.5+\zeta)^4 \qquad \text{for} \qquad \zeta<0$$

$$= 0.45714 + 0.97655\zeta + 0.39606\zeta^2$$

$$+\,0.072430\zeta^3 - 0.0291\zeta^4 \qquad \text{for} \qquad \zeta \geq 0. \tag{3.31}$$

The functions $\mathcal{H}(\zeta)$, $\mathcal{G}(\zeta)/\mathcal{H}(\zeta)$, and $\mathcal{K}(\zeta)/\mathcal{H}(\zeta)$ are shown in figure 3.3. Take a laminar shear flow for example: $e_{\tilde{x}} = \Gamma/2$ and $\zeta=0$ so that $\mathcal{G}/\mathcal{H} = 0.62832$ $(=\pi/5)$ and $\mathcal{G}/\mathcal{H}=16/35$. It is easily seen that

$$< w_r > = -R\frac{\Gamma^2}{4}\frac{\pi}{5}\frac{8}{3}/[\frac{\Gamma}{2}\frac{8}{3}] = -\frac{\pi}{10}\,\Gamma R, \tag{3.32}$$

$$< w_r^2 > = R^2\frac{\Gamma^3}{8}\frac{16}{35}\frac{8}{3}/[\frac{\Gamma}{2}\frac{8}{3}] = \frac{4}{35}(\Gamma R)^2. \tag{3.33}$$

The results of these two moments of w_r can be used to validate the present theoretical formulation by comparing with direct numerical simulation for particle collisions.

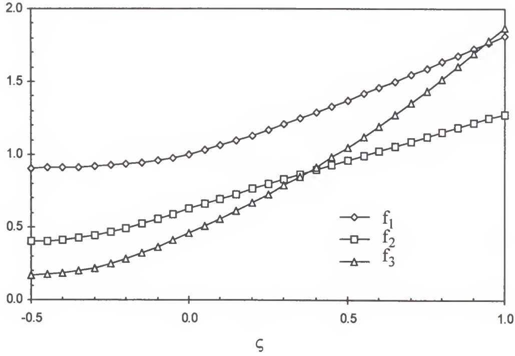

Figure 3.3 Variations of $\mathcal{H}(\zeta)$, $\mathcal{G}(\zeta)$, $\mathcal{K}(\zeta)$ with ζ where

$$f_1 = \frac{3}{8}\,\mathcal{H}(\zeta),\; f_2 = \frac{\mathcal{G}(\zeta)}{\mathcal{H}(\zeta)} \text{ and } f_3 = \frac{\mathcal{K}(\zeta)}{\mathcal{H}(\zeta)}.$$

To apply the above results to turbulent flows, we consider the following two cases: i) Gaussian isotropic turbulence; and ii) rapidly sheared homogeneous turbulence under a mean flow gradient Γ. In both cases, the turbulence can be represented using random Fourier modes and ensemble averages can be obtained without resorting to the direct numerical solutions to the Navier Stokes equations for the fluid flows. Pertinent comparison can be made with ST's prediction in the first case. Insights on the effect of mean flow shear can be gained by examining the collision rate in the rapidly sheared turbulence.

3.3 Numerical Simulation

The detailed representation of the isotropic turbulence and rapidly sheared homogeneous turbulence are given in Chapter 2. In short, the isotropic turbulence is represented in the form of

$$u_i(\mathbf{x},\ t) = \sum_{m=1}^{N}[b_i^{(m)} \cos(\mathbf{k}^{(m)} \cdot \mathbf{x} + \omega^{(m)} \cdot t) + c_i^{(m)} \sin(\mathbf{k}^{(m)} \cdot \mathbf{x} + \omega^{(m)} \cdot t)] \tag{2.6}$$

where $\mathbf{k}^{(m)}$ and $\omega^{(m)}$ are the wavenumber and frequency of the m-th mode. The random coefficients $b_i^{(m)}$ and $c_i^{(m)}$ are their corresponding amplitudes. For sheared homogeneous turbulence, the flow field is given by

$$u_i(\mathbf{x},\ t) = \sum_{m=1}^{N}[b_i^{(m)}(S) \cos(\chi^{(m)} \cdot \mathbf{x} + \omega^{(m)} \cdot t) + c_i^{(m)}(S) \sin(\chi^{(m)} \cdot \mathbf{x} + \omega^{(m)} \cdot t) + \Gamma x_2 \delta_{i1} \tag{2.18}$$

where $\chi^{(m)}$ is the new wavenumber after the distortion by the mean flow shear, $S = \Gamma t$ is the total shear by the mean flow, and $b_i^{(m)}(S)$ is the amplitude of the m-th random mode after the rapid shearing.

The scheme developed in Chen et al. (1995) is employed here to search for particle collisions. Detailed description on the collision algorithm is given in Chapter 2. Periodic boundary conditions are employed for both turbulent flow and particle motion. A number of particles (N_p) are randomly introduced in the flow field of volume π^3. The average collision velocity is obtained based on all the collision events for whole time period and all turbulence realizations.

As discussed in Chapter 2, four different post-collision treatments will give different collision rate and it is not clear which treatment is the best. In the study throughut this chapter, the 'THROW AWAY' scheme is implemented. However, an extremely low particle volume concentration is used. The initial particle volume concentration is chosen carefully so that the average number of collisions in each turbulence realization is less than 1 . The post-collision treatment thus has little practical effect on the collision statistics. A large number of turbulence realizations are used to obtain sufficient ensemble average. A subsequent cumulative time average smoothes out statistical noise in the collision rate.

3.4 Results and Discussions

3.4.1 Comparison with Simulation Results in a Laminar Shear Flow

In an earlier paper dealing with particle collision a laminar shear flow (Hu & Mei, 1998), comparison for the collision kernel, $\frac{4}{3}\Gamma R^3$, based on Smoluchowski's prediction and the direct numerical simulation was presented; excellent agreement was obtained. To confirm the present analyses in the laminar shear flow, we compare the collision velocity given by equations (3.32-3.33) with that based on the direct numerical simulations. Zero inertial particles of radius 0.009, 0.0125 and 0.02, respectively, are introduced into a cubic box with length L_x=2, L_y=2.0, and L_x=2.0, with the restriction $0.1<y_p<1.9$. A uniform shear flow with a shear rate Γ=1.0 is imposed and the flow velocity field is given by $v=(u, v, w) = (\Gamma y, 0, 0)$. Periodic boundary conditions are employed in the streamwise and spanwise directions. Particles near $y=0.1$ and $y=1.9$ have less collisions because there are no particles in regions of $y<0.1$ and $y>1.9$ in the simulation. A correction due to this boundary effect (Wang et al. 1997) was needed for the collision rate (Hu & Mei, 1998). However, this boundary correction has little effect on the collision velocity since the decrease in the collision kernel affects both the numerator and denominator in equation (3.25). Three hundred time steps with a step size $\Delta t=0.01$ are used to advance particles and a total of 40 realizations were employed to further increase the statistical accuracy. Ten thousand particles are used for $r=0.009$, 0.0125 while four thousand particles are used for larger size with $r=0.02$. Table 3.1 shows the comparisons for both $<-w_r>$ and $<w_r^2>$. Since $<w_r^2>$ is the second order moment of w_r, excellent agreement for these two moments indicates that the basis of the present formulation is sound. It is worth noting that a naive, Eulerian-based estimation of the average collision velocity based on the incoming particle flux, $\frac{4}{3}\Gamma R^3 n_i$, and the available collision area, $2\pi R^2$, would lead an erroneous value of $\frac{2}{3\pi}\Gamma R$ instead of $\frac{\pi}{10}\Gamma R$ for $<-w_r>$.

Table 3.1 Comparison of the collision velocity among monosized particles between prediction and direct numerical simulation in laminar shear flow.

Particle radius	$<-w_r>$ simulation	$<-w_r>$ prediction	$<w_r^2>$ simulation	$<w_r^2>$ prediction
0.009	5.6421×10^{-3}	5.6549×10^{-3}	3.7018×10^{-5}	3.7029×10^{-5}
0.0125	7.8638×10^{-3}	7.8540×10^{-3}	7.1529×10^{-5}	7.1429×10^{-5}
0.02	1.2425×10^{-2}	1.2566×10^{-3}	1.8012×10^{-4}	1.8286×10^{-4}

In a laminar shear flow, w_r=-$u_x$cosθ and the collision angle θ_c between the collision velocity **w** and the axis connecting the center of colliding particle pair, $\pi/2 \le \theta_c \le \pi$, happens to equal to θ as shown in figure 3.1. In the simulation, θ_c can be easily evaluated so that the pdf for θ_c is readily obtained. Since $(-w_r)_{w_r<0}\,\sin\theta d\theta d\phi$ is proportional to the probability of the particle striking the target surface at (θ, ϕ) with a solid angle dω=dθdϕ, it is readily seen that

$$\begin{aligned}(-w_r)dA &= -\Gamma R^3 \sin^2\theta\cos\theta\,\cos\phi\, d\theta d\phi && \text{for } (\theta,\phi)\in\Omega,\\ &= 0 && \text{elsewhere} \qquad (3.35)\end{aligned}$$

where Ω is the region defined by $(\frac{\pi}{2} \le \theta \le \pi,\ -\frac{\pi}{2} \le \phi \le \frac{\pi}{2})$ and $(0 \le \theta \le \frac{\pi}{2},\ \frac{\pi}{2} \le \phi \le \frac{3\pi}{2})$ in which $w_r \le 0$. Interpreting $\sin^2\theta\cos\theta\sin\phi$ as proportional to the probability density function of incoming particles striking the target particle near (θ, ϕ), further integrating over ϕ from 0 to 2π, treating $0 \le \theta \le \pi/2$ as the same as $\pi/2 \le \theta \le \pi$ due to symmetry, and using appropriate normalization, one obtains the pdf for the collision angle θc

$$\begin{aligned}p(\theta c) &= -B \sin^2\theta_c\cos\theta_c && \text{for } \pi \le \theta \le \pi/2\\ &= 0 && \text{for } 0 \le \theta \le \pi/2 \qquad (3.36)\end{aligned}$$

where B is a normalizing factor which is 3 for θ_c in radian and π/60 for θ_c in degree. The average angle is $<\theta c> = \int_{\pi/2}^{\pi} \theta c\, pdf(\theta c) d\theta c$ = 2.237 radian or 128.17°. The numerical simulation gives <θc> = 128.13°. Figure 3.4 compares the pdf's based on the above prediction and the direct numerical simulation using ten thousand particles of radius 0.009 over 40 realizations of initial particle positions. Excellent agreement is observed for the whole region $\pi/2 \le \theta_c \le \pi$. The present theoretical framework is thus validated in the laminar shear flow.

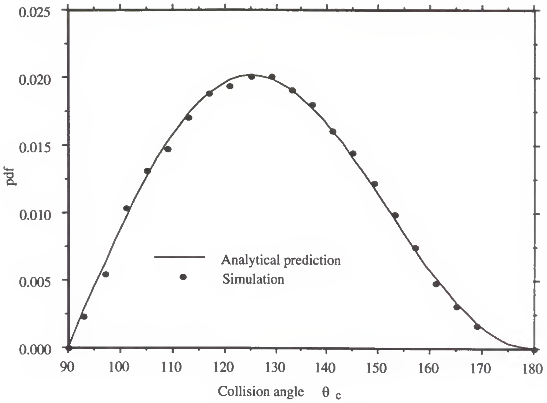

Figure 3.4 Comparison of the pdf's for the collision angles θ_c between the theory and the simulation in a laminar shear flow.

3.4.2 Collision Rate and Velocity in a Gaussian, Isotropic Turbulence

For particle collision in isotropic turbulence which is represented using equation (2.6), the dimensionless collision kernel

$$\alpha_{11}^{*} = \frac{\alpha_{11}}{R^3(\varepsilon/\nu)^{1/2}} = \frac{<e_{\tilde{x}}\mathcal{H}(\zeta)>}{(\varepsilon/\nu)^{1/2}} \tag{3.37}$$

is evaluated using N_R=500 realizations. The dissipation rate ε is based on the ensemble average of the same N_R realizations. In each realization, $e_{\tilde{x}}\ \mathcal{H}(\zeta)$ and ε/ν are computed in the flow field with 654 statistically independent data. It is found that α_{11}^{*} varies slightly with the number of the Fourier modes, N_k, used in the turbulence representation. Furthermore, it weakly depends on the power μ in equation (2.10) with which the random wavenumber is chosen. Figure 3.5 shows the variation of α_{11}^* as N_k increases from 100 to 4096 for μ=1.2 and 1.4 for $\bar{\eta}_0$= 0.05 (Re_λ=53.8). The result seems to converge after N_k=2048; $\alpha_{11}^*(\mu=1.2)$ converges to 1.2935 while $\alpha_{11}^*(\mu=1.4)$ converges to 1.2945 with a difference less than 0.1%. They are both very close to 1.2944, the value predicted by ST. It is worth commenting that due to the rapid decrease of the energy spectrum E(k) in the high k range, not all wavenumbers that are randomly generated need to be used in equation (2.10). For those high wavenumber modes that correspond to very small amplitudes, they can be simply neglected without compromising the accuracy. Thus the effective number of the random modes is smaller than the specified N_k. From the simulations, the effective number of the modes for μ=1.4 is roughly three times that for μ=1.2 for the same N_k. Hence the fact that it takes larger values of N_k for μ=1.2 than for μ=1.4 to get a converged result is not surprising. It is also interesting to note that, using N_k=1024 and μ=1.2, a higher value of Re_λ (=124.4 using $\bar{\eta}_0$=0.01) gives α_{11}^* =1.2899 as opposed to α_{11}^* =1.2912 at Re_λ=53.8. This clearly shows that shape of the energy spectrum E(k) in isotropic turbulence has little effect on α_{11}^*. With N_k=200 and μ=1.2, α_{11}^* =1.2756 which is only 1.45% less than the converged result. Thus in the following direct numerical simulation for particle collision, N_k=200 and μ=1.2 will be used.

To validate the present analyses, direct numerical simulations of particle collision in isotropic turbulence are performed. The turbulence in the periodic box of length π has the following characteristics: root-mean-squared turbulence velocity u_0=1.0, integral length scale L_{11}=0.594, Taylor micro length scale λ=0.277, Kolmogorov length scale η=0.023, Kolmogorov time scale $\tau_k=(\nu/\varepsilon)^{1/2}$=0.073, and Re_λ=40.1. With the modified Fourier modes in the periodic box, the dimensionless collision kernel based on the prediction is α_{11}^* =1.2711 as opposed to α_{11}^* =1.2756 without the modification of the wavenumbers. Initially, five hundred particles of radius r=0.005 (r/η=0.217) are randomly distributed in the box of volume π^3 with a particle volume concentration of

8.44×10^{-6}. These inertialess particles are advanced using local fluid velocity. A total time period of T=6 (i.e. $T/\tau_k=82.2$) is simulated with time step $\Delta t=0.01$. The average number of collisions within the entire period of the simulation $0<t<T=6$ in each realization is about $0.4271<1$ based on our new expression of the collision rate in §6.2. To obtain a reliable statistics, a total of 10,000 realizations is used to generate an estimated collision pairs $N_C=4271$. Figure 3.6 (a) shows the simulation result for α_{11}^* in $0\leq t/\tau_k\leq 82.2$ and the predicted value of 1.2711. There is a significant noise in the numerical simulation data due to the small number of collisions within each time step despite the fact that 10,000 realizations have been used. A cumulative average is applied to reduce the noise. Figure 3.6 (b) shows the cumulative time average of α_{11}^* from the simulation. The direct numerical simulation is less than the predicted value (1.2711) by about 2.5%. This difference may be caused by a small effect of particle size, since the theoretical predictions are expected to be accurate only in the small size limit, i.e. $r/\eta<<1$, while the particle size in numerical simulation is $r/\eta=0.217$. The effect of finite particle size on the collision rate will be explored in Chapter 6. The agreement for α_{11}^* between the simulation and the prediction is quite good.

Table 3.2 shows the results of the prediction and the numerical simulation for the two moments of particle collision velocity, $<-w_r>$ and $<w_r^2>$, in isotropic turbulence. The predicted values are based on $\mu=1.2$ and $N_k=200$ in the periodic box with $N_R=400$ realizations. The particle sizes are r/η = 0.2175 and 0.4875, respectively. Satisfactory agreements are obtained. On the other hand, ST (1956) gave an expression, equation (3.9), for the Eulerian-based average particle radial collision velocity. Using that expression, one would obtain $\frac{<-w_r>}{R(\varepsilon/\nu)^{1/2}}$ = 0.206. The present prediction for the periodic domain with $N_R=400$, after ensemble average, gives a value of 0.328 for this dimensionless radial collision velocity which agrees rather well with the direct numerical simulation show in Table 2. Since the direct numerical simulation is based on the tracking of particle trajectories, the probability-based prediction for $<-w_r>$ is consistent with the Lagrangian approach. The Eulerian-based approach for $\langle -w_r \rangle$ does not take into account the bias of the collision probability toward the high values of $-w_r$; hence it gives a lower value for $\langle -w_r \rangle$.

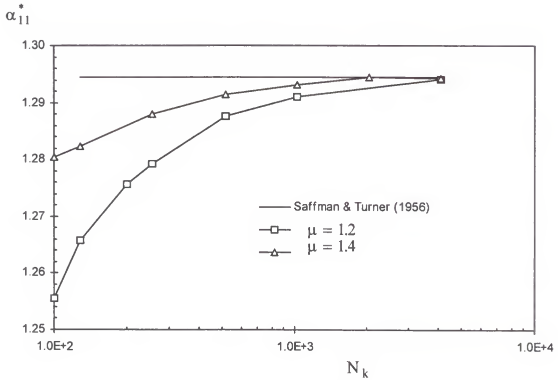

Figure 3.5 Convergence of α_{11}^* as $N_k \rightarrow 8$.

Table 3.2 Comparison of the collision velocity among monosized particles between prediction and direct numerical simulation in Gaussian, isotropic turbulence.

Particle radius (r/η)	$\langle -w_r \rangle$ simulation	$\langle -w_r \rangle$ prediction	$\langle w_r^2 \rangle$ simulation	$\langle w_r^2 \rangle$ prediction
0.217	4.5430×10^{-2}	4.5611×10^{-2}	2.7356×10^{-3}	2.7296×10^{-3}
0.4875	1.0093×10^{-1}	1.0040×10^{-1}	1.3405×10^{-2}	1.3224×10^{-2}

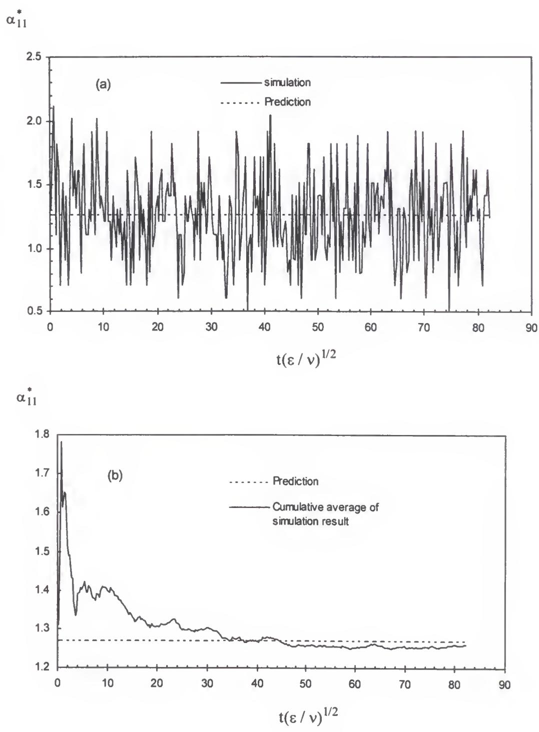

Figure 3.6 Particle collision kernel α_{11}^{*} from direct numerical simulation in Isotropic turbulence. (a) Variation of the ensemble average. (b) Cumulative time average.

3.4.3 Collision in a Rapidly Sheared Homogeneous Turbulence

The statistics of the turbulence, such as four non-zero components of the Reynolds stress tensor, generated using RDT and the random Fourier modes was first checked against the analytical values at short times ($\Gamma t \ll 1$) given by RDT (Townsend, 1976, p.84) to ensure the correct implementations. It was found through simulation that the development of the sheared turbulence with time does not depend on the Reynolds number, Re_λ, of the initial state or the energy spectrum at $t=0$. The turbulence part of the flow in the RDT is determined by the total shear $S=\Gamma t$. The complete flow field, sheared turbulence plus the mean shear flow, thus depends on two parameters: Γ and $S=\Gamma t$. Since the collision rate depends on the spatial structure of the turbulence while the turbulence structure becomes increasingly anisotropic as the total shear S increases, finding an appropriate representation of the collision rate in the homogeneous turbulent shear flow is not trivial.

To develop a better understanding on the dependence of the collision rate on the turbulent flow, it is instructive to examine the collision rate due to the sheared turbulence but without the contribution from the mean shear Γ; this part of the collision kernel will be denoted as $\overline{\alpha}_{11}$. Another word, $\overline{\alpha}_{11}$ is evaluated using the flow field given by equation (2.18) but without the last term $\Gamma x_2 \delta_{i1}$ which is deterministic. Following the definition for α_{11}^* in the isotropic turbulence case, we use the dissipation rate $(\varepsilon/\nu)^{1/2}$, which increases with S, as the turbulence characteristic shear rate to normalize $\overline{\alpha}_{11}$,

$$\bar{\alpha}_{11}^* = \frac{\bar{\alpha}_{11}}{R^3(\varepsilon/\nu)^{1/2}} \qquad \textit{(without contribution from mean shear } \Gamma\textit{)}. \qquad (3.38)$$

It is easily seen that $\bar{\alpha}_{11}^*$ depends on the total shear $S=\Gamma t$ only. Figure 3.7 (a) shows the variation of $\bar{\alpha}_{11}^*$ on S. In the high S limit, the simulation results suggest that $\bar{\alpha}_{11}^*$ approach a constant of 1.1676 in the form of

$$\bar{\alpha}_{11}^{*} \sim 1.1676 + 0.659/S \qquad \text{for } S>10. \qquad (3.39)$$

In this rage of $0 \le S \le 50$ turbulence goes from isotropic to strongly anisotropic state. The turbulence intensity becomes dominated by the longitudinal component in the x_1-direction. Based on RDT prediction which neglects the nonlinear interaction among different scales, the longitudinal component of the turbulence makes up 92.7% of the total kinetic energy at $S=\Gamma t=20$. The anisotropy invariant II_b reaches a value of -0.25 at S=20. At such large values of total shear, S, the RDT results may become a little inaccurate in comparison with DNS result. However, for the present work, since the RDT-based turbulence is strongly anisotropic, it serves our purpose to evaluate the effect of such anisotropy in the turbulence on particle collision rate. When the collision kernel is normalized using $(\varepsilon/\nu)^{1/2}$, the maximum difference in $\bar{\alpha}_{11}^{*}$ is only about 15% at the extreme limit of $S\rightarrow\infty$. If the isotropic result is used, $\bar{\alpha}_{11}^{*} \sim 1.2944$, only a maximum error of 10% will result from the limiting value of $\bar{\alpha}_{11}^{*}$ at very large total shear. This encouraging result will be used to develop an approximation for α_{11}^{*} in the presence of strong mean shear.

Now consideration is given to the particle collision kernel with contribution from both the turbulence part and the mean flow shear part as the flow field is given by the entire right-hand-side of equation (2.18). Figure 3.7 (b) shows α_{11}^{*} as a function of the ratio of the mean shear rate to the turbulence shear rate, $\Gamma/(\frac{\varepsilon}{\nu})^{1/2}$, for a range of shear rates. For a given Γ, $(\varepsilon/\nu)^{1/2}$ increases as t or S increases so that the abscissa mainly reflect the effect of t or S. To see the effect of mean flow shear rate, Γ is made dimensionless by the turbulence mean shear rate at t=0 in the isotropic state $(\varepsilon_0/\nu)^{1/2}$. Four values of $\Gamma/(\varepsilon_0/\nu)^{1/2}$ are used: 0.87, 2.18, 4.36, and 8.72; they correspond to the solid symbols in figure 3.7 (b). The open symbols specifically correspond to the cases when S=0 (or t=0) so that the turbulence is still isotropic. The dimensionless values of α_{11}^{*}

seem to collapse reasonably well. At large values of $\Gamma/(\frac{\varepsilon}{\nu})^{1/2}$, the curve becomes linear as the collision rate is increasingly dominated by the mean shear so that α_{11} scales linearly with Γ as Smoluchowski's theory predicts. A small degree of scattering exists for $\Gamma/(\frac{\varepsilon}{\nu})^{1/2}<2$. This is caused by the 15% maximum variation of $\bar{\alpha}_{11}^{*}$ over the whole range of total shear S, as already demonstrated in figure 3.7 (a). There are two possibilities for $\Gamma/(\frac{\varepsilon}{\nu})^{1/2} \ll 1$: i) both Γ and $S=\Gamma t$ are very small even comparing with $(\varepsilon_0/\nu)^{1/2}$ of the initial isotropic turbulence; ii) Γ is finite but $S=\Gamma t$ is large so that $(\varepsilon/\nu)^{1/2}$ become large comparing with $(\varepsilon_0/\nu)^{1/2}$. In the first case, the turbulence is closer to the isotropic state so that $\bar{\alpha}_{11}^{*}$ ~1.2944. In the second case, the turbulence is highly anisotropic and $\bar{\alpha}_{11}^{*}$ →1.1676 for very large values of S. No attempt is made to correlate $\bar{\alpha}_{11}^{*}$ with the total shear S since S is not relevant in practical applications such as in turbulent pipe flow. Using $\bar{\alpha}_{11}^{*}$ =1.2944 in the isotropic state to represent the turbulence part of the collision kernel, a simple interpolation is proposed to represent the effect of mean shear and turbulence on the collision rate,

$$\alpha_{11}^{*} \approx \frac{\alpha_{11}}{R^3(\varepsilon/\nu)^{1/2}} = \{1.2944^{2.2} + [\frac{1.3333\,\Gamma}{(\varepsilon/\nu)^{1/2}}]^{2.2}\}^{1/2.2}. \tag{3.40}$$

This interpolation is shown by the solid line in figure 3.7 (b). A satisfactory agreement can be observed. It is also worth commenting that when Γ is normalized using the eddy turn over time, $3u_0^2/\varepsilon_0$, of the initial isotropic turbulence, the shear-rate parameter

$$\Gamma^{*} = \Gamma 3u_0^2/\varepsilon_0, \tag{3.41}$$

corresponds to Γ^{*}=36.98 and 92.45 for $\Gamma/(\varepsilon_0/\nu)^{1/2}$ =0.87 and 2.18. In a low Reynolds number turbulent channel flow, the maximum value of Γ^{*} is around 35 at a location of 10 wall units away from the wall (Kim et al. 1987). Hence, the parameters used in figure 3.7 (b) are relevant to practical situations. Although a 10% error exists for α_{11}^{*} given by (3.40), the advantage of this simple approximation is that the total shear $S=\Gamma t$ is absent and it depends only on the spatial structure of the turbulence characteristics by the scalar quantity $(\varepsilon/\nu)^{1/2}$.

Figure 3.8 shows the radial collision velocity, $\langle -w_r \rangle$, as a function of $\Gamma/(\frac{\varepsilon}{\nu})^{1/2}$, for different values of $\Gamma/(\frac{\varepsilon_0}{\nu})^{1/2}$. Similarly, the data seem to collapse approximately into one curve in the range studied. The following interpolation fits the radial collision velocity well,

$$\frac{\langle -w_r \rangle}{R(\varepsilon/\nu)^{1/2}} \approx \{0.3245^{1.7} + [\frac{\pi}{10}\,\frac{\Gamma}{(\varepsilon/\nu)^{1/2}}]^{1.7}\}^{1/1.7}. \tag{3.41}$$

For the root-mean squared radial collision velocity, $\langle w_r^2 \rangle$, the behavior is very similar to that of $\langle -w_r \rangle$. While the data is not shown here, the following interpolation, which fits the data quite well, is provided,

$$\frac{\langle w_r^2 \rangle^{1/2}}{R(\varepsilon/\nu)^{1/2}} = \{0.3681^{1.7} + [\frac{0.3381\,\Gamma}{(\varepsilon/\nu)^{1/2}}]^{1.7}\}^{1/1.7}. \tag{3.42}$$

The application of the above expressions to turbulent channel flow, which is different from the homogeneous, rapidly sheared turbulence, is yet to be tested. However, since the rapidly sheared turbulence at large total shear S considered in this work is already drastically different from the isotropic turbulence, there are reasons to expect a similar dependence of α_{11}, $\langle -w_r \rangle$, and $\langle w_r^2 \rangle$ on Γ and $(\varepsilon/\nu)^{1/2}$ in a turbulent channel flow which is of significant industrial importance.

3.5 Summary and Conclusions

A theoretical framework has been developed to evaluate the collision rate and collision velocity of small particles in *general* turbulent flows. The classical results for the collision kernels by Smoluchowski (1917) for laminar shear flow and by Saffman & Turner (1956) for isotropic turbulence are recovered. The present approach differs significantly from that of Saffman & Turner in that the ensemble average is taken after the collision rate for a given flow realization is calculated. This avoids the assumption of isotropy, as needed in Saffman & Turner, and allows for the evaluation of the collision rate in general turbulent flows. The collision velocity predicted in both laminar shear flow and isotropic turbulence agrees well with the direct numerical simulation for particle collisions. The present theory is used to evaluate the collision rate and velocity of small particles in the rapidly sheared homogeneous turbulence. It is found that the effect of the turbulence structure on the collision rate and velocity can be mainly captured by using the mean turbulent shear rate $(\varepsilon/\nu)^{1/2}$. The combined effects of the mean shear and the sheared turbulence on the collisions are elucidated. Simple interpolations are developed to evaluate the collision rate and velocity for arbitrary mean flow shear rate and turbulence mean shear rate.

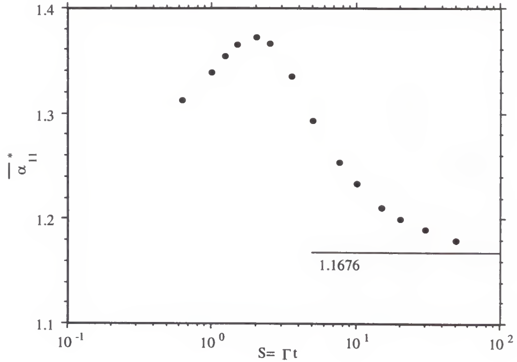

Figure 3.7 (a) Normalized particle collision kernel in a highly sheared homogeneous turbulence without contribution from the mean shear rate.

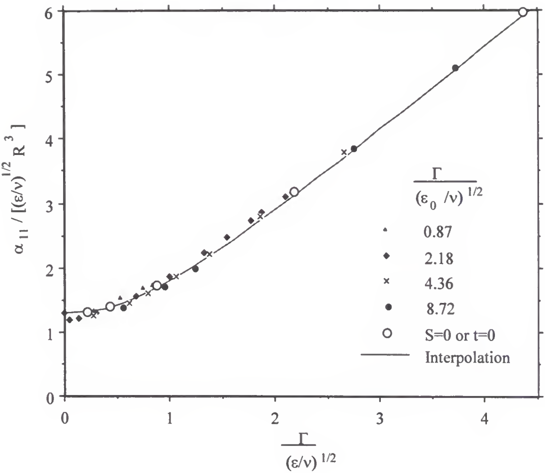

Figure 7 (b) Collision kernel in a rapidly sheared homogeneous turbulence. ε_0 denotes the dissipation rate of the isotropic state at t=0.

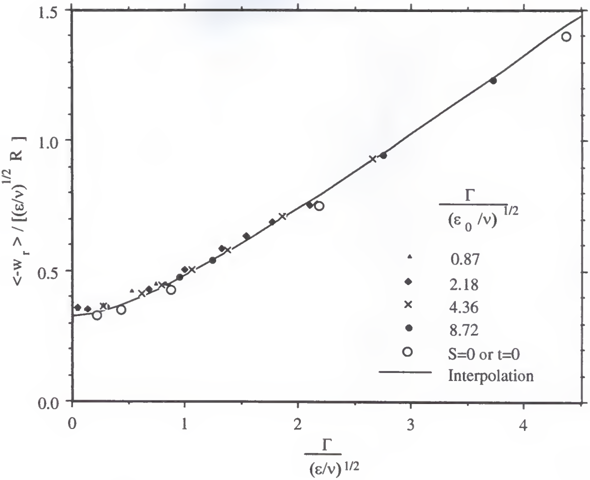

Figure 3.8 Collision velocity in a rapidly sheared homogeneous turbulence. ε_0 denotes the dissipation rate of the isotropic state at t=0.

CHAPTER 4
EFFECT OF INERTIA ON THE PARTICLE COLLISION VELOCITY AND COLLISION ANGLE IN GAUSSIAN TURBULENCE

Numerical simulation of particle collisions in isotropic, Gaussian turbulence is carried out to study the effects of particle inertia on the turbulence induced collision velocity and collision angle. An asymptotic analysis is developed to predict the effect of the small particle inertia on the collision velocity. A PDF-based method is also implemented to predict the effect of the small particle inertia on the collision velocity. The analysis predicts that the increase in the collision velocity is proportional to the terms $(\beta\tau_k)^{-1}$ and $(\beta\tau_k)^{-2}$, in which β^{-1} is the particle response time and τ_k is the Komogorov time scale. Good agreement is obtained among three different methods: the numerical simulation, asymptotic prediction, and the PDF-based method, for the collision velocity of particles with small inertia. The effects of both particle inertia and size on the collision angle have also been investigated. It is found that collision angle can be significantly affected by both inertia and size. Average collision angle and the variation of collision angle increase as the inertia increases, while the decrease in the size will also reduce both the average collision angle and the variation of collision angle.

4.1 Introduction

Particle collisions can take place through a variety of collision mechanisms. Particles may be brought together by inertial centrifugal and gravitational forces. The velocity gradient is responsible for collisions among particles in laminar shear flow and is a dominant factor for particle collisions in turbulence. Brownian motion and Van der

Waal forces can also affect the collisions. One of the common characteristics of these collision mechanisms is the ability to generate a negative relative velocity between two particles along the line connected with two particle centers. Of significance are the statistics of the relative velocity of two particles at contact (hereinafter referred as collision velocity) and the relative angle between the velocities of two particles at contact (hereinafter referred as collision angle). For solid particles, collision causes momentum exchange among particles and may influence the local and global particulate flow conditions. The suspended solid particles are produced during the manufacturing process of materials, the combustion of heavy fuel and pulverized coal. The collisions among suspended particles will greatly affect the properties of particulate flow and thus influence the performance of the systems. Adhesion may occur when two colliding solid particles have small collision velocity, while large collision velocity will produce large restitutive rebounce velocities for the colliding particles and may overcome the bonding force determined by cohesive surface energy. The collision also affects the angular momentum of particles. Tangential velocity components will be imposed to the colliding particles if the collision angle θ_{12} is not equal to zero. The particle rotation will be either enhanced or reduced depending on the collision angle θ_{12}, which determines the orientation of the particle tangential velocities upon collision. Gunaraj et al. (1997) peroformed experiments measuring the collision angle θ_{12} between heavy particles (silica sand particles with 1000-1500 μm in diameter) in turbulent channel flow.

The collision velocity is also a critical quantity in determining the collision kernel and collision rate. In uniform shear flow, Smolochowski (1917) integrated the volume flow rate using collision velocity along the spherical surface of collision radius R ($=r_i + r_j$, where r_i and r_j are the radii of collision pair respectively) and obtained collision kernel for uniform shear flow. In turbulent flow, particle collisions are affected by local turbulence fluctuations. In the absence of any other force creating relative motion between particles, these local fluctuations entirely control relative velocity distribution which determines the collision kernel. In most of the previous theories, the collision kernel in a particle-laden system is linearly related to the collision velocity, the first moment of the relative velocity distribution of colliding particles. Thus the scale and form of these particle relative velocity distributions directly determine the collision rate. The fact that the collision rate and collision kernel in previous studies are all proportional to the collision velocity explains the critical importance of the prediction of collision velocity (Saffman & Turner 1956, Williams & Crane 1983, Kruis & Kusters 1996, et al).

The particle collision has been studied in two different ways. One is based on Eulerian method, which is favorable to theoretical prediction and was followed by previous studies on the theoretical evaluation of both collision velocity and collision kernel. The other is to use Lagrangian tracking in direct numerical simulation of particle collisions. For inertialess particles in both uniform laminar shear flow and isotropic turbulence, the collection of collision velocities using Lagrangian method shows a biased average in favor of those regions where w_r is high, as shown clearly in Chapter 3. Saffman & Turner (1956) obtained the collision velocity using average integration on the spherical collision surface by Eulerian method without considering the influence of the biased average. Although their formulation correctly predicts the velocity correlation between two points for turbulent flow, it has been incorrectly interpreted as the collision velocity upon collisions. The effect of particle inertia on the collision velocity was recently studied also by Sundaram and Collins (1997). They used two statistical variables: g(R), the particle radial distribution function at contact, and P(**w**/R), the conditional relative velocity probability density function at contact, where **w** is the relative velocity of two particles at contact. It is noted that in Sundaram and Collins' work, in additional to the assumption of the exponential form for P(**w**/R), the g(R) was evaluated based on their numerical extrapolation form for distances smaller than the first numerically evaluated point. However, the usefullness of g(R) and P(**w**/R) is rather questionable.

In this work, we study the effect of particle inertia on increasing particle collision velocity and collision angle by carrying out numerical simulation of particle collisions in an isotropic, Gaussian turbulence, and developing an asymptotic analysis to predict the effect of small particle inertia on the collision velocity based on Lagrangian description. An integration method is also implemented to predict the effect of the small particle inertia on the collision velocity. The increase in the particle collision velocity due to inertia predicted by both the asymptotic analysis and integration method is in agreement with the numerical simulation results. The analysis predicts that the increase in the collision velocity contains terms that are proportional to $(\beta\tau_k)^{-1}$ and $(\beta\tau_k)^{-2}$. Good agreement is obtained by the numerical simulation, asymptotic prediction and the integration method for the collision velocity of particles with small inertia. The effects of particle inertia and size on the collision angle have also been investigated. It is found that collision angle are significantly affected by both inertia and size. Average collision angle and the variation of collision angle increase as the inertia increases, while the decease in the size will reduce both the average collision angle and the variation of collision angle.

4.2 Saffman & Turner's Analysis

In Saffman & Turner's (1956) prediction of the collision rate among inertialess particles, the volume flow rate of particles towards a target particle was evaluated by an integration, $<\int_{w_r<0} -w_r dS>$, where w_r is the radial component of the relative velocity. The integration was carried out over the entire spherical surface of radius R, as shown in figure 4.1. Because of the continuity of fluid flow,

$$
\begin{aligned}
<\int_{w_r<0} -w_r dS> &= <\int_{\text{entire sphere}} |w_r| dS> \\
&= \int_{\text{entire sphere}} <|w_r|> dS. \qquad (4.1)
\end{aligned}
$$

For isotropic turbulence, which is true at small scales for anisotropic turbulence, the above becomes

$$<\int_{w_r<0} -w_r dS> = 2\pi R^2 <|w_x|> \qquad (4.2)$$

where x is the local coordinate parallel to the line connecting the centers of the colliding particles as shown in figure 4.2 and < > denotes ensemble averaging.

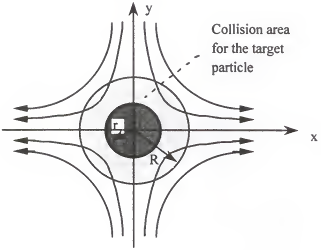

Figure 4.1 Sketch of particle collision scheme

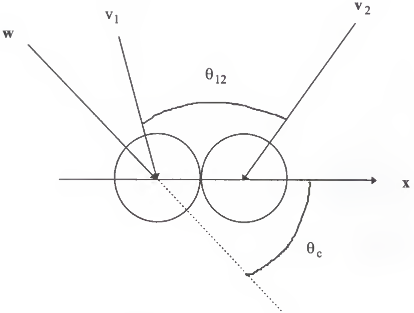

$$\mathbf{w} = \mathbf{v}_1 - \mathbf{v}_2$$

$$w_x = v_{1x} - v_{2x}$$

Figure 4.2 Sketch of particle collision velocity and collision angles (θ_{12} & θ_c). The separation distance is $x_2 - x_1 = \pm R = \pm(r_1 + r_2)$.

In the limit of zero particle inertia, particle velocity **v** follows the fluid velocity **u** very well so that the radial component of relative velocity $\mathbf{w} = \mathbf{v}_1 - \mathbf{v}_2$ upon collision is

$$|w_x| \sim |u_{1x} - u_{2x}| \sim R\left|\frac{\partial u}{\partial x}\right| = R\left(\frac{2}{15\pi}\frac{\varepsilon}{\nu}\right)^{1/2} \tag{4.3}$$

and
$$< w_x^2 > = 5\ R^2 < \left(\frac{\partial u}{\partial x}\right)^2 > = \frac{1}{15}R^2\frac{\varepsilon}{\nu} \tag{4.4}$$

where w_x is the collision velocity.

For particles with inertia, the volume flow rate of particles to a target particle was expressed as $\iiint_{\text{entire sphere}} |\mathbf{w}|\ P(\mathbf{w})d\mathbf{w}$, where $P(\mathbf{w})$ is the probability density function (PDF) of **w** and contains the effects of the spatial variations of velocity in the fluid, the turbulent accelerations due to the relative motion with the turbulence, and gravity. The volume flow rate can be integrated assuming $P(\mathbf{w})$ to be a normal distribution function. For monodisperse particles,

$$\iiint_{\text{entire sphere}} |\mathbf{w}|\ P(\mathbf{w})d\mathbf{w} = \frac{2}{3}R^3\left(\frac{2\pi\varepsilon}{\nu}\right)^{1/2}. \tag{4.5}$$

Compared with the equation (4.2), the equivalent collision velocity based on equation (4.5) can be evaluated

$$|w_x| \sim \frac{2}{3}R^3\left(\frac{2\pi\varepsilon}{\nu}\right)^{1/2}/(2\pi R^2) = \frac{2}{3}R\left(\frac{\varepsilon}{2\pi\nu}\right)^{1/2} \tag{4.6}$$

and
$$< w_x^2 > \sim \frac{1}{9}R^2\frac{\varepsilon}{\nu}. \tag{4.7}$$

It is noted that equation (4.7) is independent of the inertia parameter β. For the small inertia limit $\beta\rightarrow\infty$, comparing equations (4.6) & (4.7) with equations (4.3) & (4.4), an inconsistency that (4.6) & (4.7) can not recover (4.3) & (4.4) occurs, which is physically incorrect.

4.3 Present Analysis

4.3.1 Asymptotic Analysis

To understand and predict the effect of inertia on the collision velocity w_x, it is assumed that the particle size is much less than the Taylor micro-length scale, and the gravitational force is negligible. For simplicity it is assumed that turbulence is isotropic and Gaussian. The particle dynamic equation in the absence of (or weak) gravity is

$$\frac{d\mathbf{v}}{dt} = \beta(\mathbf{u} - \mathbf{v}). \tag{4.8}$$

The above can be written as

$$\mathbf{v} = \mathbf{u} - \frac{1}{\beta}\frac{d\mathbf{v}}{dt}. \tag{4.9}$$

For large values of β, repeatedly substituting the left hand side into the right hand side gives

$$\begin{aligned} \mathbf{v} &= \mathbf{u} - \frac{1}{\beta}\frac{d\mathbf{u}}{dt} + \frac{1}{\beta^2}\frac{d^2\mathbf{v}}{dt^2} = \mathbf{u} - \frac{1}{\beta}\frac{D\mathbf{u}}{Dt} + \frac{1}{\beta}(\mathbf{u}-\mathbf{v})\cdot\nabla\mathbf{u} + \frac{1}{\beta^2}\frac{d^2\mathbf{v}}{dt^2} \\ &\sim \mathbf{u} - \frac{1}{\beta}\frac{D\mathbf{u}}{Dt} + O\left(\frac{1}{\beta^2}\right). \end{aligned} \tag{4.10}$$

The variance of $w_x = v_{1x} - v_{2x}$ in which particle 1 and particle 2 are separated by a distance of $|x_2 - x_1| = R$ is

$$\begin{aligned} \mathrm{var}(w_x) &\sim \mathrm{var}\left(u_{1x} - u_{2x} - \frac{1}{\beta_1}\frac{Du_{1x}}{Dt} + \frac{1}{\beta_2}\frac{Du_{2x}}{Dt}\right) \\ &= <(u_{1x} - u_{2x})^2>|_{x_2-x_1=\pm R} + <\left(\frac{1}{\beta_1}\frac{Du_{1x}}{Dt} - \frac{1}{\beta_2}\frac{Du_{2x}}{Dt}\right)^2>|_{x_2-x_1=\pm R} \\ &\quad - 2<(u_{1x} - u_{2x})\left(\frac{1}{\beta_1}\frac{Du_{1x}}{Dt} - \frac{1}{\beta_2}\frac{Du_{2x}}{Dt}\right)>|_{x_2-x_1=\pm R} \\ &= \text{term I} + \text{term II} + \text{term III}. \end{aligned} \tag{4.11}$$

The first term can be expanded as

$$\text{term I} = <(u_{1x} - u_{2x})^2>|_{x_2 - x_1 = \pm R} = <u_{1x}^2> + <u_{2x}^2> - 2<u_{1x}u_{2x}>|_{x_2 - x_1 = \pm R}$$

$$= 2<u_x^2> - 2<u_x^2>f(r{=}R) = 2\,u_0^2\,[1-f(R)] \qquad (4.12)$$

where u_0^2 is the mean square intensity of turbulence and f(r) is the standard longitudinal velocity correlation coefficient. If the particle size is much less than the Taylor micro-length scale λ, the above can be simplified to

$$\text{term I} = <(u_{1x} - u_{2x})^2>|_{x_2 - x_1 = \pm R} \sim 2\,u_0^2\,\frac{1}{2}\left(\frac{R}{\lambda}\right)^2 = \frac{1}{15}R^2\frac{\varepsilon}{\nu}$$

$$\text{for} \quad R \ll \lambda. \qquad (4.13)$$

Term II in equation (4.11) can be similarly handled,

$$\text{term II} = <\left(\frac{1}{\beta_1}\frac{Du_{1x}}{Dt} - \frac{1}{\beta_2}\frac{Du_{2x}}{Dt}\right)^2>|_{x_2 - x_1 = \pm R} = \frac{1}{\beta_1^2}<\left(\frac{Du_{1x}}{Dt}\right)^2> + \frac{1}{\beta_2^2}<\left(\frac{Du_{2x}}{Dt}\right)^2>$$

$$- 2\frac{1}{\beta_1\beta_2}<\frac{Du_{1x}}{Dt}\frac{Du_{2x}}{Dt}>|_{x_2 - x_1 = \pm R} \qquad (4.14)$$

where $<\frac{Du_{1x}}{Dt}\frac{Du_{2x}}{Dt}>|_{x_2 - x_1 = \pm R}$ is the spatial correlation of $\frac{Du_x}{Dt}$ in the x-direction with a separation distance of R. Noting that var($\frac{Du_{1x}}{Dt}$) = var($\frac{Du_{2x}}{Dt}$) and expanding the correlation for small R, we obtain

$$<\frac{Du_{1x}}{Dt}\frac{Du_{2x}}{Dt}>|_{x_2 - x_1 = \pm R} \sim <\left(\frac{Du_x}{Dt}\right)^2>\left[1 + \frac{R^2}{2}\frac{\partial^2 f_D(0)}{\partial x^2} + \ldots\right] \qquad (4.15)$$

where f_D is the correlation coefficient of $\frac{Du_x}{Dt}$. Defining the micro length scale of the fluid acceleration $\frac{Du_x}{Dt}$ as

$$\frac{1}{\lambda_D^2} = -\frac{1}{2}\frac{\partial^2 f_D(0)}{\partial x^2} \qquad (4.16)$$

term II can be expressed as

$$\text{term II} \sim <\left(\frac{Du_x}{Dt}\right)^2>\left(\frac{1}{\beta_1^2} + \frac{1}{\beta_2^2}\right) - \frac{2}{\beta_1\beta_2}<\left(\frac{Du_x}{Dt}\right)^2>\left(1 - \frac{R^2}{\lambda_D^2}\right)$$

$$\sim <(\frac{Du_x}{Dt})^2>(\frac{1}{\beta_1} - \frac{1}{\beta_2})^2 + \frac{2}{\beta_1\beta_2}<(\frac{Du_x}{Dt})^2>\frac{R^2}{\lambda_D^2} \qquad \text{for } R<<\lambda_D. \qquad (4.17)$$

Finally, equations (4.13) & (4.17) lead to

$$\mathrm{var}(w_x) \sim \frac{1}{15}R^2\frac{\varepsilon}{\nu} + <(\frac{Du_x}{Dt})^2>(\frac{1}{\beta_1} - \frac{1}{\beta_2})^2 + \frac{2}{\beta_1\beta_2}<(\frac{Du_x}{Dt})^2>\frac{R^2}{\lambda_D^2}$$

$$- 2 <(u_{1x} - u_{2x})(\frac{1}{\beta_1}\frac{Du_{1x}}{Dt} - \frac{1}{\beta_2}\frac{Du_{2x}}{Dt})>. \qquad (4.18)$$

For the like particles, $\beta_1 = \beta_2 = \beta$,

$$\mathrm{var}(w_x) \sim \underbrace{\frac{1}{15}R^2\frac{\varepsilon}{\nu}}_{\text{(i)}} \underbrace{- \frac{2}{\beta} <(u_{1x} - u_{2x})(\frac{Du_{1x}}{Dt} - \frac{Du_{2x}}{Dt})>}_{\text{(ii)}} + \underbrace{\frac{2}{\beta^2}<(\frac{Du_x}{Dt})^2>\frac{R^2}{\lambda_D^2}}_{\text{(iii)}},$$

(4.19)

where term (i) is the mean-squared collision velocity for inertialess particles, terms (ii) & (iii) are contributed by the inertia. The net increase of the mean-squared collision velocity due to the inertia can be expressed as

$$<\Delta w_x^2> \sim \underbrace{- \frac{2}{\beta} <(u_{1x} - u_{2x})(\frac{Du_{1x}}{Dt} - \frac{Du_{2x}}{Dt})>}_{\text{(ii)}} + \underbrace{\frac{2}{\beta^2}<(\frac{Du_x}{Dt})^2>\frac{R^2}{\lambda_D^2}}_{\text{(iii)}}. \qquad (4.20)$$

It is noted that term (ii) represents the first-order effect of the inertia and term (iii) contains the second-order effect of the inertia. The present prediction, equations (4.19) & (4.20), differs from the equation (4.7) in two aspects. First, the collision velocity in the limit $\beta \to \infty$ is consistent with the equation (4.4). Second, the present analysis includes two additional terms in the effect of inertia, as seen from equations (4.19) & (4.20) when $\beta_1 = \beta_2$. The effect of inertia does not vanish when $\beta_1 = \beta_2$ while it does in Saffman & Turner's analysis. It should be mentioned that $<\Delta w_x^2>$ in (4.20) is computed based on Lagrangian tracking of all colliding particles.

4.3.2 PDF-Based Method

For inertialess particles, the collision velocity can be evaluated by the direct integration (Mei & Hu 1998) in both uniform shear flow and turbulent flows.

$$< w_r >= \frac{\int_{w_r<0} w_r(-w_r)dS}{\int_{w_r<0}(-w_r)dS} \tag{4.21}$$

and

$$< w_r^2 >= \frac{\int_{w_r<0} w_r^2(-w_r)dS}{\int_{w_r<0}(-w_r)dS} \tag{4.22}$$

where $(-w_r)dS$ in the numerator can be interpreted as proportional to the probability of a particle striking the target surface over an area dS. The denominator is the normalizing factor for the probability. The product, $w_r(-w_r)$, clearly indicates that $<w_r>$ is a biased average in favor of these regions where $(-w_r)$ is high.

Equations (4.21) & (4.22) may be extended for particles with inertia. For small inertia, as shown in §4.3.1, the particle velocity to the first order β is

$$\mathbf{v} = \mathbf{u} - \frac{1}{\beta}\frac{D\mathbf{u}}{Dt}. \tag{4.23}$$

The collision velocity may be expressed as

$$w_r = w_x = v_{1x} - v_{2x} = u_{1x} - u_{2x} - \frac{1}{\beta_1}\frac{Du_{1x}}{Dt} + \frac{1}{\beta_2}\frac{Du_{2x}}{Dt} \tag{4.24}$$

$$\int_{w_r<0} -w_r dS = \int_{w_r<0} -(u_{1x} - u_{2x} - \frac{1}{\beta_1}\frac{Du_{1x}}{Dt} + \frac{1}{\beta_2}\frac{Du_{2x}}{Dt})dS. \tag{4.25}$$

For monodisperse particles, $\beta_1 = \beta_2 = \beta$, equation (4.25) may be rewritten as

$$\int_{w_r<0} -w_r dS = \int_{w_r<0} [u_{2x} - u_{1x} + \frac{1}{\beta}(\frac{Du_{1x}}{Dt} - \frac{Du_{2x}}{Dt})]dS. \tag{4.26}$$

From the equations (4.21), (4.24) and (4.26), the collision velocity is then found

$$< w_r > = \frac{< \int_{w_r<0} -[u_{2x} - u_{1x} + \frac{1}{\beta}(\frac{Du_{1x}}{Dt} - \frac{Du_{2x}}{Dt})]^2 dS >}{< \int_{w_r<0} [u_{2x} - u_{1x} + \frac{1}{\beta}(\frac{Du_{1x}}{Dt} - \frac{Du_{2x}}{Dt})] dS >} . \quad (4.27)$$

Similarly, the mean-squared collision velocity is

$$< w_r^2 > = \frac{< \int_{w_r<0} [u_{2x} - u_{1x} + \frac{1}{\beta}(\frac{Du_{1x}}{Dt} - \frac{Du_{2x}}{Dt})]^3 dS >}{< \int_{w_r<0} [u_{2x} - u_{1x} + \frac{1}{\beta}(\frac{Du_{1x}}{Dt} - \frac{Du_{2x}}{Dt})] dS >} . \quad (4.28)$$

The integrations in right hand side of (4.28) are evaluated using Eulerian method .

4.4 Results and Discussions

The direct numerical simulations of the particle collisions in Gaussian turbulence is performed to assess present asymptotic analysis and to predict collision angle. Initially, a given number of particles are randomly distributed in the box of volume π^3. The inertial parameter $\beta\tau_k$ varies from 0.022 to ∞. The particle sizes D/η=0.435, 0.957, 1.739, 2.522, 4.348 are considered, and the corresponding initial number of particles are 24000, 10000, 5000, 3000 and 1000 respectively. The particle collision detection is turned on until all particles have reached dynamic equilibrium. The overlapping particles are eliminated to avoid the false counting of the collisions before the collision detection turned on. The particles are advanced by time step Δt=0.01. The total time steps, varying from 200 to 600 after the equilibrium state, depend on the inertia. A total of 40 realizations is used for smooth statistics.

Figure 4.3 shows the comparisons of direct numerical simulations, asymptotic analysis and PDF-based method for D/η=0.957. Very good agreement is observed among the three methods for small inertia $\beta\tau_k$>3.6, so equation (4.20) is validated for prediction of small inertia effect on the collision velocity. However, large deviation is observed for $\beta\tau_k$<3.6 since the asymptotic analysis cannot be applied for particles with large inertia.

The reason is that the first order approximation (4.23) is no longer valid when the β becomes small for particles with large inertia. The PDF results of collision velocity can be found in figures 4.4 (a) & (b). The collision velocities are all negative, because collision occurs only if the pair of particles are approaching each other. For not very large inertia, say $\beta\tau_k \geq 1$, due to the strong correlation between particle velocity and fluid velocity, the PDF curves are sharp and narrowed with a small variance and peak at almost the same location, while zero inertia curve is at highest level. The PDFs are sharper for small particle size ($D/\eta=0.957$) at $\beta\tau_k \geq 1.023$, shown in figure 4.4 (a), compared with figure 4.4 (b). However, the PDF curves become flatter and the location of the peak shifts to larger $|w_r|$ for $\beta\tau_k \leq 0.073$ due to little correlation between particle velocity and fluid velocity at large inertia.

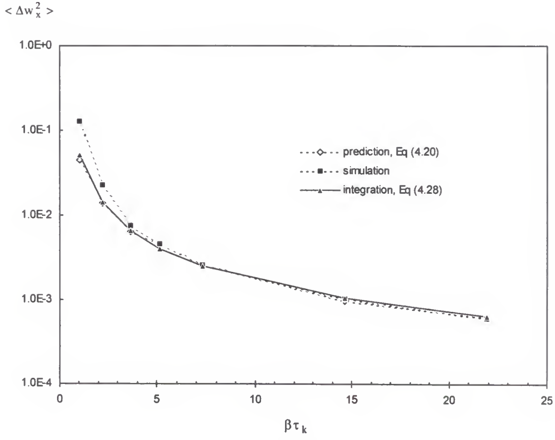

Figure 4.3 Comparison for the increased collision velocity due to the particle inertia between numerical simulation and theoretical prediction, $D/\eta=0.957$.

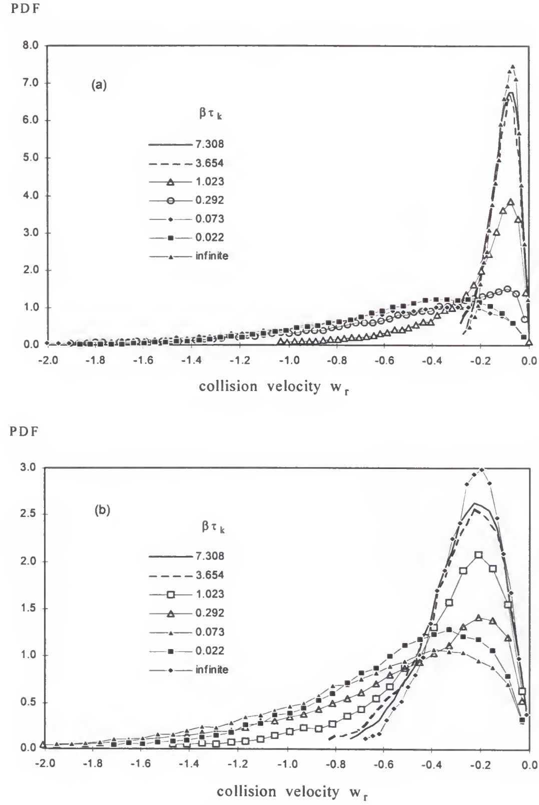

Figure 4.4 Effect of particle inertia on the probability density function of the particle collision velocity w_r. (a) $D/\eta=0.957$. (b) $D/\eta=2.522$.

The effect of particle inertia on collision angle among monodisperse particles can be found in figures 4.5 (a-c), 4.6 & 4.7. It is seen that the collision angles θ_{12} & θ_c strongly depend on the inertia. For not very large inertia, $\beta\tau_k \geq 1.023$, the mean collision angle $\bar{\theta}_{12}$ is less than 20^0 at $D/\eta=0.957$, as shown in figure 4.5 (a) & 4.6, and it is less than 30^0 at $D/\eta=2.522$, as shown in figures 4.5 (b) & 4.6. However, for very large inertia, $\beta\tau_k \leq 0.073$, the mean collision angle $\bar{\theta}_{12}$ is greater than 80^0, which reflects little biased orientation of collisions due to very weak correlation between the particles and turbulent flow. It is noted that the PDF curves for $\beta\tau_k \geq 1.023$ are much sharper and narrower than those for $\beta\tau_k \leq 0.073$ and the variation of collision angle increases as the particle inertia increases, as shown in figure 4.7. Figure 4.5 (c) shows the effect of inertia on θ_c. It is seen that the increase in inertia results in the collision angle θ_c approaching to symmetrical distribution with the mean 45^0.

The effect of particle size on the collision angle θ_{12} can be seen in figure 4.8, which clearly shows that the particle size has a significant effect on the collision angle. The average collision angle θ_{12} increases as the size increases. For $D/\eta \leq 1.739$, the maximum θ_{12} is located at somewhere between 0^0 and 10^0, and the average θ_{12} is around 10^0. However, for larger particles with large inertia, shown in figure 4.8, the collision angle θ_{12} is around 20^0, which is within the range of $14^0 \sim 32^0$ obtained from the experiments for heavy particles in a turbulent channel flow (Gunaraj et al. 1997). Since little information is reported on the turbulent channel flow, the comparison is only qualitative.

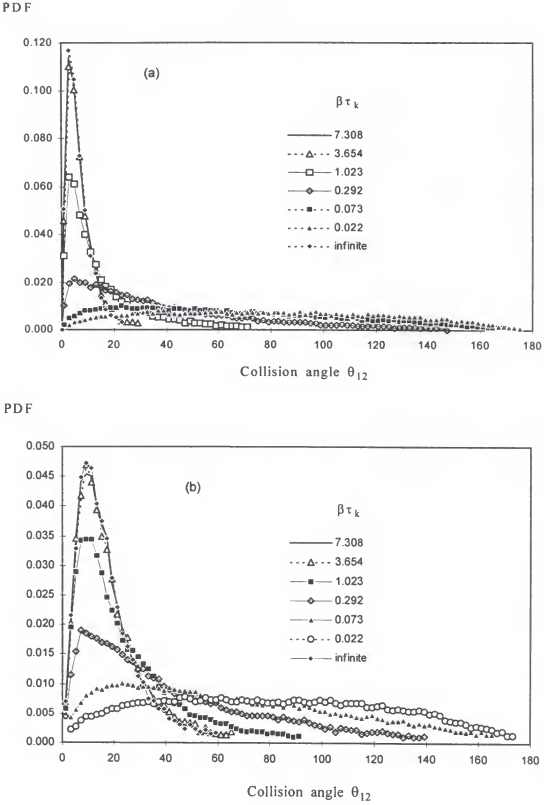

Figure 4.5 Effect of particle inertia on the probability density function of the particle collision angle θ_{12}. (a) $D/\eta=0.957$. (b) $D/\eta=2.522$.

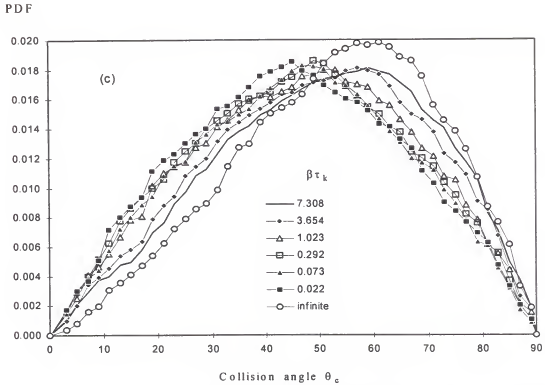

Figure 4.5 (c) Effect of particle inertia on the probability density function of the particle collision angle θ_c, $D/\eta=0.957$.

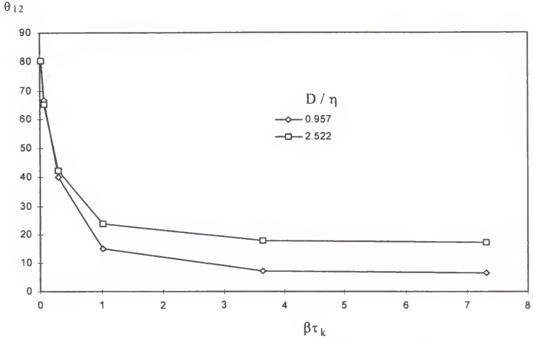

Figure 4.6 Effect of particle inertia on the mean collision angle $\overline{\theta}_{12}$ in isotropic, Gaussian turbulence.

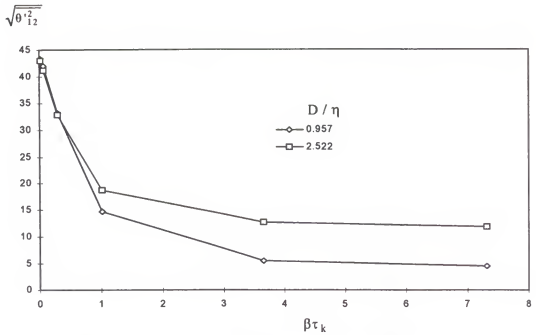

Figure 4.7 Effect of particle inertia on the standard deviation of collision angle θ_{12} in isotropic, Gaussian turbulence.

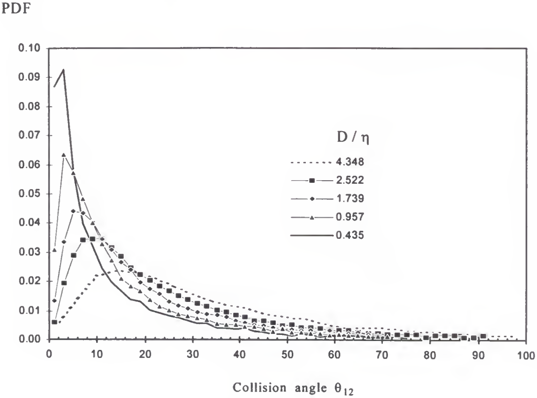

Figure 4.8 Effects of particle inertia and size on the probability density function of the particle collision angle θ_{12}, $\beta\tau_k$=1.023.

4.5 Summary and Conclusions

Numerical and analytical studies on particle collision velocity and angle in isotropic, Gaussian turbulence have been carried out. The effects of particle inertia and particle size on the collision velocity and collision angle are examined.

An asymptotic analysis has been developed to predict the effect of small particle inertia on the particle collision velocity. The asymptotic prediction for the increased collision velocity agrees well with the results of numerical simulation and PDF-based method. The collision velocity is found to contain terms that are proportional to $(\beta\tau_k)^{-1}$ and $(\beta\tau_k)^{-2}$.

Particle collision angle strongly depends on particle inertia and size. The average collision angle and the variation of the collision angle increase as the inertia increases. Both the average collision angle and the variation of the collision angle decrease as the particle size decreases.

CHAPTER 5
QUANTIFICATION OF PARTICLE CONCENTRATION NON-UNIFORMITY IN TURBULENCE

For heavy particles with finite inertia, small scale structure of turbulence induces particle preferential concentration. Particles tend to collect in the regions of high strain rate and low vorticity, as has been observed in many Lagrangian simulations. Quantification of the extent of the non-uniform particle concentration distribution has been difficult because the particle concentration based on the Lagrangian statistics is highly noisy. A method is developed to calculate reliably the variant of the particle concentration, $<n'^2>$, in which n is the instantaneous particle number concentration and the prime is the fluctuation in a small cube of volume $(\Delta x)^3$, from the Lagrangian simulations of the particle motions in an isotropic turbulence. The concentration non-uniformity is measured using a new parameter Δ_β based on the first two lower order moments of n. It is observed that the non-uniformity varies with Δx, suggesting a fractal nature of the particle concentration distribution. For particles with zero size, the non-uniformity scales with Δx as $\Delta_\beta \sim (\Delta x)^{-b}$ (b around 1) for small values of Δx. However, for finite-size particles, the non-uniformity reaches a maximum value (around order one or less) at $\Delta x/D = 2.0 \sim 3.5$, in which D is the particle diameter; it drops to zero as $\Delta x/D$ gets close to one. It is noted that the maximum value of the $<n'^2>/<n>^2$ is attained when the ratio of particle response time to the Kolmogorov time scale is close to one, which has been previously observed for the zero-size case based on other physical quantities.

5.1 Introduction

In many statistical problems, the lower order moments are often of interest. For large number of monodisperse particles, the collision rate is $\dot{n}_c=\alpha_{11}n^2$. The first moment of particle concentration is clearly the average concentration $\bar{n}$, i.e., the number of particles per unit volume. The second order moment $<n^2>$ can then be expressed as

$$<n^2> = \bar{n}^2 + <n'^2> = \bar{n}^2 \left(1+\frac{<n'^2>}{\bar{n}^2}\right) \tag{5.1}$$

where < > denotes ensemble average. The first moment $\bar{n}$ does not tell how the number of particles varies with the volumes at different locations and gives no reflection of turbulence structure at small scale levels. However, the second order moment, $<n^2>$, consists of two terms: $\bar{n}^2$ and $<n'^2>$. The variance of particle concentration, $<n'^2>$, measures the variation of particle number density in the cells, i.e. the non-uniformity of the particle distribution. Thus it is fundamentally important to the particle collision rate. Since $\bar{n}$ is a simple average of particle concentration in a turbulent flow while $<n'^2>$ depends on the turbulence structure and particle inertia, etc., our attention is given to the behavior of $<n'^2>$.

In this study, we use the normalized variance of particle concentration, $<n'^2>/\bar{n}^2$ to quantify the concentration non-uniformity in turbulent flows. The normalized variance is obtained via direct numerical simulation. As will demonstrated in §5.2, the inherent statistical noise is eliminated from the $<n'^2>/\bar{n}^2$. By this new method no assumption regarding the particle-particle interactions is needed. The effects of particle size and inertia on the concentration non-uniformity can be quantified separately. It is found that the concentration non-uniformity can be greatly overestimated if the particle size is ignored. For particles with zero size, the non-uniformity scales with Δx as $<n'^2>/<n>^2 \sim (\Delta x)^{-b}$ (b around 1) for small values of Δx for particles whose response time is comparable with turbulence Kolmogorov time scale, where Δx is the length of a small cube of volume $(\Delta x)^3$ used in the Lagrangian simulations of the particle motions in turbulence. However, for finite-size particles, the non-uniformity reaches a maximum value (around order one or less) at $\Delta x/D = 2.0\sim3.5$, in which D is the particle diameter and η is Kolmogorov length scale; it drops to zero as $\Delta x/D$ gets close to one. The maximum value of the $<n'^2>/<n>^2$ is obtained when the ratio of particle response time to the Kolmogorov time scale is around one.

5.2 Quantification Method

5.2.1 Inherent Noise of the Concentration Non-uniformity

Suppose the computational domain L^3 is divided into N_c equal-volume cells each with length Δx so that $N_c = (L/\Delta x)^3$. Obviously $\bar{n} = N/N_c$ is the first moment of n.

For zero-size, inertialess particles, the probability of a particle residing in a particular cell is $p = 1/N_c$. With N particles in the domain, the probability of k particles residing in a specific cell of volume $(\Delta x)^3$ obeys the Bernoulli distribution,

$$P(k) = \frac{N!}{k!(N-k)!}\, p^k (1-p)^{N-k}. \tag{5.2}$$

The second moment of n is, by definition,

$$<n^2> = \sum_{k=0}^{N} k^2 P(k)\,. \tag{5.3}$$

Thus the variance of the particle concentration for a given cell is

$$<n'^2> = <n^2> - \bar{n}^2 = \sum_{k=0}^{N} k^2 P(k) - \bar{n}^2\,. \tag{5.4}$$

For $Np(1-p) >> 1$, P(k) given by (5.2) can be expressed as

$$P(k) \sim \frac{1}{\sqrt{2\pi Np(1-p)}}\, \exp[-(k-Np)^2/2Np(1-p)], \tag{5.5}$$

for k in the neighborhood of N*p*, which is known as DeMoivre-Laplace theorem. In the limit of large N*p*(1- *p*), which is very close to $\bar{n}$ for small *p*, an asymptotic integration gives

$$<n^2> = \int_0^N k^2 P(k)\, dk \sim \bar{n}^2 + \bar{n}(1-p)\,. \tag{5.6}$$

Denoting $<n'^2_\infty>$ as $<n'^2>$ for zero-size, inertialess particles ($\beta \to \infty$), we obtain

$$<n'^2_\infty> = <n^2> - \bar{n}^2 = \bar{n}(1-p)\,. \tag{5.7}$$

Denoting r as the ratio of $<n'^2>$ to $\bar{n}^2$,

$$r = \frac{<n'^2>}{\bar{n}^2}\,, \tag{5.8}$$

it follows for zero-size, inertialess particles that

$$r_\infty \equiv \frac{<n'^2_\infty>}{\bar{n}^2} = \frac{1-p}{\bar{n}}\,. \tag{5.9}$$

For $\bar{n} = O(1)$ or smaller, the DeMoivre-Laplace theorem does not hold anymore. In DNS the number of particles used is relatively small from the point view of smooth statistics, as mentioned in Section I. In DNS, $\bar{n}$ may be much less than one as cell size becomes small. With finite-size particles, the ultimate number distribution of particles is reduced to either zero or one per cell as the cell size is smaller than 0.5773D, where D is the particle diameter. For $\bar{n} << O(1)$, particle number concentration is more likely to obey Poisson distribution

$$P(k) = \frac{\lambda^k e^{-\lambda}}{k!}\,, \tag{5.10}$$

where $\lambda = Np$. The second moment of n is then

$$<n^2> = \sum_{k=0}^{N} k^2 P(k) = \sum_{k=0}^{N} k^2 \frac{\lambda^k e^{-\lambda}}{k!}\,, \tag{5.11}$$

and the variance of the particle concentration for a given cell is

$$<n'^2> = <n^2> - \bar{n}^2 = \sum_{k=0}^{N} k^2 \frac{\lambda^k e^{-\lambda}}{k!} - \bar{n}^2 . \tag{5.12}$$

For N >>1,

$$\sum_{k=0}^{N} k^2 \frac{\lambda^k e^{-\lambda}}{k!} = \sum_{k=0}^{\infty} k^2 \frac{\lambda^k e^{-\lambda}}{k!} = \sum_{k=0}^{\infty} [k(k-1)+k] \frac{\lambda^k e^{-\lambda}}{k!}$$

$$= \sum_{k=0}^{\infty} k(k-1) \frac{\lambda^k e^{-\lambda}}{k!} + \sum_{k=0}^{\infty} k \frac{\lambda^k e^{-\lambda}}{k!}$$

$$= \lambda^2 e^{-\lambda} \sum_{k=0}^{\infty} \frac{\lambda^{k-2}}{(k-2)!} + \lambda e^{-\lambda} \sum_{k=0}^{\infty} \frac{\lambda^{k-1}}{(k-1)!}$$

$$= \lambda^2 e^{-\lambda} e^{\lambda} + \lambda e^{-\lambda} e^{\lambda}$$

$$= \lambda^2 + \lambda . \tag{5.13}$$

Since $\lambda = Np = \bar{n}$, the variance of n can be expressed as

$$<n'^2> = \sum_{k=0}^{N} k^2 \frac{\lambda^k e^{-\lambda}}{k!} - \bar{n}^2 \sim \lambda^2 + \lambda - \bar{n}^2$$

$$= \bar{n}^2 + \bar{n} - \bar{n}^2 = \bar{n} . \tag{5.14}$$

It follows for zero-size, inertialess particles that

$$r_\infty \equiv \frac{<n'^2_\infty>}{\bar{n}^2} = \frac{1}{\bar{n}} . \tag{5.15}$$

For $\bar{n} >> 1$, seen from both equations (5.9) and (5.15), $r_\infty = <n'^2_\infty>/\bar{n}^2 \to 0$ so that the variance of the particle concentration distribution is very small when it is normalized by the square of the first moment of n. However, if N is fixed while N_c takes a large value in the limit, we have $\bar{n} << 1$ and $r_\infty \sim 1/\bar{n} >> 1$. In a practical simulation of particle motions in turbulence, N is always finite and fixed. Since we are interested in quantifying the small-scale variation of the particle concentration, it is necessary to reduce successively the size of the cell, $(\Delta x)^3$, on which $\bar{n}$ and $<n'^2>$ are computed. It is noted that the relatively large value of $<n'^2_\infty>$ for inertialess particles is entirely due to the fact that there is not enough particles in each cell as the size is reduced and $r_\infty \sim 1/\bar{n}$ contains no contribution from the preferential concentration. As far as the inertial effect is concerned, $r \sim 1/\bar{n}$ is purely the inherent statistical noise which can be improved by using large values of $\bar{n}$ in principle. As the inertia of the particles increases, $<n'^2>$ will contain an increasing effect of the inertia bias. The fact that $r_\infty \sim 1/\bar{n} >> 1$ for inertialess particles when $\bar{n} << 1$ implies, however, that $r = <n'^2>/\bar{n}^2$ is dominated completely by the inherent statistical noise $r_\infty \sim 1/\bar{n}$. The contribution from the inertial effect to $<n'^2>$ or r thus must be isolated from the statistical noise. Figure 5.1 shows the comparison between the DNS results r_∞ for inertialess particles and the inherent noise $1/\bar{n}$, where $<n'^2>/\bar{n}^2$ at every instant was recorded and a total of 300 time steps and 40 turbulence realizations are used in our DNS. The details regarding turbulence representation, the characteristics of the turbulence and particle collision detection scheme have been given in §2.1.3. It clearly shows that $<n'^2>/\bar{n}^2$ is indeed dominated by $1/\bar{n}$ which has to be subtracted.

5.2.2 Concentration Non-uniformity Parameter

For particles with finite inertia, the variance of the particle concentration can be computed in direct numerical simulations

$$< n'^2 (\beta) > = \frac{1}{N_c} \sum_{j=1}^{N_c} (n_j - \bar{n})^2 . \tag{5.16}$$

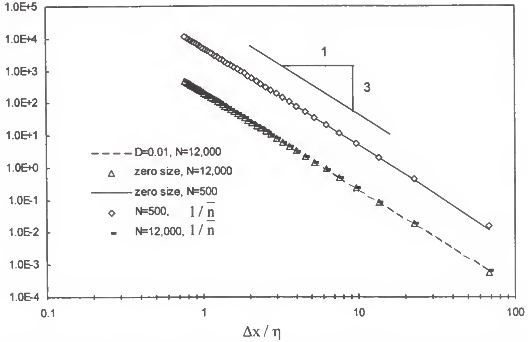

Figure 5.1 The normalized variance of the concentration as function of cell size for inertialess particles in isotropic turbulence. $\beta\tau_k = 1.023$.

The above variance of the concentration non-uniformity is dominated by the statistical noise, as shown in figure 5.1. For zero-size, inertialess particles, the above should approach to $\langle n'^2_\infty \rangle = \bar{n}(1-p)$ for $\bar{n} > O(1)$, and $\langle n'^2_\infty \rangle = \bar{n}$ for $\bar{n} \ll O(1)$. Defining the normalized difference between above $\langle n'^2(\beta) \rangle$ and $\langle n'^2_\infty \rangle$ as

$$\left\langle \frac{n'^2_\beta}{\bar{n}^2} \right\rangle = \left\langle \frac{n'^2_\beta(\beta)}{\bar{n}^2} \right\rangle - \left\langle \frac{n'^2_\infty}{\bar{n}^2} \right\rangle$$

$$= \left\langle \frac{n'^2_\beta(\beta)}{\bar{n}^2} \right\rangle - \frac{1-p}{\bar{n}} \qquad \text{for } \bar{n} > O(1), \qquad (5.17)$$

and

$$\left\langle \frac{n'^2_\beta}{\bar{n}^2} \right\rangle = \left\langle \frac{n'^2_\beta(\beta)}{\bar{n}^2} \right\rangle - \left\langle \frac{n'^2_\infty}{\bar{n}^2} \right\rangle$$

$$= \left\langle \frac{n'^2_\beta(\beta)}{\overline{n}^2} \right\rangle - \frac{1}{\overline{n}} \qquad \text{for} \quad \overline{n} \ll O(1). \qquad (5.18)$$

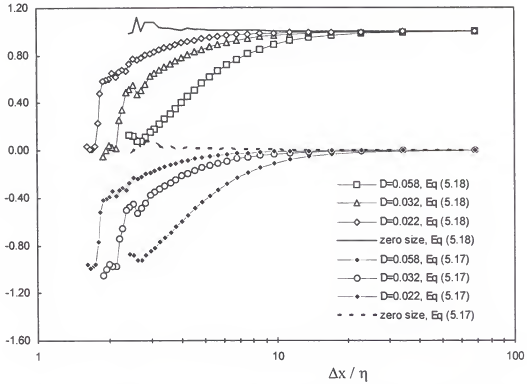

Figure 5.2 The expressions (5.17) & (5.18) of the concentration non-uniformity as function of cell size for inertialess particles in isotropic turbulence. $\beta\tau_k = \infty$.

The effect of inertia on the variance of n can be identified. Both equations (5.17) and (5.18) represent the contribution to $\langle n'^2 \rangle$ from the inertial effect for $\overline{n} > O(1)$ and $\overline{n} \ll O(1)$, respectively. Figure 5.2 shows the results of equations (5.17) and (5.18) for isotropic turbulent flow. Equation (5.17) obviously gives very small value for large Δx/D for $\overline{n} \gg O(1)$, while equation (5.18) on other hand gives small values for small Δx/D for $\overline{n} \ll O(1)$. For inertialess particles, $\langle n'^2_\beta \rangle / \overline{n}^2$ from both expressions has O(1) variation over cell size. Equation (5.17) gives $\langle n'^2_\beta \rangle / \overline{n}^2 \rightarrow -1$ as cell size Δx approaches to zero while equation (5.18) gives $<n'^2_\beta>/\bar{n}^2 \to 1$ as Δx increases. This is physically unsound because the preferential concentration is an inertial phenomenon and should not appear in turbulent flows with inertialess particles. Figure 5.3 shows the DNS results of $<n'^2_\beta>$ using equations (5.17) & (5.18) in a uniform shear flow for inertialess particles. The uniform shear flow is represented by $\mathbf{u}=(\Gamma y, 0, 0)$ with the velocity gradient $\Gamma=1.0$. Comparing with figure 5.2, very similar behavior for $<n'^2_\beta>/\bar{n}^2$ is obtained even for a uniform shear flow. The results are unphysical because there is no mechanism to drive inertialess particles to form non-uniform concentration in a uniform shear flow. Thus, one should not expect to apply the equation (5.17) or (5.18) to quantify the concentration non-uniformity. However, the above results gave us a valuable hint. That is, the results obtained by both equations (5.17) & (5.18) can be interpreted as an additional statistical noise for both inertialess and inertial particles. It is hence suggested that the actual contribution of the inertia to $<n'^2>$ for an arbitrary β may be expressed as

$$<\Delta n'^2_\beta> = [<n'^2(\beta)> - \bar{n}(1-p)]_\beta - [<n'^2(\beta=\infty)> - \bar{n}(1-p)]_{\beta=\infty}, \tag{5.19}$$

or

$$<\Delta n'^2_\beta> = [<n'^2(\beta)> - \bar{n}]_\beta - [<n'^2(\beta=\infty)> - \bar{n}]_{\beta=\infty}. \tag{5.20}$$

Apparently, zero concentration non-uniformity is obtained for inertialess particles in both turbulence and uniform shear flows based on equations (5.19) & (5.20). It is noted that $<\Delta n'^2_\beta>$ is a function of β and $\bar{n}$ in equation (5.20), while $<\Delta n'^2_\beta>$ is mainly determined by β and $\bar{n}$ in (5.19). The influence of p on $<\Delta n'^2_\beta>$ in (5.19) may be negligible as far as a small p is concerned, i.e. $<\Delta n'^2_\beta>= f(\beta, \bar{n})$, since p appears in both first and second terms in right side of equation (5.19). A large p, however, means the large cell size (the box size is the limit), which usually gives approximately uniform particle distribution. It is also noted that $<\Delta n'^2_\beta> \to 0$ as $\bar{n} \to \infty$ (or $N \to \infty$). Thus, it is expected that the effect of inertia on the concentration non-uniformity can be captured using equations (5.19) & (5.20). To quantify the extent of the concentration non-uniformity using the second moment of n, a dimensionless quantity Δ_β called concentration non-uniformity parameter, is defined as

$$\Delta_\beta = \left[\frac{<n'^2_\beta>}{\bar{n}^2} - \frac{(1-p)}{\bar{n}}\right]_\beta - \left[\frac{<n'^2(\beta=\infty)>}{\bar{n}^2} - \frac{(1-p)}{\bar{n}}\right]_{\beta=\infty}, \tag{5.21}$$

or

$$\Delta_\beta = \left[\frac{<n'^2_\beta>}{\bar{n}^2} - \frac{1}{\bar{n}}\right]_\beta - \left[\frac{<n'^2(\beta=\infty)>}{\bar{n}^2} - \frac{1}{\bar{n}}\right]_{\beta=\infty}. \tag{5.22}$$

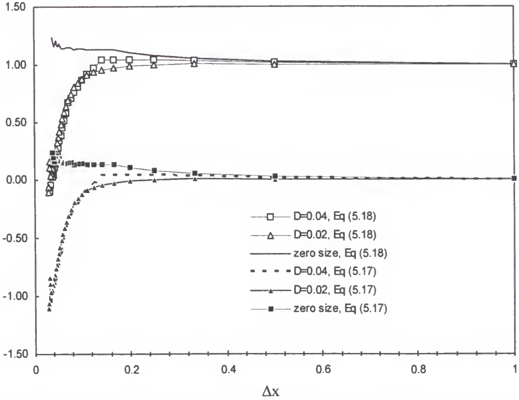

Figure 5.3 The expressions (5.17) & (5.18) of the concentration non-uniformity as function of cell size for inertialess particles in uniform shear flow. $\beta/\Gamma=\infty$.

Figure 5.4 shows the concentration non-uniformity parameter for the uniform shear flow using equations (5.21) & (5.22). It is seen that Δ_β is very small for all cases in a uniform shear flow. Figure 5.5 shows Δ_β in turbulent flows for a large range of sizes for particles with zero inertia. It is also shown that, for zero-size particles, the concentration non-uniformity at small inertia ($\beta\tau_k=7.3$) still increases with the decreasing cell size.

The detailed discussions about the size effect on the collision rate will be given in §5.3. The above results obtained by (5.21) & (5.22) are reasonable and hence strongly suggest that equations (5.21) & (5.22) can be used to quantify and predict the particle concentration non-uniformity induced by particle inertia in general turbulence. It should also be noticed that both equations (5.21) and (5.22) always yield the same shape differed by a constant (≅1). To facilitate the subsequent discussions, equation (5.22), which does not contain *p* and is thus in a simpler form, is used hereinafter.

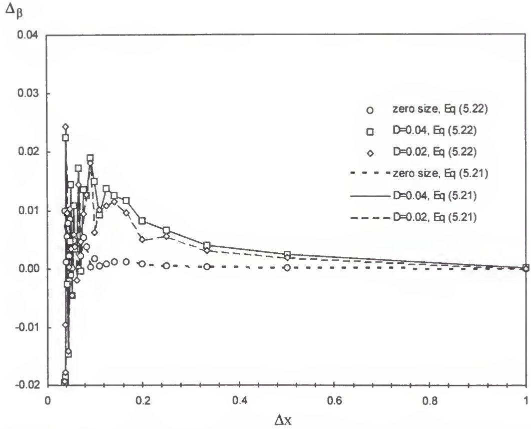

Figure 5.4 The concentration non-uniformity parameter Δ_β as function of cell size in uniform shear flow. $\Gamma=1.0$, $\beta/\Gamma=1.0$.

Figure 5.6 shows the effect of total particle number N on the concentration non-uniformity parameter Δ_β. It is seen that Δ_β remains almost on the same curve when N increases from 25,000 to 50,000 and 100,000 for all values of N_c (from 2^3 to 278^3).

Even when N decrease to 12,000, 5,000 and 2,000, Δ_β does not change much from those at N=100,000. This suggests that Δ_β is only very weakly dependent on N and the results for Δ_β obtained at finite N (2,000-12,000) can be used to represent Δ_β of $N \rightarrow \infty$. Hence, Δ_β defined by (5.21) & (5.22) contains only the effect of inertia and can be used conveniently as a measure for small scale concentration non-uniformity. It should be also pointed out that while Δ_β has a minimal statistical error due to finite N, it still contains statistical errors due to finite number of turbulence realizations.

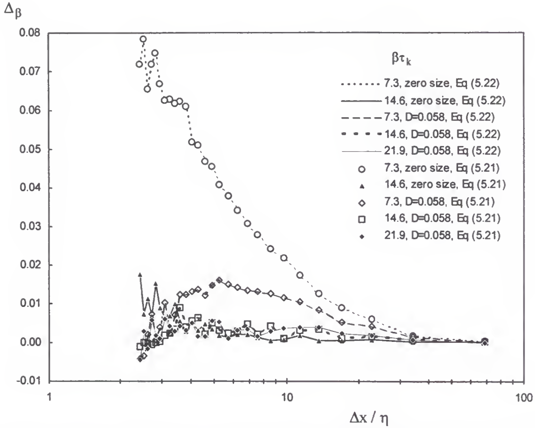

Figure 5.5 The concentration non-uniformity as function of cell size for small inertia particles in isotropic turbulence.

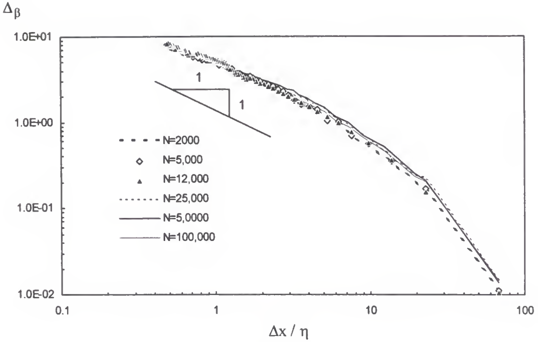

Figure 5.6 The concentration non-uniformity as function of cell size for various particle number densities at a given inertia in isotropic turbulence. $\beta\tau_k = 1.023$.

5.3 Results and Discussions

Since this chapter is focused on quantifying the concentration non-uniformity in order to investigate the effects of particle inertia and finite size on the collision rate, the "THROW AWAY" scheme is employed for finite-size particles. Both the tracking of the motions of particles and the collision detection are carried out in a Lagrangian frame. The semi-implicit finite difference scheme with 2nd order accuracy is implemented to integrate the equation of particle motion and to detect collision.

To examine the effects of the inertia and size on particle concentration non-uniformity induced by the small-scale structure of turbulence, N particles are randomly seeded in a box of π^3 in an isotropic turbulence. Initially, the velocities of the particles are set to be the same as that of the turbulence at corresponding locations. There are two categories of particles considered: zero-size and finite-size particles. For zero-size particles, following previous studies on the preferential concentration, no particle collision detection is needed so that particles can overlap in space, which is equivalent to the use of the "OVERLAPPING" scheme. For finite-size particles, however, collision between particles has to be detected, and the collided pair will disappear from their current size groups as far as geometrical collision is concerned. Periodical boundary conditions are imposed on both the particles and turbulence. Instantaneous particle concentration fields are obtained by tracking 2000, 5000, 12000, 25,000 to 50,000 and 100,000 particles respectively. The box is divided into N_c equal-volume cells each with length Δx so that $N_c = (\pi/\Delta x)^3$. The isotropic turbulence in the periodic box has the following characteristics: integral length scale L=0.594, Taylor micro length scale λ =0.277, Kolmogorov length scale η=0.023, Kolmogorov time scale $\tau_k = (\nu / \varepsilon)^{1/2}$=0.073, and Re_λ=40.1. The time step used in this study is dt=0.01 and the ratio of total time (after the particles have reached dynamic equilibrium) to Kolmogorov time is 82 for most of the cases in the following discussions. The instantaneous non-uniform concentration is calculated and recorded at every time step after particles have reached dynamically equilibrium. The average concentration non-uniformity is obtained based on the recorded concentration non-uniformity by all time steps and all turbulence realizations.

Figure 5.7 shows the effects of inertia on the concentration non-uniformity for sizeless particles. It can be seen that the maximum value of Δ_β occurs around $\beta\tau_k$=1.0, which agrees with the results of Wang & Maxey (1993). It is noted that all curves for different inertia increase monotonically as the cell size decreases, and the slopes are all close to -1 in the small cell size limit except that the curve for $\beta\tau_k$=0.511 has a slightly smaller slope at the same region. Evidently, the results in figure 5.7 show the divergence of Δ_β as cell size becomes small, so does figure 5.6. The singular behavior of Δ_β is unphysical for finite-size particles because the particle concentration becomes either 0 or 1 per cell when the cell size falls below particle diameter. Analytically it can be easily shown from equations (5.21) & (5.22) that Δ_β is equal to zero if the 0-1 Poisson distribution is reached.

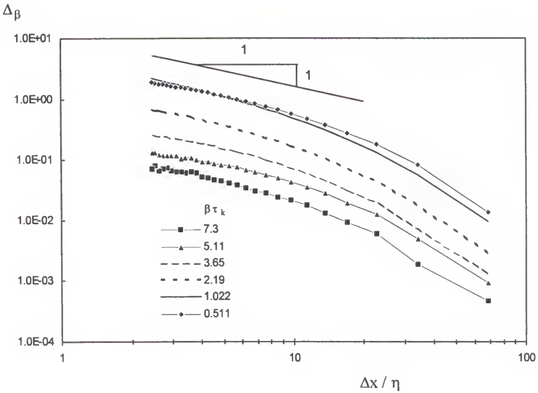

Figure 5.7 The concentration non-uniformity of sizeless particles as function of cell size for various inertia in isotropic turbulence.

Figures 5.8 (a-b) show the non-uniformity parameter Δ_β for finite-size particles over the whole range of cell sizes. The collection of the maximum values of concentration non-uniformity parameter Δ_β for finite-size particles as function of particle inertia in isotropic turbulence is shown in figure 5.9. For $\beta\tau_k \geq 0.5$, the non-uniformity parameter Δ_β increases as the inertia increases. The maximum Δ_β is reached at $\beta\tau_k$=0.5. For very large inertia $\beta\tau_k$<0.5, however, the non-uniformity parameter Δ_β decreases as the inertia further increases. It is observed that Δ_β varies with inertia as $(\beta\tau_k)^{-2}$ for large values of $\beta\tau_k$. It is also noted from figure 5.9 that the non-uniformity Δ_β at D/η=0.957 is larger than that at larger particle size D/η=2.522. Detailed discussions on the relationship between the non-uniformity parameter Δ_β and the collision rate will be given in Chapter 6.

Figure 5.10 compares Δ_β of small finite-size particles with that of zero size for $\beta\tau_k \sim 1$. It can be seen that there exists a maximum Δ_β for all finite-size particles for all different inertia. Clearly, the use of sizeless particles not only results in a singular concentration non-uniformity in the limit of small cell size but also overestimates the value Δ_β even at finite cell size. Figures 5.11 (a) & (b) show that the value of the maximum Δ_β increases as the particle size becomes small. A maximum value of Δ_β always exists for all finite-size particles. It is reasonable to expect that the maximum Δ_β will ultimately become infinite if one uses infinite small size of particles such as sizeless particles. It is seen that the maximum Δ_β is reached at normalized cell size $\Delta x/D=2.0\sim2.5$ for all particle sizes ($D/\eta=0.957\sim2.522$) *except* for the smallest particles in figures 5.11 (a) & (b), where the maximum Δ_β is reached at $\Delta x/D=3.5$ for $D/\eta=0.435$.

The effects of particle size on the particle concentration non-uniformity may be explained as follows. A reason for particle size to play an important role in quantification of the concentration non-uniformity may be explained by the mechanism of binary collisions between particles. Since particles are pairing to form the non-uniformity before they collide each other as turbulent flow evolves in time, the most meaningful scaling quantity should be able to measure the degree of the number of particles closely paired at every instant. The dimensionless cell size $\Delta x/D=2.0\sim3.5$, with being able to contain more than a pair of particles, is a proper frame to capture this significant phenomenon.

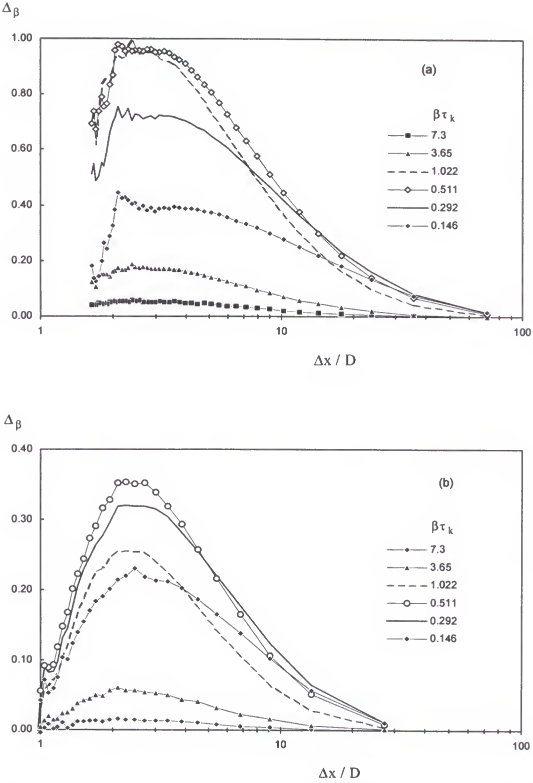

Figure 5.8 The concentration non-uniformity parameter Δ_β of finite-size particles as function of cell size for various inertia in isotropic turbulence. (a) $D/\eta=0.957$. (b) $D/\eta=2.52$.

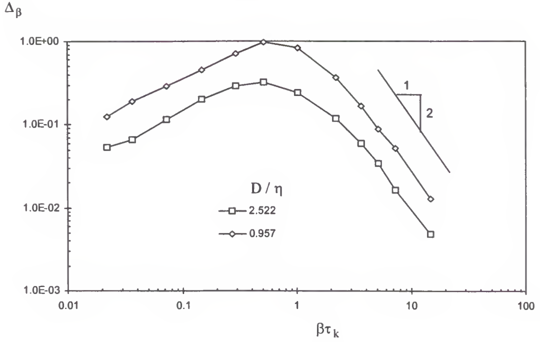

Figure 5.9 The maximum concentration non-uniformity parameter Δ_β of finite-size particles as function of particle inertia in isotropic turbulence.

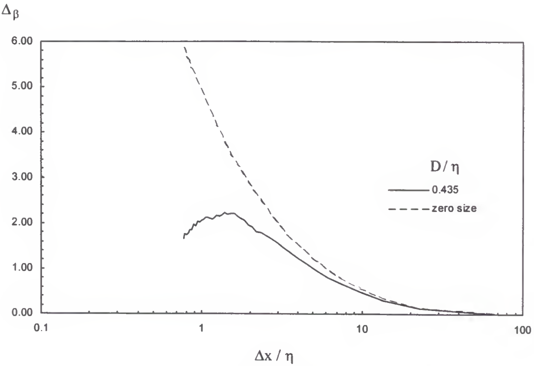

Figure 5.10 The concentration non-uniformity parameter Δ_β as function of $\Delta x/\eta$ for small-size and zero-size particles in isotropic turbulence. $\beta\tau_k$=1.023.

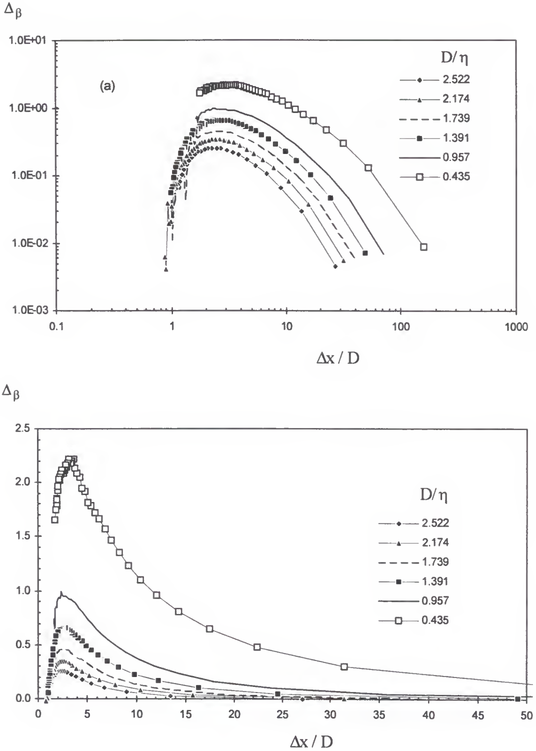

Figure 5.11 The concentration non-uniformity of particles at a given inertia as function of $\Delta x/D$ cell size for various sizes in isotropic turbulence. (a) Log scale in x-axis. (b) in normal scale in x-axis.

5.4 Summary and conclusions

A new method is developed to calculate reliably the normalized concentration non-uniformity parameter $<n'^2>/\overline{n}^2$, in which n is the instantaneous particle number concentration and the prime is the fluctuation in a small cube of volume $(\Delta x)^3$, from the Lagrangian simulations of the particle motions in turbulence, and $\overline{n}$ is the mean concentration of particles. The inherent statistical noise is eliminated from the parameter $<n'^2>/\overline{n}^2$. The effects of particle size and inertia on the concentration non-uniformity can be quantitatively examined using present method. It is found that the concentration non-uniformity parameter will be greatly overestimated if the effect of particle size is neglected. For particles with zero size, the non-uniformity varies with the inverse of Δx, i.e. $\Delta_\beta \sim 1/\Delta x$ for small values of Δx when particle response time is comparable with turbulence Kolmogorov time scale. However, for finite-size particles, the concentration non-uniformity parameter reaches a maximum value instead of unbounded value for sizeless particles. For finite-size particles, the maximum non-uniformity is reached at $\Delta x/D = 2.0$~3.5 while it becomes zero when $\Delta x/D$ approaches to one. Particle size is an important length scale in quantifying particle concentration non-uniformity. The maximum value of the concentration non-uniformity is reached when the ratio of particle response time to the Kolmogorov time scale is close to one.

CHAPTER 6
COLLISION RATE AT FINITE PARTICLE INERTIA AND SIZE IN GAUSSIAN TURBULENCE

The effects of particle inertia, size, concentration and gravity on the collision kernel are investigated in an isotropic, Gaussian turbulence. An asymptotic analysis is developed to predict the effect of the increased collision velocity on the collision rate due to small particle inertia. A unified expression of the collision kernel including effects of the increases in both collision velocity and concentration non-uniformity is proposed for small inertia particles. Good agreement is obtained between the simulation results and the prediction by the unified expression for particles with small inertia. The theoretical prediction of the collision kernel for zero inertia particles is critically examined by carrying out the direct numerical simulations at both a very dilute concentration with small number of particles and a dilute concentration with large number of particles. It is found that the normalized collision kernel α_{11}^{*} decreases as particle size or mean concentration increases. In contrast to Saffman & Turner's prediction for the effect of particle gravity on α_{11}^{*}, the gravitational settling is found to reduce α_{11}^{*} for monodisperse particles. It is found that "HARD SPHERE" model suffers from multiple collision problem and the collision kernel predicted by the "HARD SPHERE" model is dependent on time step size for small inertia particles. The classical result of Smoluchowski for the collision rate of monodisperse particles in a laminar shear flow is shown to be inaccurate due to the inclusion of the self-collisions. The present work extends Smoluchowski's result by excluding the self-collisions in the counting of collision pairs.

6.1 Introduction

As pointed out in Chapter 1, the particle inertia affects the particle collision rate through various mechanisms: increase in the collision velocity, particle concentration non-uniformity, and compressibility of the particulate phase in the continuum sense. Zhou et al. (1997) made an attempt to include all these mechanisms in a mechanistic analysis for particle collision rate. In particular, the effects of the concentration non-uniformity were modeled with an adjustable parameter that is based on the simulation results of the collision using the "OVERLAPPING" scheme. It must be pointed out that the "OVERLAPPING" scheme for particle detection scheme is equivalent to having a zero particle size as far as the particle concentration non-uniformity is concerned. It has clearly been demonstrated in Chapter 5 that neglecting particle size leads to a significant over-estimation of the concentration non-uniformity. Hence, the model of Zhou et al. (1997) contains a serious over-estimation on the effect of particle inertia through an over-estimation of the concentration non-uniformity.

In addition to particle inertia measured by $\beta\tau_k$, the particle size also plays complicated roles on the collision rate. Consider the zero inertia limit for example. For particles with small size, $D<\eta$, the collision velocity **w** is linearly proportional to the particle size D and $(\varepsilon / \nu)^{1/2}$. This is so because for $|\mathbf{x}_i - \mathbf{x}_j| \sim D < \eta$, Taylor series expansion can be applied to obtain fluid velocity difference, $\Delta\mathbf{u}$, between two close points separated by a distance $|\mathbf{x}_i - \mathbf{x}_j| = R$ in space in the form of

$$<|\mathbf{w}|> \sim <|\Delta\mathbf{u}|> \sim |(\mathbf{x}_i - \mathbf{x}_j)\cdot\nabla\mathbf{u} + \ldots| \sim R(\varepsilon / \nu)^{1/2} + \ldots \qquad (6.1)$$

On average the leading order term for **w** is thus proportional to $(\varepsilon / \nu)^{1/2}$ and D. For $|\mathbf{x}_i - \mathbf{x}_j| \sim D >> \eta$, the velocity difference $\Delta\mathbf{u}$ between two points in space is given by the inertial subrange scaling law as

$$|\Delta\mathbf{u}| \sim (\varepsilon R)^{1/3} + \ldots \qquad (6.2)$$

which is independent of viscosity. Note that the dependence of $|\Delta \mathbf{u}|$ on R is only to the one-third power which is quite less than the linear behavior for $R<\eta$. Hence, in addition to reducing the particle concentration non-uniformity, an increase in particle size also reduce the rate of increase in the collision velocity. When this is coupled with particle inertia and finite particle volume concentration, the situation becomes much more complicated. A detailed numerical study on the effects of particle inertia, particle size, and particle concentration on the collision rate in turbulence is warranted.

To that end, an asymptotic analysis is first developed to predict the effect of the small particle inertia on the collision kernel due to the increase in collision velocity. The effect of particle size on the collision kernel is critically examined by carrying out the direct numerical simulation at a very dilute concentration for zero inertia particles. It is found that the collision kernel decreases as particle size increases. The collision kernel is found to be affected by particle mean concentration of the system. A unified expression of the collision kernel including effects of the increase in collision velocity and concentration non-uniformity is proposed for small inertia particles. The unified expression is evaluated through direct numerical simulations. The effect of gravitational settling on the collision kernel is observed through DNS result and explained by the affected collision velocity and concentration non-uniformity. The results of three collision models: "THROW AWAY", "KEEP ALL" and "HARD SPHERE" are presented and compared. It is found that good agreement between the "THROW AWAY" and "KEEP ALL" models are reached and verified by Smoluchowski's result in laminar shear flow, while the "HARD SPHERE" model gives quite different result due to the multiple collision mechanism. It is observed through DNS that, even at a large inertia such as $\beta\tau_k=1$ and with long time $\beta T=52$, the collision kernel using "HARD SPHERE" model appears continuously increasing with time, but the results of both the "THROW AWAY" and "KEEP ALL" models are quite steady from the beginning and also in a good agreement. The Smoluchowski's collision rate for monodisperse particles (1.5) in a laminar shear flow is found to be inaccurate due to the inclusion of the self-collisions. A correction to Smoluchowski's formulation has been made by excluding the self-collisions in the counting of collision pairs. A numerical simulation for particle collisions in a laminar shear flow at very low concentration is carried out to validate the present result.

6.2 Correction of Smoluchowski's theory

As mentioned in Chapter 2, the collision rate and kernel may vary with the collision models. In order to minimize the effects of the collision models on the collision rate and kernel, numerical simulation of particle collisions has to be carried out at a very dilute particle concentration in the system. Although equations (1.3) and (1.5) are used usually for systems involving a large number of particles so that the number concentration in the continuum sense is well defined, the calculation of the collision rate given by equation (1.3) is not necessarily limited to the systems with large number of particles. There has been recent development in the numerical studies of particle collision in fluids in which a finite number of particle trajectories, instead of continuous particle cloud, are studied. It has come to our attention that equation (1.5) involves the counting of self collisions among monodisperse particles, despite the factor of $\frac{1}{2}$ which has already been introduced. This issue can be easily seen in the Lagrangian framework.

Suppose there are N_i particles of *i*th-size group and N_j particles of *j*th-size group in the fluid of volume $\forall$ at a given instant. The number of collisions among *i*th-size and *j*th-size particles is related to the number of possible combinations among these two groups. The number of possible combinations among *i*th-size and *j*th-size groups is N_iN_j so that the collision rate can be related to the number of possible combinations as

$$\dot{n}_{C_{ij}} = \alpha_{ij} N_i N_j / \forall^2. \tag{6.3}$$

However, considering the collisions among the same size group, the number of possible combinations of particles is $\frac{1}{2}N_i(N_i-1)$, not $\frac{1}{2}N_i^2$. Take $N_i=2$ for example. There can be only one possible collision in the system. However, equation (1.5) implies that there are two possible collisions. Based on the number of possible combinations, the collision rate among the same size group in the given volume should be

$$\dot{n}_{C_{ii}} = \frac{1}{2} N_i(N_i\text{-}1)\ \frac{4}{3}\Gamma(2r_i)^3\ \forall^{-2} \tag{6.4}$$

or

$$\dot{n}_{C_{ii}} = \frac{1}{2} n_i(n_i\ \text{-}1/\forall)\ \frac{4}{3}\Gamma(2r_i)^3 \qquad\qquad \text{for } n_i > 1/\forall \tag{6.5}$$

where $n_i = N_i/\forall$ and $n_j = N_j/\forall$ are simply the average number of particles per unit volume. For a large value of N_i, or $n_i\forall \gg 1$, equation (6.5) recovers equation (1.5).

Using the number of possible combinations, equation (6.4) can also be consistently derived from equation (6.3) as a special case. Considering $N_i=2^M$ particles of radius r_i in a given volume $\forall$ and separating these particles into two groups each having 2^{M-1} particles, the number of collision candidates among these two groups is $2^{2(M-1)}$. However, there are collisions among the particles within each group. To find the number of collisions within the group, all the particles in the group can be further divided into two sub-groups, each with 2^{M-2} particles on such second level sub-group. The total number of the collision candidates in the second level sub-groups is $2\text{x}2^{2(M-2)}$. This process can be continued until there is only one particle in each sub-group on the last level so that all possible combinations are counted. Summing up the collisions among all sub-groups of different levels yields

$$\begin{aligned} \dot{n}_{C_{ii}} &= \frac{4}{3}\Gamma(2r_i)^3\ [2^{2(M-1)} + 2\text{x}2^{2(M-2)} + 2^2\text{x}2^{2(M-3)+} + \ldots + 2^{M-2}\,2^2 + 2^{M-1}2^0\,] \\ &= \frac{4}{3}\Gamma(2r_i)^3\ 2^M(2^M\text{-}1)/2 = \frac{1}{2}N_i(N_i\text{-}1)\ \frac{4}{3}\Gamma(2r_i)^3. \end{aligned} \tag{6.6}$$

Thus equation (6.4) is now consistent with equation (6.3) and is indeed a special case of equation (6.3).

To confirm the validity of equation (6.4) in the context of particle collision in fluid flows, a direct numerical simulation is carried out to examine the collisions among the like particles. Fifty particles of radius $r_i=0.02$ are randomly introduced at $t=0$ into a cubical box with length $Lx=2$, $Ly=1.8$, and $Lz=2.0$ so that $\forall=7.2$, with the restriction

$0.1<y_p<1.9$. A uniform shear flow with a shear rate $\Gamma=1.0$ is imposed and the flow velocity field is given by $\mathbf{v}=(u, v, w) = (\Gamma y, 0, 0)$. All particles move with the fluid along the x-direction. The motion of particles is updated with a time step $\Delta t=0.03$ and a total of three hundred time steps is used in each realization. Periodic boundary conditions are employed along x- and z-directions so that the particles that have left the box at the end of the *n*th time step are reintroduced, at *(n+1)*th time step, by image particles entering the box from the opposite side. In a uniform shear flow, no periodic condition can be imposed along the y-direction and particles near $y=0.1$ and $y=1.9$ have less collisions because there are no particles in regions of $y<0.1$ and $y>1.9$ in direct numerical simulation. A correction on the collision rate due to this boundary effect (Wang et al 1997) is thus employed for the number of collisions

$$\dot{n}_{C_{ii}} = [\dot{n}_{C_{ii}}]_{simu} /(1- \frac{3\pi}{16}\frac{2r_1}{L_y}) \tag{6.7}$$

in the shear flow. There is another possible correction (Wang et al 1997) due to the finite volume fraction of the particles in the volume. However, the volume fraction in the present case is 0.0233% so that the maximum volume correction suggested is less than 0.1% according to the correction scheme (Wang et al 1997); this correction is neglected here. An efficient scheme (Chen et al 1995) is used to search for particle collisions. The "THROW AWAY" collision model is employed. However, since the collision kernel is so low considered in this case that the probability of having two collisions in the entire 300 time steps within one realization is very small so that the treatment of the collided particles is not a concern at all in the present case.

Based on equation (6.4) and taking $N_i=50$, it is seen that the average number of collisions within $0\le t\le T=9$ in each realization is

$$\dot{n}_{C_{ii}} \forall T = \frac{1}{2} N_i(N_i-1) \frac{4}{3}\Gamma(2r_i)^3 \forall^{-1} T = 0.13067. \tag{6.8}$$

In order to achieve a reliable statistics, 10,000 collisions are desirable so that a total of $N_R=100{,}000$ realizations are used to generate an estimated collisions $N_C=13{,}067$ based on equation (6.8).

From the direct numerical simulation of N_R=100,000 realizations, with a 1.31% boundary correction given by equation (6.7), the total number of collisions is N_C=13,093. This agrees with our estimate (N_C=13,067) within 0.2%. If equation (6.10) is used, the estimated number of collisions would be N_C=13,333 which is nearly 2% larger than the simulation result.

As seen from equation (6.4), if there is more than one collision in $0 \leq t \leq T=9$, N_i on the right hand side will not remain a constant, nor does $\dot{n}_{C_{ii}}$. However, the ratio, $\dot{n}_{C_{ii}} \forall^2 / [\frac{1}{2} N_i(N_i-1)]$ which gives the collision kernel α_{ii}, should remain constant. Based on the counting of the number of collisions in each time step from the simulation, the collision kernel α_{ii} can be calculated using

$$\alpha_{ii} = \frac{\dot{n}_{C_{ii}} \forall}{\frac{1}{2} N_i (N_i - 1) \forall^{-1}}. \tag{6.9}$$

On the other hand, if equation (6.10) is applied, one would obtain, numerically, a different collision kernel by

$$\tilde{\alpha}_{ii} = \frac{\dot{n}_{C_{ii}} \forall}{\frac{1}{2} N_i N_i \forall^{-1}}. \tag{6.10}$$

Figure 6.1 (a) shows the numerically obtained value of α_{ii} for $0 \leq t \leq 9$. It is seen that there is a significant noise due to the small number of collisions within each time step despite the fact that 100,000 realizations have been used. In order to obtain reliable data, a time average is then employed for α_{ii}. Figure 6.1 (b) shows the cumulative time average of α_{ii} and $\tilde{\alpha}_{ii}$ together with the prediction by Smolouchowski [$\alpha_{ii} = \frac{4}{3} \Gamma (2r_i)^3$]. It is clearly seen from the time averaged result that the present formulation using $\frac{1}{2} N_i(N_i-1)$ gives a collision kernel that is consistent with equation (6.9) while the original formulation using $\frac{1}{2} N_i N_i$ is consistently smaller by about 2% comparing with that given by equation (6.9).

An extended version is thus suggested for the formulation of the population balance equations in view of the foregoing analyses. The evolution equations of particle population are

$$\frac{dn_1}{dt} = -\alpha_{11} n_1 [n_1 - 1/\forall]_+ - \alpha_{12} n_1 n_2 - \alpha_{13} n_1 n_3 - \ldots$$

$$\frac{dn_2}{dt} = \frac{1}{2}\alpha_{11} n_1 [n_1 - 1/\forall]_+ - \alpha_{12} n_1 n_2 - \alpha_{22} n_2 [n_2 - 1/\forall]_+ - \alpha_{23} n_2 n_3 - \ldots$$

$$\frac{dn_3}{dt} = \alpha_{12} n_1 n_2 - \alpha_{13} n_1 n_3 - \alpha_{23} n_2 n_3 - \alpha_{33} n_3 [n_3 - 1/\forall]_+ - \ldots$$

$$\cdots\cdots\cdots\cdots\cdots\cdots$$

$$\text{for } n_i\forall > 1, \quad i = 1, 2, 3, \ldots \tag{6.11}$$

where $[\ f\ ]_+$ denotes that this term is zero if $f<0$. Mathematically, $n_i\forall$ can be a non-integer in the population balance equations. The restriction on taking only the non-negative value of $\alpha_{ii}\, n_i[n_i - 1/\forall]$ ensures that there is no generation in the *i*th group due to the collisions among the like particles.

It needs to be pointed out that the effect of the correction in equation (6.11) is relatively minor. For a system with large number of particles ($N_i \gg 1$), the present correction carries no tangible impact on the evolution of the particle size distribution. However, the present analyses place the evaluation of particle collision rate, as given by equation (6.5), on a more consistent footing.

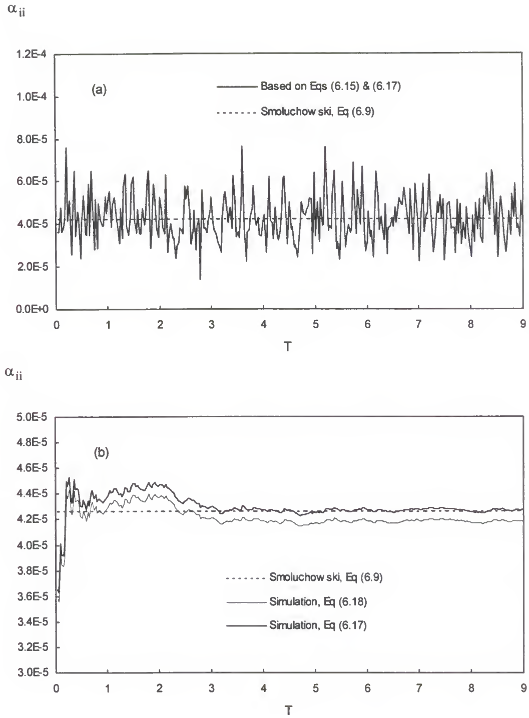

Figure 6.1 Collision kernel α_{ii} against time in laminar shear flow. Γ=1.0, D=0.04. (a) Variation of ensemble average. (b) Cumulative average.

6.3 An Analysis on the Effect of Particle Inertia on the Collision Rate

6.3.1 Saffman & Turner 's Analysis

Saffman & Turner presented the first theory for inertialess particles which follow fluid motion completely. The collision rate among particle groups 1 and 2 is evaluated as

$$\dot{n}_{C12} = n_1 n_2 < \int_{w_r<0} -w_r dS > \tag{6.12}$$

where w_r is the radial component of the relative velocity, $-n_1 n_2\, w_r$ is the particle flux moving inward to the target particle, and the integration is carried over the entire spherical surface of radius R, as shown in figure 4.1. Because of the continuity of fluid flow,

$$\begin{aligned} \dot{n}_{C12} &= \frac{1}{2} n_1 n_2 < \int_{\text{entire sphere}} |w_r| dS > \\ &= \frac{1}{2} n_1 n_2 \int_{\text{entire sphere}} <|w_r|> dS . \end{aligned} \tag{6.13}$$

The integration in right side of equation (6.13) may be expressed by equation (4.2) for isotropic turbulence, then the collision rate yields

$$\dot{n}_{C12} = n_1 n_2\, 2\pi R^2 <|w_x|> . \tag{6.14}$$

Recall that x is the local coordinate parallel to the line connecting the centers of the colliding particles and < > denotes ensemble averaging. It should be noted that for the particles with zero inertia, the ensemble averaged collision velocity $<|w_x|>$ is expressed by (4.3), so that

$$\dot{n}_{C12} = n_1 n_2\, R^3 \left(\frac{8\pi}{15}\frac{\varepsilon}{\nu}\right)^{1/2} = 1.294\, n_1 n_2\, R^3 \left(\frac{\varepsilon}{\nu}\right)^{1/2} = \alpha_{12}\, n_1 n_2 \tag{6.15}$$

where $$\alpha_{12} = 1.294\, R^3 \left(\frac{\varepsilon}{\nu}\right)^{1/2} . \tag{6.16}$$

For particles with inertia and gravity, Saffman & Turner gave their second prediction for identical particles

$$\alpha_{11}=1.67R^3(\frac{\varepsilon}{\nu})^{1/2} \tag{6.17}$$

An inconsistency occurs that the constant 1.67 in equation (6.17) differs with the constant 1.294 in equation (6.16) as particle inertia goes to zero.

6.3.2 Effect of Small Inertia on the Collision Kernel

To understand the effect of inertia on particle collisional rate, we consider an asymptotic theory for small inertia. It is assumed that the particle size is much less than the Taylor micro-length scale, and the gravitational force is negligible. As in Saffman & Turner (1956), we also assume that turbulence is isotropic and Gaussian.

Since the collision velocity $|w_x|$ is more relevant to the collision kernel as seen from equation (6.13), we start with $|w_x|$ to examine the effect of small particle inertia. Based on the asymptotic analysis of collision velocity, the mean-squared collision velocity is expressed by equation (4.19) for small inertia, and the net increase of the mean-squared collision velocity due to the inertia is given by the equation (4.20). Notice that the collision velocity is the relative velocity of two particles upon contact and hence $w_x(=v_{1x}-v_{2x})$ is always a negative value by projecting the relative velocity $(\mathbf{v}_1-\mathbf{v}_2)$ along the radial direction $(\mathbf{x}_1-\mathbf{x}_2)$,

$$w_x|_{x_2-x_1=\pm R} < 0 \qquad \text{for all collisions,} \tag{6.18}$$

and

$$<w_x>|_{x_2-x_1=\pm R} < 0. \tag{6.19}$$

Although $\mathbf{u}$ and $\mathbf{v}$ are Gaussian, w_x does not follow Gaussian distribution because of equations (6.18) & (6.19), and it is demonstrated in the figures 4.4 (a) & (b), the PDF of collision velocity for various inertia. Clearly, w_x is not Gaussian mainly because the curves of the PDF distributions are not symmetrical to the y-axis (the vertical line w_x=0). However, careful observation also tells that, for small inertia, the PDFs of the collision velocity are almost symmetrical to the vertical line at w_x=$<w_x>$ and appear close to be Gaussian distributions with respect to $w_x=<w_x>$. It is also noticed that the collision velocity PDFs of small inertia particles peak at the same w_x. That is to say, if the mean collision velocity $<w_x>$ at zero inertia is taken out from the raw w_x, the remained is $\Delta w_x = w_x(\beta) - <w_x(\beta \to \infty)>$, the net increase of the collision velocity due to the inertia, and it is quite close to symmetrical and may be approximated by Gaussian distribution. Thus we have

$$<|\Delta w_x|> = \sqrt{\frac{2}{\pi} < \Delta w_x^2 >}, \tag{6.20}$$

where $< \Delta w_x^2 >$ is the net increase of the mean-squared collision velocity due to the inertia as defined by equation (4.20) for identical particles. Substituting $< \Delta w_x^2 >$ by equation (4.20) into (6.20),

$$<|\Delta w_x|> = \sqrt{\frac{2}{\pi}} [- \frac{2}{\beta} <(u_{1x} - u_{2x})(\frac{Du_{1x}}{Dt} - \frac{Du_{2x}}{Dt})> + \frac{2}{\beta^2} <(\frac{Du_x}{Dt})^2> \frac{R^2}{\lambda_D^2}]^{1/2}. \tag{6.21}$$

Denoting $\alpha_{11}(\beta)$ as the collision kernel at arbitrary inertia and $\alpha_{11}(\beta \to \infty)$ as the collision kernel at zero inertia, the net increase of the collision kernel for identical particles due to the inertia is defined as $\delta\alpha_{11}$,

$$\begin{aligned} \delta\alpha_{11} &= \alpha_{11}(\beta) - \alpha_{11}(\beta \to \infty) \\ &= 2\pi R^2 <|\Delta w_x|>, \end{aligned} \tag{6.22}$$

and denoting the normalized collision kernel as

$$\alpha_{11}^* = \frac{\alpha_{11}}{R^3 (\frac{\varepsilon}{\nu})^{1/2}}, \tag{6.23}$$

then the net increase of normalized collision kernel can be expressed as $\delta\alpha_{11}^*$,

$$\delta\alpha_{11}^* = \frac{\delta\alpha_{11}}{R^3 (\frac{\varepsilon}{\nu})^{1/2}}. \tag{6.24}$$

Combining (6.21), (6.22) & (6.24), we have

$$\delta\alpha_{11}^{*}=\sqrt{\frac{8\pi\nu}{\varepsilon}}\,[-\,\frac{2}{\beta R^{2}}<(u_{1x}-u_{2x})(\frac{Du_{1x}}{Dt}-\frac{Du_{2x}}{Dt})>+\frac{2}{\beta^{2}\lambda_{D}^{2}}<(\frac{Du_{x}}{Dt})^{2}>]^{1/2},\tag{6.25}$$

and the net increase of collision rate for the system of a large number of particles due to particle inertia may be written as

$$\delta\,\dot{n}_{c_{11}}=\frac{1}{2}n_{1}^{2}\sqrt{\frac{8\pi\nu}{\varepsilon}}\,R^{2}[-\,\frac{2}{\beta}<(u_{1x}-u_{2x})(\frac{Du_{1x}}{Dt}-\frac{Du_{2x}}{Dt})> + \frac{2}{\beta^{2}}<(\frac{Du_{x}}{Dt})^{2}>\frac{R^{2}}{\lambda_{D}^{2}}]^{1/2}.\tag{6.26}$$

For non-identical particles 1 and 2, the net increase of the normalized collision kernel is

$$\delta\alpha_{11}^{*}=\sqrt{\frac{8\pi\nu}{\varepsilon}}\,[\frac{1}{R^{2}}<(\frac{Du_{x}}{Dt})^{2}>(\frac{1}{\beta_{1}}-\frac{1}{\beta_{2}})^{2}-\frac{2}{R^{2}}<(u_{1x}-u_{2x})(\frac{1}{\beta_{1}}\frac{Du_{1x}}{Dt}-\frac{1}{\beta_{2}}\frac{Du_{2x}}{Dt})> + \frac{2}{\beta_{1}\beta_{2}\lambda_{D}^{2}}<(\frac{Du_{x}}{Dt})^{2}>]^{1/2},\tag{6.27}$$

and the net increase of collision rate due to particle inertia may be expressed as

$$\delta\,\dot{n}_{c_{12}}=n_{1}n_{2}\sqrt{\frac{8\pi\nu}{\varepsilon}}\,R^{2}[<(\frac{Du_{x}}{Dt})^{2}>(\frac{1}{\beta_{1}}-\frac{1}{\beta_{2}})^{2} - 2<(u_{1x}-u_{2x})(\frac{1}{\beta_{1}}\frac{Du_{1x}}{Dt}-\frac{1}{\beta_{2}}\frac{Du_{2x}}{Dt})>+\frac{2}{\beta_{1}\beta_{2}}<(\frac{Du_{x}}{Dt})^{2}>\frac{R^{2}}{\lambda_{D}^{2}}]^{1/2}.\tag{6.28}$$

The present prediction, equation (6.25), differs from the second theory of Saffman & Turner in two aspects. First, $\delta\alpha_{11}^{*}\to 0$ in the limit $\beta\to\infty$, which is consistent with the result of inertialess particles, while Saffman & Turner's second prediction has $\alpha_{11}^{*}=1.67$ which is inconsistent with the first result. Second, the present analysis includes two additional terms for inclusion of the effect of the inertia, as seen from equation (6.25). The effect of inertia does not vanish in (6.25) while it does in Saffman & Turner's prediction when $\beta_{1}=\beta_{2}$, shown in equation (6.17). These two terms would have disappeared if $\frac{Du_{x}}{Dt}$ was assumed to be perfectly correlated or $\lambda_{D}\to\infty$ which was essentially assumed by Saffman & Turner (1956, p.26) by stating that "the air velocities near two close particles are the same". These two additional terms dominate the effect of inertia on the collision kernel for particles of nearly equal inertia.

6.3.3 A Proposed Expression on Collision Kernel

As mentioned previously, in addition to the increased collision kernel due to the increased collision velocity, the collision kernel is also affected by the preferential concentration due to the inertia. In Chapter 5, a net increase of the concentration non-uniformity can be quantified by the new quantity Δ_β, the equation (5.22). To include the effects of both collision velocity and the concentration non-uniformity on the collision kernel due to the inertia, the total collision rate for the system of a large number of identical particles due to the inertia may be expressed as

$$\begin{aligned} \dot{n}_{c_{11}} &= \bar{n}^2 (1+\Delta_\beta)[\alpha^*_{11}(\beta \to \infty)+\delta\alpha^*_{11}(\beta)]\ R^3 (\frac{\varepsilon}{\nu})^{1/2} \\ &= \bar{n}^2\ \alpha^*_{11} R^3 (\frac{\varepsilon}{\nu})^{1/2} \end{aligned} \tag{6.29}$$

where $\bar{n}$ is the mean concentration, $\alpha^*_{11}(\beta \to \infty)$ denotes the normalized collision kernel at zero inertia, $\delta\alpha^*_{11}(\beta)$ is the increased part of normalized collision kernel due to the finite inertia, and α^*_{11} represents the overall normalized collision kernel

$$\alpha^*_{11}=(1+\Delta_\beta)[\alpha^*_{11}(\beta \to \infty)+\delta\alpha^*_{11}(\beta)]. \tag{6.30}$$

It should be mentioned that in previous theories α^*_{11} was treated as a constant, the terms Δ_β and $\delta\alpha^*_{11}(\beta)$ have not been included. The net increase of normalized collision kernel at any inertia is then

$$\begin{aligned} \Delta\alpha^*_{11} &= (1+\Delta_\beta)[\alpha^*_{11}(\beta \to \infty)+\delta\alpha^*_{11}(\beta)] - \alpha^*_{11}(\beta \to \infty) \\ &= \Delta_\beta[\alpha^*_{11}(\beta \to \infty)+\delta\alpha^*_{11}(\beta)]+\delta\alpha^*_{11}(\beta). \end{aligned} \tag{6.31}$$

For small inertia, $\delta\alpha_{11}^{*}(\beta)=\delta\alpha_{11}^{*}$, where $\delta\alpha_{11}^{*}$ is defined by equation (6.25). Combining the equations (5.22), (6.25) & (6.31) yields the final form of the total net increase of normalized collision kernel

$$\Delta\alpha_{11}^{*}=\{[\frac{<n'^2_\beta>}{\bar{n}^2}-\frac{1}{\bar{n}}]_\beta-[\frac{<n'^2(\beta=\infty)>}{\bar{n}^2}-\frac{1}{\bar{n}}]_{\beta=\infty}\}\{\alpha_{11}^{*}(\beta\to\infty)$$
$$+\sqrt{\frac{8\pi\nu}{\varepsilon}}[-\frac{2}{\beta R^2}<(u_{1x}-u_{2x})(\frac{Du_{1x}}{Dt}-\frac{Du_{2x}}{Dt})>+\frac{2}{\beta^2\lambda_D^2}<(\frac{Du_x}{Dt})^2>]^{1/2}\}$$
$$+\sqrt{\frac{8\pi\nu}{\varepsilon}}[-\frac{2}{\beta R^2}<(u_{1x}-u_{2x})(\frac{Du_{1x}}{Dt}-\frac{Du_{2x}}{Dt})>+\frac{2}{\beta^2\lambda_D^2}<(\frac{Du_x}{Dt})^2>]^{1/2}. \tag{6.32}$$

Equation (6.32) is referred as "unified expression" of the collision kernel for simplicity in the following discussions. Obviously, $\Delta\alpha_{11}^{*}$ is a complicated function of the inertia instead of constant or zero-value predicted by previous theories.

6.4 Comparison of the Analysis with Simulation Results

In this section, only monodisperse particles in Gaussian turbulence are considered, and "THROW AWAY" collision model is employed. The variation of the collision kernel with particle inertia, size, number concentration and gravitational settling will be discussed in succession.

6.4.1 Effect of Particle Inertia

To isolate the effect of the inertia on the collision kernel in our simulation and compare with the unified expression (6.32), the inertialess part of collision kernel $\alpha_{11}^{*}(\beta\to\infty)$ must be taken out from the raw collision kernel $\alpha_{11}^{*}(\beta)$. The inertial part of collision kernel is then obtained as $\Delta\alpha_{11}^{*}=\alpha_{11}^{*}(\beta)-\alpha_{11}^{*}(\beta\to\infty)$. Figures 6.2 (a) & (b) show the variation of the collision kernel $\Delta\alpha^*_{11}$ with the inertia. The contributions from the preferential concentration, Δ_β, and from the collision velocity increase, $\delta\alpha^*_{11}$, due to inertia are also plotted. To facilitate a comparison between the prediction and simulation, the unified prediction based on equation (6.32) is also plotted in figure 6.2 (a), where the particle size is less than Kolmogorov length scale, i.e. $D/\eta=0.957$. Figure 6.2 (b) shows similar results for larger particle size at $D/\eta=2.522$. The inertial increase $\delta\alpha^*_{11}$ due to the increased collision velocity is calculated based on equation (6.25) using the multiplication factor obtained at zero inertia. The inertial part due to the preferential concentration is obtained by taking the maximum of the Δ_β curves over the whole range of the cell sizes discussed in Chapter 5. It is noted that the application of the multiplication factor obtained at zero inertia may be only meaningful for small inertia. The unified prediction is then computed by equation (6.32) based on $\delta\alpha^*_{11}$ and Δ_β determined. The inertial part of normalized collision kernel $\Delta\alpha^*_{11}$ increases as the inertia increases. The inertial increase $\Delta\alpha^*_{11}$ is observed to reach a maximum at $\beta\tau_k=0.146$ and decreases thereafter for both $D/\eta=0.957$ and $D/\eta=2.522$. However, the maximum Δ_β due to inertia is reached at $\beta\tau_k=0.5$ for both $D/\eta=0.957$ and $D/\eta=2.522$, as discussed in Chapter 5. The reason for the maximum $\Delta\alpha^*_{11}$ is that increasing the inertia decorrelates particles from the turbulent flow, and both the collision velocity and concentration non-uniformity increase, so the collision kernel is enhanced. However, the inertial increase will also reduce the ability for particles to pick up energy from the turbulence. Further increase of the inertia will eventually disable particles to get energy from the neighboring fluid and particles tend to be randomly distributed so that the concentration non-uniformity will be reduced till disappeared. Comparison between figures 6.2 (a) & (b) also shows quite different magnitudes of the increased collision kernel by different particle sizes, that is, more enhancement of the collision kernel is observed as the size becomes smaller. It is noted that the predicted $\Delta\alpha^*_{11}$ based on the unified expression appears to agree with the simulation for small inertia particles. However, large deviation is seen for $\beta\tau_k < 2$. This is expected since the asymptotic analysis assumes small particle inertia.

6.4.2 Effect of Particle Size

In order to understand the effects of particle size and concentration, zero inertia is first considered. Figures 6.3 & 6.4 show the collision kernel as a function of the size at different range of particle concentration. Figure 6.3 is for very dilute particle concentration. Only 500 particles for the size $D/\eta=0.435$, 300 particles for $D/\eta=0.609$, 200 particles for $D/\eta=0.87$ and 50 particles for $D/\eta=0.957$, 2.522, 3.478 are used in the simulation. The reason for using such dilute concentration is to avoid the dependence of the collision kernel on the post-collision treatment, as discussed in Chapter 3. Further discussions on the effects of the post-collision treatment will be given in §6.6. Since the particles have zero inertia in figures 6.3 & 6.4, the effect of particle size on the normalized collision kernel can be clearly observed. The normalized collision kernel obtained by simulation is expected to recover the theoretical prediction ($\alpha^*_{11}=1.271$) as particle size approaches to the small limit ($D/\eta<<1$). However, increasing particle size will reduce the normalized collision kernel. It appears difficult to investigate the collision kernel for very small particles because of enormous computer capacity required, and it is also infeasible to investigate the collision kernel for large size $D/\eta>5$ in a "very dilute regime", because keeping "very dilute concentration" may not have enough particles to generate reliable statistics while a given enough number of particles may violate the condition "very dilute concentration". It is seen from figure 6.3 that α^*_{11} approaches constant for large particles. Figure 6.4 shows the effect of particle size on the collision kernel for large number of particles, where the total particles are N=36000 - 500 and the corresponding sizes are $D/\eta=0.217$ - 13.36. Compared with figure 6.3, the difference is that the magnitudes of the collision kernel are smaller and continue reducing as the size increases after $D/\eta>8$. The dependence of the normalized collision kernel α^*_{11} on the size, shown in figures 6.3 & 6.4, reveals that the simple cubic law ($\alpha_{11} \sim R^3$) can not accurately describe the effect of particle size on the collision kernel α_{11}.

6.4.3 Effect of Particle Mean Concentration

Based on the results of the effect of particle size on the collision kernel in §6.4.2, different magnitudes of the collision kernel observed between figure 6.3 and figure 6.4 gave us a hint that the average particle concentration may also affect α_{11}^*. This has been confirmed by figure 6.5, where the total number of particles N=500, 1,000, 5,000, 12,000 and 24,000 with a diameter $D/\eta=0.435$ are used for five sets of direct numerical simulations. It clearly shows that the increase in the particle concentration will reduce α_{11}^*.

6.4.4 Effect of Particle Gravitational Settling

As discussed in §1.3, Saffman & Turner's prediction of collision kernel for monodisperse particles reduced to a constant $\alpha_{11}^*=1.67$ in the presence of gravity. To examine their results, a set of numerical simulations is carried out with inclusion of particle gravity. In figure 6.6, the effects of gravitational settling on the collision kernel α_{11}^* are plotted against the settling velocity for the particles of diameter $D/\eta=2.52$ with inertia at $\beta\tau_k=1.023$. As contrast with Saffman & Turner's prediction, increase in particle settling velocity will reduce the collision kernel. The collision kernel drops down quickly as settling velocity increases from 0 to 8, and further increase of settling velocity causes the collision kernel to be reduced slowly. The reason for above effect may be explained as follows. The turbulence is consisted of numerous eddies ranging from small eddies to large eddies. Large eddies are responsible for advecting both the particles and small eddies. The relative velocity between nearby particles is mainly generated by the small eddies which are critical to the particle collisions. As the settling velocity increases, the time period for the particles moving through the small eddies decreases, thus the effects of the small eddies on the particles also decrease. Due to the decreasing effects of the small eddies on the particles, the relative velocity between nearby particles decreases. This has been confirmed by figure 6.7 (a), which shows that the collision velocity indeed decreases as the settling velocity increases. Decreasing effects of the small eddies will also reduce the forces driving particles to form preferential concentration seen in figure 6.7 (b). It clearly shows that the concentration non-uniformity varies with settling velocity in a similar way as the collision kernel does.

6.5 Collision Rate in Polydisperse Suspension

In the following simulations, monosize particles are initially introduced into the system, and the "KEEP ALL" collision model is applied to consider the particle agglomeration and size evolution. The same turbulence as above is generated. The number of particles will decrease as the collision proceeds and large particles are formed. The particle size evolution and the variation of the collision kernel with particle inertia and gravitational settling will be discussed as follows.

Figures 6.8 (a) & (b) show the turbulence ensemble average of the collision kernel against time for inertialess polydisperse particles. The collision kernel decreases at the beginning and becomes stable after $T/\tau_k > 7.0$. The difference between the simulation and prediction may be due to the effects of both the mean particle concentration and the size, as mentioned in §6.4.2 and §6.4.3. The collision kernel against turbulence realization is given in figures 6.9 (a) & (b). Very smooth collision kernels are obtained by forty turbulence realizations for polydisperse particles at the inertia $\beta\tau_k = \infty$, 1.023, 0.512 & 0.292.

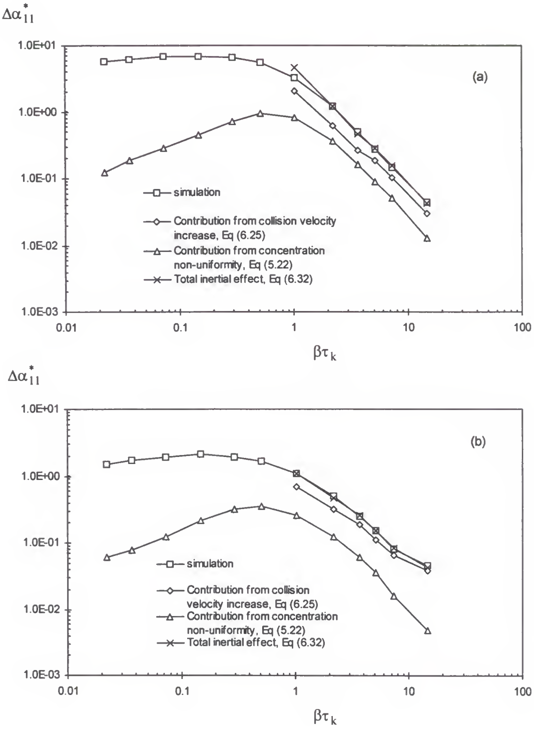

Figure 6.2 The effect of particle inertia on the increased collision kernel $\Delta\alpha^*_{11}$ for monodisperse particles for (a) $D/\eta=0.957$. (b) $D/\eta=2.52$.

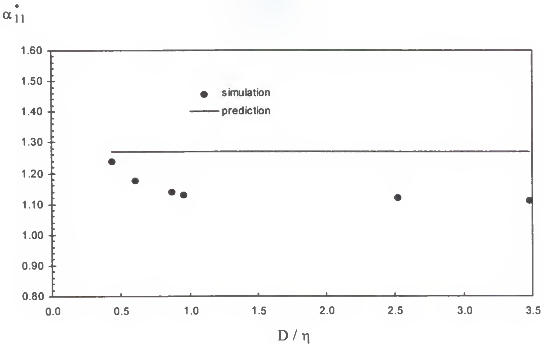

Figure 6.3 The effect of particle size on the collision kernel α^*_{11} for monodisperse particles at a very dilute system. $\beta\tau_k = \infty$.

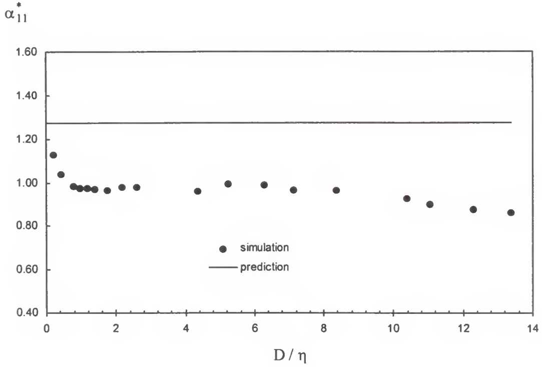

Figure 6.4 The effect of particle size on the collision kernel α^*_{11} for monodisperse particles at 'not' very dilute system. $\beta\tau_k = \infty$.

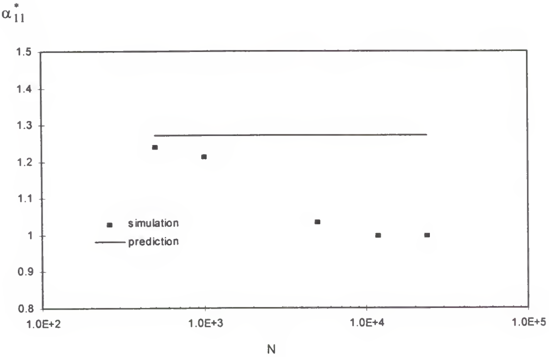

Figure 6.5 Variation of the collision kernel α^*_{11} against particle number concentration for monodisperse particles. $\beta\tau_k = \infty$, D/η=0.435.

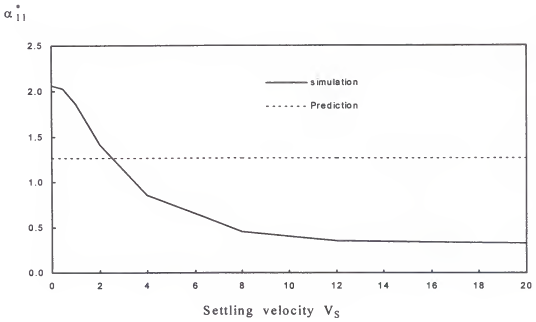

Figure 6.6 The effect of gravitational settling on the collision kernel α^*_{11} for monodisperse particles. $\beta\tau_k$=1.023, D/η=2.52.

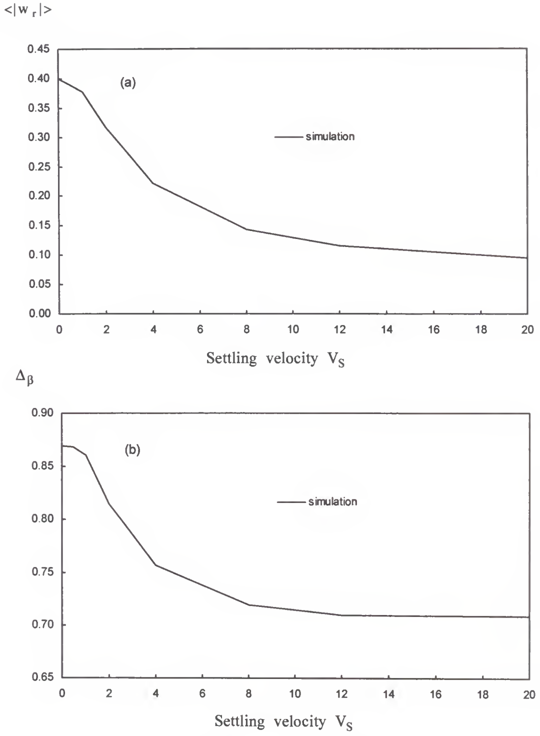

Figure 6.7 The effect of gravitational settling for monodisperse particles. $D/\eta=2.52$, $\beta\tau_k=1.023$. (a) on the collision velocity. (b) on the concentration non-uniformity.

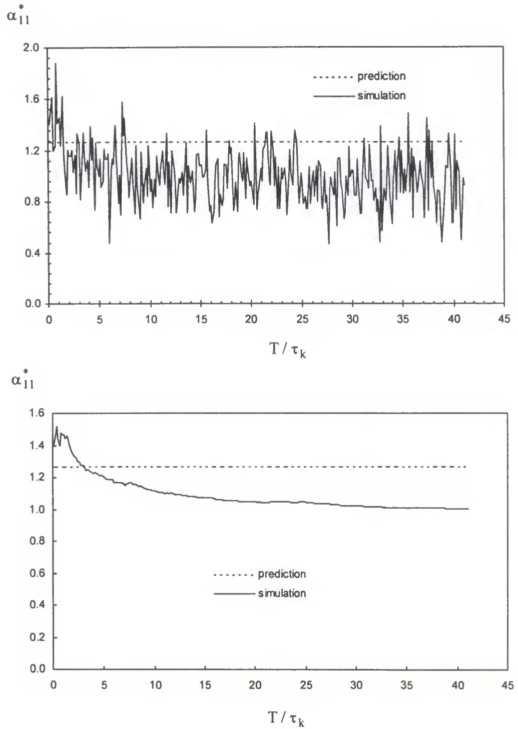

Figure 6.8 Collision kernel α^*_{11} of polydisperse particles against time. $\beta\tau_k = \infty$, D/η=0.957. (a) Variation of the collision kernel. (b) Cumulative average.

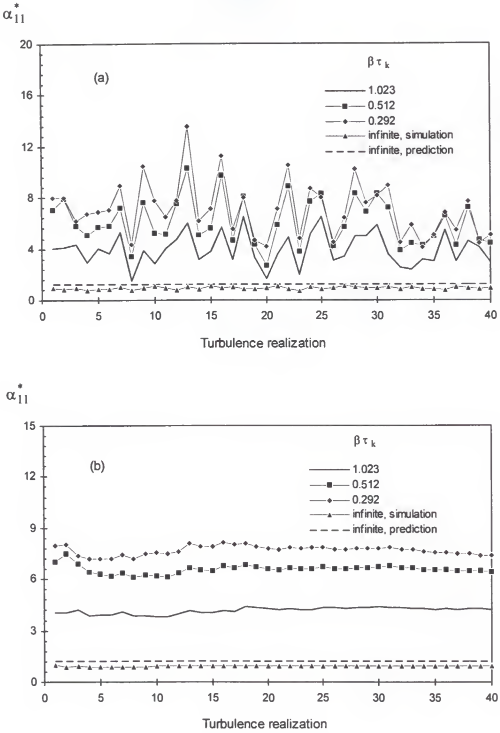

Figure 6.9 Collision kernel α^*_{11} of polydisperse particles with various inertia against turbulence realization. D/η=0.957. (a) Variation of the collision kernel. (b) Cumulative average of the collision kernel.

6.5.1 Particle Size Spectrum

Figure 6.10 shows the size distribution at three time instants. The slope of the size evolution keeps changing as the collision proceeds with time. It appears that no dynamic equilibrium of particle size spectrum exists in present particle-laiden system, while a slope of -2 was reported by Pearson et al (1984) and Balachandar (1988) for the so-called dynamic equilibrium of particle size distribution. It is noted that a constant rate of primary particles was introduced into the system and large particles were removed from the systems in Monte Caro simulations of Pearson et al. and in Balachandar, while present simulation does not add any extra particles or remove any large particles. Figures 6.11 (a) & (b) show the number evolution of both primary and secondary size particles, where 5,000 particles of diameter D/η=0.957 are initially distributed. It is seen that the instant number of primary particles and the generation of secondary size particles are greatly affected by particle inertia. The population of new particles grows quickly as the inertia increases.

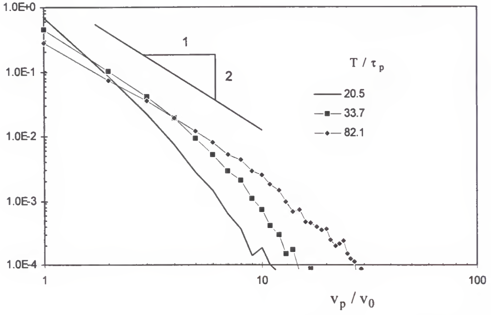

Figure 6.10 The evolution of particle size distribution at various instants for polydisperse particles. D/η=2.17, $\beta\tau_k$=1.023.

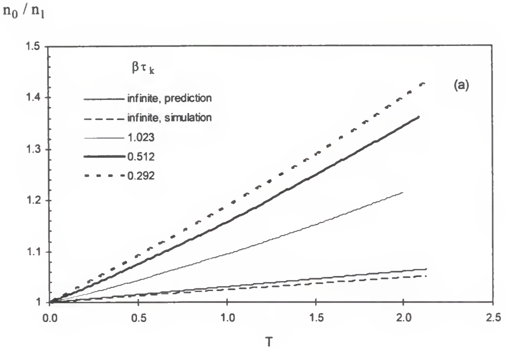

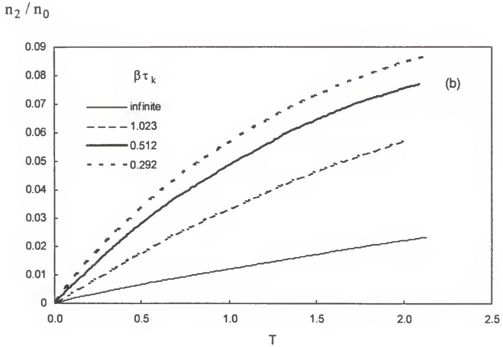

Figure 6.11 Inverse of total number of particles against time for polydisperse particles. $D/\eta=0.957$. (a) primary size (v_0) particles. (b) secondary size ($2 v_0$) particles.

6.5.2 Effect of Particle Inertia

To investigate the effects of the inertia on the collision kernel for polydisperse particles, the inertial part of collision kernel $\Delta\alpha_{11}^{*}=\alpha_{11}^{*}(\beta)-\alpha_{11}^{*}(\beta\rightarrow\infty)$ is calculated first. Figures 6.12 (a) & (b) show the variation of the collision kernel $\Delta\alpha_{11}^{*}$ with the inertia. The effects of the increase in inertia on Δ_{β}, $\delta\alpha_{11}^{*}$ and the unified prediction (6.32) are also plotted in figures 6.12 (a) & (b) for comparison. The particle sizes are D/η=0.957 and 2.52 in figures 6.12 (a) & (b) respectively. The number of particles used in simulation is 5,000 and 2,000 respectively. Similar to the monodisperse suspension, the $\delta\alpha_{11}^{*}$ due to increased collision velocity is calculated based on the prediction (6.25) using the multiplication factor obtained by inertialess polydisperse particles, and the inertial part due to the preferential concentration is collected based on the maximum of the Δ_{β} curves. It should be pointed out that the Δ_{β} curves for polydisperse suspension are obtained by calculating the concentration non-uniformity among the primary size particles, so that it represents the pure contribution from the non-uniform distribution of primary particles. The unified prediction is obtained by $\delta\alpha_{11}^{*}$ and Δ_{β} determined. It is seen that the inertial part of the collision kernel increases as the inertia increases. Similar to monodisperse particles, the inertial part $\Delta\alpha_{11}^{*}$ is also observed to reach a maximum at $\beta\tau_{k}$=0.146 and decreases thereafter for both D/η=0.957 and D/η=2.522, and the maximum Δ_{β} due to inertia is also reached at $\beta\tau_{k}$=0.5 for both D/η=0.957 and D/η=2.522. The reason for the maximum $\Delta\alpha_{11}^{*}$ is similar to the monodisperse particles. Increasing the inertia decorrelates particles from the turbulent flow, and both the collision velocity and particle non-uniformity increase, so the collision kernel is enhanced. However, increasing inertia will also reduce the ability for particles to pick up energy from the turbulence. Further increase of the inertia will eventually disable particles to get energy from the neighboring fluid and particles tend to be randomly distributed so that the concentration non-uniformity will be disappeared. It is observed by comparison between figures 6.12 (a) & (b) that larger collision kernel is obtained by smaller size $D/\eta=0.957$. Since all parameters used in figures 6.12 (a) & (b) are the same except the size of primary particles, it is evident that particle size has a significant effect on the enhancement of the inertial part $\Delta\alpha_{11}^{*}$. It is also noted that the unified prediction of collision kernel $\Delta\alpha_{11}^{*}$ seems to be in agreement with the simulation at small inertia for polydisperse particles. Similar to the monodisperse particles, large deviation is observed for $\beta\tau_k < 2$. This is also expected since the asymptotic analysis assumes small particle inertia. As seen from previous discussions, the collision kernel is complicated by the collision velocity and preferential concentration and possibly also by the compressibility of the particle velocity field. Based on the simulation results of both monodisperse particles and polydisperse particles, however, it may be concluded that the increases in both collision velocity and preferential concentration due to the inertia are the dominant factors enhancing the collision kernels for small inertial particles.

6.5.3 Effect of Particle Gravitational Settling

The effect of gravitational settling on the collision kernel α_{11}^{*} can be found in figure 6.13. The increase in particle settling velocity will reduce the collision kernel of polydisperse particles. The collision kernel varies rapidly in the region $0<V_s<8$ and then slows down and seems to approach a constant at $V_s>8$. The similar mechanisms as discussed in previous section may be applied here to explain the similar physics for polydisperse particles. Because of the decreasing effects of the small eddies on the particles, the collision velocity is expected to decrease as the settling velocity increases, as shown in figure 6.14 (a). Similarly, the concentration non-uniformity of polydisperse particles is also expected to decrease as the gravitational settling is enhanced, which has been consistently shown by the figure 6.14 (b). It is also observed that small difference between the figures 6.14 (a) & (b) and figures 6.7 (a) & (b) is consistent with the similar comparison of the collision kernel between the figure 6.13 and figure 6.6.

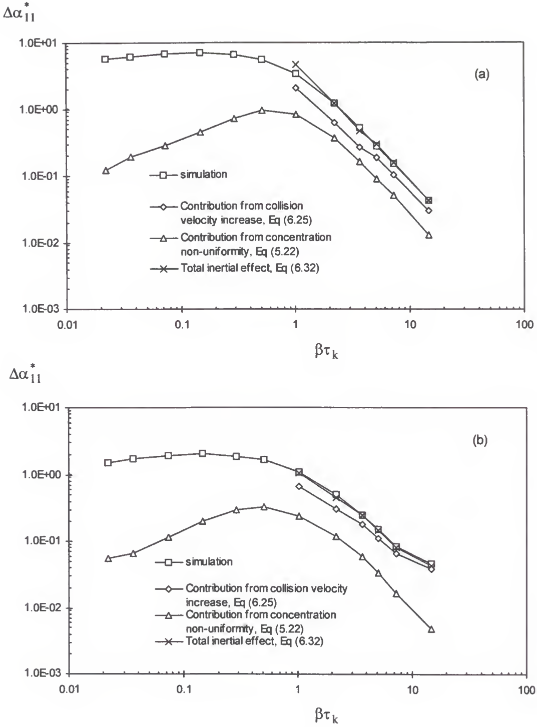

Figure 6.12 The effect of particle inertia on the increased collision kernel $\Delta\alpha_{11}^*$ for polydisperse particles for (a) $D/\eta=0.957$. (b) $D/\eta=2.52$.

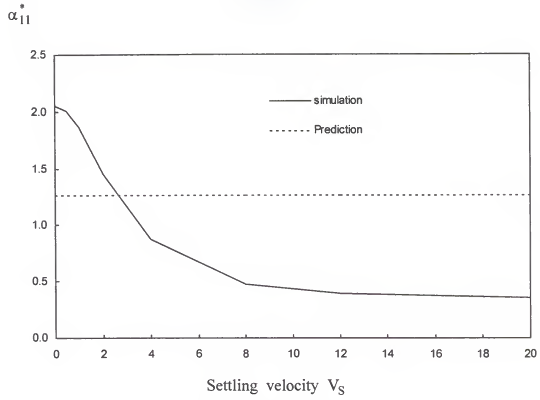

Figure 6.13 The effect of gravitational settling on the collision kernel α^*_{11} for polydisperse particles. $\beta\tau_k$=1.023, D/η=2.52.

6.6 Collision Rate in Hard Sphere Suspension and Assessment of Collision Models

As mentioned in chapter 2, the "HARD SPHERE" model generates multiple collisions and may not be used for particles with small inertia. In addition to the issue on multiple collisions, we have found that Smoluchowski's result in laminar shear flow cannot be recovered by the "HARD SPHERE" collision model. Figures 6.15 (a) & (b) show the simulation results of hard sphere particles in laminar shear flow with various shear rates and inertia. Figures 6.16 (a) & (b) show the comparison of three collision models with Smoluchowski's prediction. While the "KEEP ALL" and "THROW AWAY" models can give good agreement with the Smoluchowski's result, the "HARD SPHERE" model, however, underpredicts the collision kernel by a large percentage.

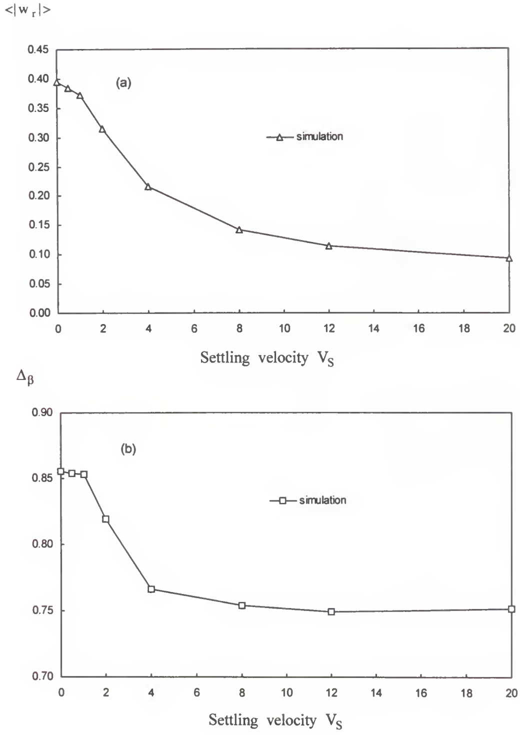

Figure 6.14 The effect of gravitational settling for polydisperse particles. $D/\eta=2.52$, $\beta\tau_k=1.023$. (a) on the collision velocity. (b) on the concentration non-uniformity.

Figures 6.17 (a) & (b) show the effect of particle inertia on the collision kernel using "HARD SPHERE" model in Gaussian turbulence. Maximum collision kernel is reached at $\beta\tau_k$=2.192 does not make sense, which is mainly due to multiple collision mechanism as discussed above. The fact that the collision kernel increases with time even at $\beta\tau_k$=1.023 may suggest that the "HARD SPHERE" model may be appropriate for simulating collision kernel only if $\beta\tau_k$<<1. It is seen from figures 6.17 (a) & (b) that the collision kernel appears to reach steady value at $\beta\tau_k$=0.512 or 0.146. Figures 6.18 (a) & (b) show the comparison of three collision models for prediction of the collision kernel α^*_{11} at $\beta\tau_k$=1.023. The collision kernels against time can be observed for the "KEEP ALL" and "THROW AWAY" models and good agreement is also obtained between these two models, while the "HARD SPHERE" model results in twice the collision kernel and seems still diverging as βT=51. The comparison among three collision models at a larger inertia, $\beta\tau_k$=0.292, is given in figures 6.19 (a) & (b). The good agreement between the "KEEP ALL" and "THROW AWAY" model is again observed. Although the collision kernel obtained by using "HARD SPHERE" model is steady at $\beta\tau_k$=0.292, it differs considerably from the results of other two models.

6.7 Summary and Conclusions

The classical result of Smoluchowski for the collision rate of monodisperse particles in a laminar shear flow is shown to be inaccurate due to the inclusion of the self-collisions. The present work extends Smoluchowski's result by excluding the self-collisions in the counting of collision pairs. A numerical simulation for particle collisions in a laminar shear flow at very low concentration is carried out to validate the extended result of Smoluchowski.

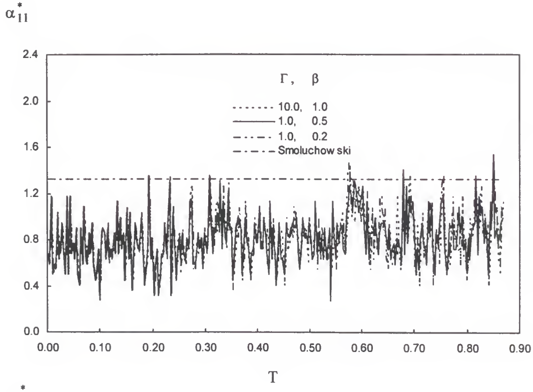

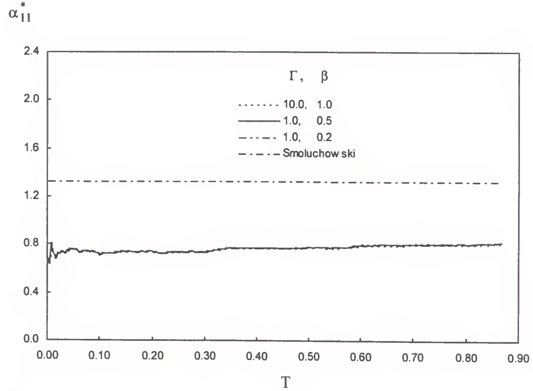

Figure 6.15 Collision kernel α^*_{11} of hard sphere particles with various inertia against time in laminar shear flow. D=0.04. (a) Variation of the collision kernel. (b) Cumulative average.

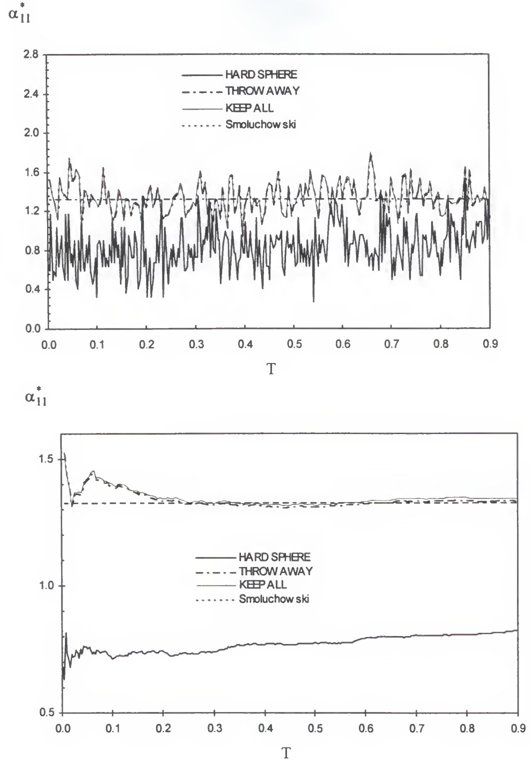

Figure 6.16 The effects of the collision schemes on the collision kernel α^*_{11} against time in laminar shear flow. Γ=1.0, D=0.04. (a) Variation of the collision kernel. (b) Cumulative average of the collision kernel.

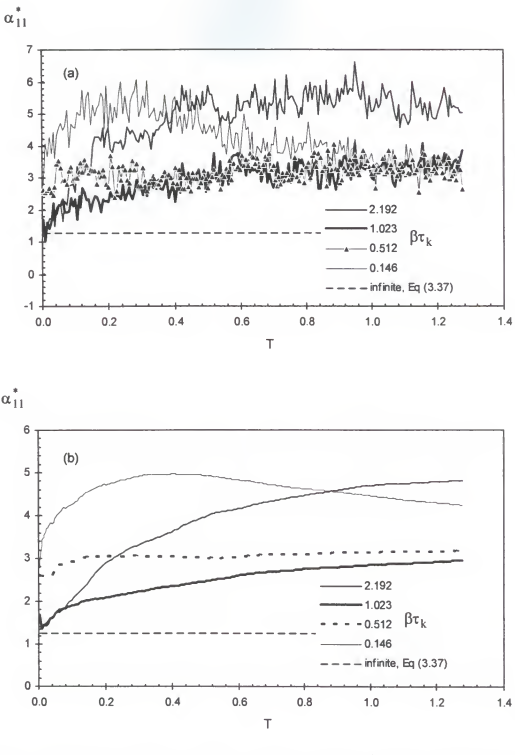

Figure 6.17 The effects of the inertia on the collision kernel α^*_{11} against time for hard sphere particles in Gaussian turbulence. D/η=0.957. (a) Variation of the collision kernel. (b) Cumulative average of the collision kernel.

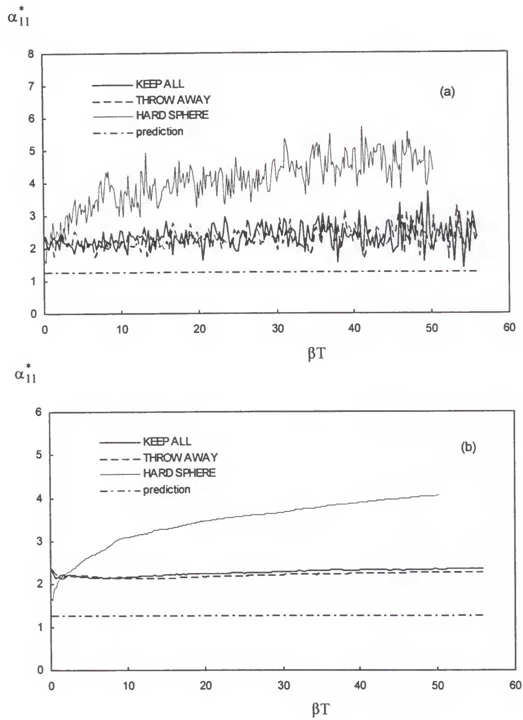

Figure 6.18 The effects of the collision schemes on the collision kernel α^*_{11} against time in Gaussian turbulence. $D/\eta=2.174$, $\beta\tau_k=1.023$. (a) Variation of the collision kernel. (b) Cumulative average of the collision kernel.

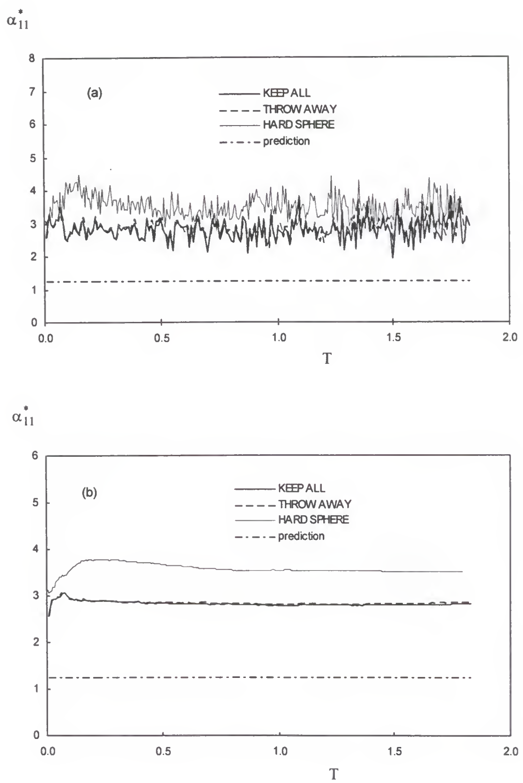

Figure 6.19 The effects of the collision schemes on the collision kernel α^*_{11} of hard sphere particles in Gaussian turbulence. $D/\eta=0.957$, $\beta\tau_k=0.292$. (a) Variation of the collision kernel. (b) Cumulative average of the collision kernel.

The theoretical prediction of the collision kernel for zero inertia particles is critically examined by carrying out the direct numerical simulation at a very dilute concentration with small number of particles in isotropic, Gaussian turbulence. It is found that the simulation results of finite size particles ($D/\eta \geq 0.435$) are asymptotically approaching to the theoretical prediction. The normalized collision kernel α^*_{11} decreases as particle size increases, while α^*_{11} is a constant based on all theoretical predictions. The direct numerical simulations at a dilute concentration with a large number of particles have also been carried out for examining the size effect on α^*_{11} in the turbulence. The normalized collision kernel α^*_{11} decreases as particle size increases. The effect of particle mean concentration on α^*_{11} is examined. It is found that α^*_{11} decreases as the mean concentration increases, while previous theories showed no effect of the mean concentration on α^*_{11}.

The effect of particle inertia on the collision kernel is investigated by both analysis and numerical simulations in an isotropic, Gaussian turbulence. A unified expression of the collision kernel including effects of the increased collision velocity and concentration non-uniformity is proposed for small inertia. Good agreement is obtained between the simulation results and the unified expression for particles with small inertia.

In contrast to Saffman & Turner's prediction for the effect of particle gravity on the collision kernel. The gravitational settling is found to reduce the collision kernel among monodisperse particles. Sharp decrease in the collision kernel is observed when the dimensionless settling velocity increases from 0 to 8, and further increase in the settling velocity will also result in the decrease of the collision kernel but a slow rate of decrease.

The effect of various collision models on the collision kernel is also examined. It is found that the theoretical prediction of collision rate at small size and zero inertia limit can be recovered by both "THROW AWAY" and "KEEP ALL" models, while the "HARD SPHERE" model cannot be used for prediction of collision rate at small inertia even for laminar shear flow due to the multiple collision mechanism. Reliable calculation for the collision kernel using the "HARD SPHERE" model requires extremely small time step for small inertia particles. Steady values of collision kernel can be reached only for very large inertia using "HARD SPHERE" model. In general, the collision kernel based on the "HARD SPHERE" model is larger than the results obtained by both the "THROW AWAY" and "KEEP ALL" models for particles with large inertia in Gaussian turbulence.

CHAPTER 7
SUMMARY AND CONCLUSIONS

A new theoretical framework is developed to evaluate the collision rate and collision velocity of very small particles in *general* turbulent flows. The classical results for the collision kernel by Smoluchowski (1917) for laminar shear flow and by Saffman & Turner (1956) for isotropic turbulence are recovered. The present approach differs significantly from that of Saffman & Turner in that the ensemble average is taken after the collision rate for a given flow realization is calculated. This avoids the assumption of isotropy and allows for the evaluation of the collision rate in general turbulent flows. The collision velocity predicted in both laminar shear flow and isotropic turbulence agrees well with the results from direct numerical simulation of particle collisions. The present theory is used to evaluate the collision rate and velocity of small particles in the rapidly sheared homogeneous turbulence. It is found that the effect of the turbulence structure on the collision rate and velocity can be mainly captured by using the mean turbulent shear rate $(\varepsilon/\nu)^{1/2}$. The combined effects of the mean shear and the sheared turbulence on the collisions are elucidated. Simple interpolations are developed to evaluate the collision rate and velocity for arbitrary mean flow shear rate and turbulence mean shear rate.

As particle inertia increases, the collision velocity increases and particle concentration becomes increasingly non-uniform. These factors significantly affect the particle collision rate in turbulence. The effect of inertia on the collision rate is examined by considering these two distinctive contributions: the effect of the increased collision velocity and the effect of the increasing concentration non-uniformity.

Numerical and analytical studies on particle collisions in isotropic and Gaussian turbulence are carried out. The effect of particle inertia on the collision velocity is examined. An asymptotic analysis is developed to predict the effect of small particle inertia on the particle collision velocity. Asymptotic prediction for the increased collision velocity agrees well with the results of numerical simulation. The collision velocity is found to contain terms that are proportional to $(\beta\tau_k)^{-1}$ and $(\beta\tau_k)^{-2}$. The effects of both particle inertia and size on the collision angle are examined through numerical simulations. The collision angle depends strongly on the particle inertia and particle size. The average collision angle and the standard deviation of the collision angle increase with the increases of both inertia and particle size.

In order to examine the effect of concentration non-uniformity on the collision rate quantitatively, a new method has been developed to quantify the particle concentration non-uniformity using a concentration non-uniformity parameter. The concentration non-uniformity parameter is the ratio of the variance of particle concentration to the square of average particle concentration with inherent statistical noise removed. The effects of both particle size and inertia on the concentration non-uniformity are quantitatively examined. The concentration non-uniformity will be greatly overestimated if the effect of finite particle size is not included. For sizeless particles with particle response time comparable to the turbulence Kolmogorov time scale, the measure of concentration non-uniformity parameter is inversely proportional to the cell length Δx, in which the concentration non-uniformity is measured, for small values of Δx. However, for finite-size particles, the concentration non-uniformity parameter reaches a maximum value instead of unbounded for sizeless particles. For finite-size particles, the maximum non-uniformity is reached at $\Delta x/D = 2.0$~3.5 while it becomes zero when $\Delta x/D$ is close to one. Particle size is an important quantity that affects particle concentration non-uniformity. The maximum value of the concentration non-uniformity is reached when particle response time is close to the Kolmogorov time scale.

The effects of the inertia on the collision velocity and concentration non-uniformity are combined to predict the effect of particle inertia on the collision kernel. A unified expression of the collision kernel including both of these is proposed for small inertia. Good agreement is obtained between the simulation results and the unified expression for particles with small inertia.

The effect of particle size on the collision kernel in turbulence is examined for particles with zero inertia at a very dilute concentration limit. The normalized collision kernel $\alpha_{11}^{*} = \alpha_{11} / [R_{ii}^{3} (\varepsilon / \nu)^{1/2}]$ decreases as particle size increases. The theoretically predicted value for α_{11}^{*} is only asymptotically observed in the small size and very dilute limit. At higher concentration, α_{11}^{*} is also observed to decrease with increasing particle size. As the mean concentration increases, α_{11}^{*} decreases which suggests that the theoretically predicted value for α_{11}^{*} is only valid in a very dilute limit.

The classical result of Smoluchowski for the collision rate of monodisperse particles in a laminar shear flow is shown to be inaccurate due to the inclusion of the self-collisions. The present work extends Smoluchowski's result by excluding the self-collisions in the counting of collision pairs. The extended result for the collision rate is validated by a numerical simulation for particle collisions in a laminar shear flow at very low concentration.

Finally, the effect of various collision models on the collision kernel is investigated. Theoretical prediction for collision rate at small size and zero inertia limit can be recovered by both "THROW AWAY" and "KEEP ALL" models, while the "HARD SPHERE" model cannot be used for predicting the collision rate at small inertia even in laminar shear flow due to an unphysically large number of multi-collisions between the same pair. Calculation of the collision kernel using the "HARD SPHERE" model requires extremely small time step for small inertia particles. Steady values of collision kernel can be reached only for very large inertia using "HARD SPHERE" model. In general, the collision kernel based on the "HARD SPHERE" model is larger than the results obtained by both the "THROW AWAY" and "KEEP ALL" models for particles with large inertia in Gaussian turbulence.

REFERENCES

Abrahamson, J. 1975 "Collision rates of small particles in a vigorously turbulent fluid," Chemical Engineering Science 30, 1371-1379.

Bachalo, W. D. , Bachalo, E. J. , Hanscom, J. & Sankar, S. V. 1993 "An investigation of spray interaction with large-scale eddies," AIAA 93-0696.

Balachandar, S. 1988 "Particle Coagulation in Homogeneous Turbulence," Ph.D. thesis, Division of Engineering, Brown University, RI.

Beard, K. V. & Ochs, H. T. 1983 "Measured collection efficiencies for cloud drops," J. Atmos. Sci. 40, 146-154.

Camp, T. R. & Stein, P. C. 1943 "Velocity gradients and internal work in fluid motion," J. Boston Soc. Civil Engrs. 30, 219-228.

Chen, M., Kontomaris, K. & Mclaughlin, J. B. 1995 "Dispersion, growth, and deposition of coalescing aerosols in a direct numerical simulation of turbulent channel flow," Gas-particle Flow, FED-Vol. 228, 27-32.

Chein, R. & Chung, J. N. 1987 "Effects of vortex pairing on particle dispersion in turbulent shear flows," Int. J. Multiphase Flow 13, 785-802.

Chein, R. & Chung, J. N. 1988 "Particle dynamics in a gas-particle flow over normal and inclined plates," Chem. Engng Sci. 43, 1621-1636.

Chung, J. N. & Troutt, T. R. 1988 "Simulation of particle dispersion in an axisymmetric jet," J. Fluid Mech. 186, 199-222.

Crowe, C. T., Chung, J. N. & Troutt, T. R. 1988 "Particle mixing in free shear flows," Prog. Energy Combust. Sci. 14, 171-194.

Crow, C, T., Trout, T. R. & Chung, J. N. 1996 "NumericaJ models for two-phase turbulent flows," Annu.Rev. Fluid Mech. 28, 11-43.

Davies, R. N. 1953 Dust is dangerous, Faber and Faber Limited, London.

Delichatsios, M. A. 1980 "Particle coagulation in steady turbulent flows: application to smoke aging," J. Colloid and Interface Science, 78, 163-174.

Eaton, J. K. & Fessler, J. R. 1994 "Preferential concentration of particles by turbulence," Int. J. Multiphase Flow 20, suppl., 169-209.

Fathikalajahi, J., Taheri, M. & Talaie, M.R. 1996 "Theoretical study of nonuniform droplets concentration distribution on venturi scrubber performance," Particulate Science and Technology 14, 2, 153-164.

Fung, J. C. H. & Perkins, R. J. 1989 "Particle trajectories in turbulent flow generated by true-varying random Fourier modes," In Advances in Turbulence 2 (Edited by Fernholz, H. H. & Fiedler, H. E.), Springer, New York.

Gunaraj, J. A. & Tabakoff, W. & Siravuri, S. 1997 "Experimental investigation of solid particles interaction in particulate flow," The Proceedings of the 1997 ASME Fluids Engineering Division Summer Meeting, FEDSM97-3628, Vancouver, British Columbia, Canada, June 22-26.

Hansell, D., Kennedy, I. M. & Kollman, W. 1992 "A simulation of particle dispersion in a turbulent jet," Int. J. Multiphase Flow 18, 559-576.

Hocking, L. M. & Jonas, P. R. 1970 "The collision efficiency of small drops," Q. J. R. Met. Soc. 96, 722-729.

Hu, K. C. & Mei, R. 1998 "On particle collision rate in fluid flows," Phys. Fluids. 10, 4, 1028-1030.

Hu, K. C. & Mei, R. 1997 "Effect of inertia on the particle collision coefficient in Gaussian turbulence," The Proceedings of the 1997 ASME Fluids Engineering Division Summer Meeting, FEDSM97-3608, Vancouver, British Columbia, Canada, June 22-26.

Hunt, J. C. R. & Carruthers, D. J. 1990 "Rapid distortion theory and the 'problems' of turbulence," J. Fluid Mech., 212, 497-532.

Hunt, J. C. R., Buell, J. C. & Wray, A. A. 1987 "Big whorls carry little whorls," In Proceedings of the Summer Program 1987, Center for Turbulence Research, Stanford University, Calif.

Hunt, J. R. 1982 "Self-similar particles-size distributions during coagulation: theory and experimental verification," J. Fluid Mech. 122, 169-185.

Ishima, T., Hishida, K. & Maeda, M. 1993 "Effect of particle residence time on particle dispersion in a plane mixing layer," Trans ASME, J. Fluids Engng 115, 751-759.

Jonas, P. R. & Goldsmith, P. 1972 “The collection efficiencies and small droplets falling through a sheared air flow,” J. Fluid Mech. 52, 593-608.

Kamalu, N., Wen, F., Troutt, T. R., Crowe, C. T. & Chung, J. N. 1988 “Particle dispersion by ordered motion in mixing layers,” ASME Cavitation Multiphase Flow Forum FED 64, 150-154.

Kallio, G. A. & Reeks, M. W. 1989 “A numerical simulation of particle deposition in turbulent boundary layers,” Int. J. Multiphase Flow 15, 433-446.

Kim, J., Moin, P. & Mosers, R. D. 1987 "Turbulence statistics in fully developed channel flow at low Reynolds number," J. Fluid Mech., 177, 133-166.

Klett, J. D. & Davis, M. H. 1973 “Theoretical collision efficiencies of cloud droplets at small Reynolds numbers,” J. Atmos. Sci. 30, 107-118.

Kobayashi, H., Masutani, S. M., Azuhata, S., Arashi, N. & Hishinuma, Y. 1988 “Dispersed phase transport in a plant mixing layers,” In Transport Phenomena in Turbulent Flow, Hemisphere, New York, 433-446.

Kraichnan, R. 1970 "Diffusion by a random velocity field," Phys. Fluids 13, 22-31.

Kruis, F. E. & Kusters, K. A. 1996 “The collision rate of particles in turbulent media,” J. Aerosol Sci. 27, S263-264.

Kulick, J. D., Fessler, J. R. & Eaton, J. K. 1994 “Particle response and turbulence modification in fully developed channel flow,” J. Fluid Mech. 277, 109-134,

Lavieville, J., Deutsch, E. & Simonin, O. 1995 “Large eddy simulation of interactions between colliding particles and homogeneous isotropic turbulence field,” ASME/FED Vol 228, Gas-Particle Flows, 347-357.

Lazaro, B. J. & Lasheras, J. C. 1992 “Particle dispersion in the developing shear layer. Part 2. forced flow,” J. Fluid Mech. 235, 143-178.

Lee, M. J., Kim, J. & Moin, P. 1990 "Structure of turbulence at high shear rate," J. Fluid Mech., 216, 561-583.

Levich, V.G. 1962 Physicochemical hydrodynamics, Prentice-Hall, Englewood Cliffs, New Jersey.

Lin, C. L. & Lee, S. C. 1975 “Collision efficiency of water drops in the atmosphere,” J. Atmos. Sci. 32, 1412-1421.

Longmire, E. K. & Eaton, J. K. 1992 "Structure of a particle-laden round jet," J. Fluid Mech. 236, 217-257.

Lun, C. K. K. 1991 "Kinetic theory for granular flow of dense, slightly inelastic, slightly rough spheres," J. Fluid Mech. 233, 539-559.

Lun, C. K. K. & Savage, S. B. 1987 "A simple kinetic theory for granular flow of rough, inelastic, spherical particles," Trans. ASME E: J. Appl. Mech. 54, 47-53.

Maxey, M. R. & Corrsin, S. 1986 "Gravitational settling of aerosol particles in randomly oriented cellular flow fields. J. Atmospher. Sci. 43, 1112-1134.

Mclaughlin, J. B. 1989 "Aerosol particle deposition in numerically simulated channel flow," Phys. Fluids A 1, 1211-1224.

Mei, R. & Hu, K. C. 1998 "On the collision rate of small particles in turbulent flows," J. Fluid Mechanics, in review.

Mei, R. & Adrian, R. J. 1994 "Effect of Reynolds-Number-Dependent Turbulence Structure on the Dispersion of Fluid and Particles," TAM Report. No. 747, Department of Theoretical and Applied Mechanics, University of Illinois, Urbana, Illinois.

Mei, R. & Adrian, R. J. 1995 "Effect of Reynolds number on isotropic turbulent dispersion," ASME J. Fluids Eng, 117(3), 402-409.

Mei, R. 1996 "Velocity fidelity of flow tracer particles," Experiments in Fluids, 22, 1-13.

Pearson, H. J., Valioulis, I. A. & List, E. J. 1984 "Monte Carlo simulation of coagulation in discrete particle-size distributions. Part I. Brownian motion and fluid shearing," J. Fluid Mech. 143, 367-385.

Pearson, H. J. & Valioulis, I. A. & List, E. J. 1984 "Monte Carlo simulation of coagulation in discrete particle-size distributions. Part II. Interparticle forces and quasi-stationary equilibrium hypothesis," J. Fluid Mech. 143, 387-411.

Presser, C. & Gupta, A. K. 1993 "Behavior of droplets in pressure-atomized fuel sprays with coflowing air swirl," Heat Transfer in Fire and Combustion Systems - 1993 American Society of Mechanical Engineers, Heat Transfer Division, HTD v 250, Publ by ASME, New York, 79-91.

Rashidi, M., Hetsroni, G. & Banerjee, S. 1990 "Particle-turbulence interaction in a boundary layer," Int. J. Multiphase Flow 16, 935-949.

Rouson, D. M. I. & Eaton, J. K. 1994 "Dirct numerical simulation of turbulent channel flow with immersed particles," ASME/FED Vol. 185, Numerical Methods in Multiphase Flows, 47-57.

Saffman, P. G. & Turner, J. S. 1956 "On the collision of drops in turbulent clouds," J. Fluid Mech., 1, 16-30.

Sato, Y. & Yamamoto, K. 1987 "Lagrangian measurement of fluid-particle motion in an isotropic turbulent field," J. Fluid Mech. 175, 183-199.

Smoluchowski, M. V. 1917 "Versuch einer mathematischen theorie der koagulationskinetic kolloider losunggen," Z. Phys. Chem. 92, 129.

Squires, K. D. & Eaton, J. K. 1991 "Preferential concentration of particles by turbulence," Phys. Fluids A 3, 1169-1178.

Squires, K. D. & Eaton, J. K. 1994 "Effect of selective modification of turbulence on two-equation models for particle-laden turbulent flows," Journal of Fluids Engineering, Transactions of the ASME 116, 4, 778-784.

Sundaram, S. & Collins, L. R. 1997 "Collision statistics in an isotropic, particle-laden turbulence suspension. I. direct numerical simulations," J. Fluid Mech. 335, 75-109.

Tang, L., Wen, F., Yang, Y., Crowe, C. T., Chung, J. N. & Troutt, T. R. 1992 "Self-organizing particle dispersion mechanism in a plane wake," Phys. Fluids A 4, 2244-2251.

Tanaka, T., Yonemura S. & Tsuji, Y. 1995 "Effects of' particle properties on the structure of clusters," ASME FED-VO1.228, Gas-Particle Flows, 297-302.

Tanaka T., Yonemura, S., Kiribaymhi K. & Tsuji, Y. 1996 "Cluster formation and particle-induced lnstability in gas-solid flows predicted by the dsmc method," JSME International Journal, Ser. B 39, 2, 239-245.

Townsend, A. A. 1976 The structure of turbulent shear flow, 2nd ed. Cambridge University Press.

Tu, J. Y., Lee, B. E. & Fletcher, C. A. J. 1996 "Eulerian modeling of particle-wall collisions in confined gas-particle flows via a Lagrangian approach," American Society of Mechanical Engineers, Fluids EngineeringDivision FED v 236, nl, ASME, New York, 751-758.

Walton, O. R. & Braun, R. L. 1986 "Stress calculations for assemblies of inelastic spheres in uniform shear," Acta Mech. 63, 73-86.

Wang, L. 1992 "Dispersion of particles injected nonuniformly in a mixing layer," Phys. Fluids A 4, 1599-1601.

Wang, L. P. & Maxey, M. R. 1993 "settling velocity and concentration distribution of heavy particles in homogeneous isotropic turbulence," J. Fluid Mech. 256, 27-68.

Wang, L. P., Wexler, A. S. & Zhou, Y. 1997 "On the collision rate of small particles in isotropic turbulence. Part 1. zero-inertia case," The Proceedings of the 1997 ASME Fluids Engineering Division Summer Meeting, Vancouver, British Columbia, Canada, June 22-26.

Wang, Q. & Squires, K. D. 1996 "Large eddy simulation of particle-laden turbulent channel flow," Phys. Fluids A 8, 1207-1223.

Wen, F., Kamalu, N., Chung, J. N., Crowe, C. T. & Troutt, T. R. 1992 "Particle dispersion by vortex structures in plane mixing layers," Trans. of ASME, J. Fluids engng 114, 657-666.

William, J. J. E. & Crane, R. I. 1983 "Particle collision rate in turbulent flow," J. Multiphase Flow, Vol. 9, 421-435.

Yang, Y., Crowe, C. T., Chung, J. N. & Troutt, T. R. 1993 "Quantitative study of particle dispersion in a bluff-body wake flow," ASME FED-Vol. 166, Gas-Solid Flows, 231-236.

Yonemura, S., Tanaka, T. & Tsuji, Y. 1993 "Cluster formation in gas-solid flow predicted by the DSMC method," ASME/FED-Vol. 166, Gas-Solid Flows, 303-309.

Young, J. B. & Hanratty, T. D. 1991 "Optical studies on the turbulent motion of solid particles in a pipe flow," J. Fluid Mech. 231, 665-688.

Zhou, Y., Wang, L. P. & Wexler, A. S. 1997 "On the collision rate of small particles in isotropic turbulence. Part 2. finite inertia case," The Proceedings of the 1997 ASME Fluids Engineering Division Summer Meeting, Vancouver, British Columbia, Canada, June 22-26.

BIOGRAPHICAL SKETCH

Kevin Cunkuo Hu (his original Chinese name: Cunkuo Hu) was born on February 25, 1963 in Ruian, Zhejiang province, People's Republic of China. He earned his bachelor's degree and master's degree in aerospace propulsion, Beijing University of Aeronautics and Astronautics, Beijing, People's Republic of China, in 1983 and 1986, respectively. During the period of studying for his master's degree, he specialized in the area of gas-liquid two-phase flow. From 1986 to 1993, he worked as an aerospace engineer and was involved in the areas of two-phase flow, fuel atomization and combustion in the 31st Research Institute of the Ministry of Aviation and Space Industry, Beijing, P.R. China. Since fall 1993, he has been working in the fields of fluid mechanics and particle science as a Ph.D. candidate in the Department of Aerospace Engineering, Mechanics and Engineering Science at University of Florida, Gainesville, Florida, United States of America.

I certify that I have read this study and that in my opinion it conforms to acceptable standards of scholarly presentation and is fully adequate, in scope and quality, as a dissertation for the degree of Doctor of Philosophy.

Renwei Mei

Renwei Mei, Chairman
Associate Professor of Aerospace Engineering,
Mechanics and Engineering Science

I certify that I have read this study and that in my opinion it conforms to acceptable standards of scholarly presentation and is fully adequate, in scope and quality, as a dissertation for the degree of Doctor of Philosophy.

Corin

Corin Segal
Associate Professor of Aerospace Engineering,
Mechanics and Engineering Science

I certify that I have read this study and that in my opinion it conforms to acceptable standards of scholarly presentation and is fully adequate, in scope and quality, as a dissertation for the degree of Doctor of Philosophy.

Ulrich H. Kurzweg

Ulrich H. Kurzweg
Professor of Aerospace Engineering, Mechanics
and Engineering Science

I certify that I have read this study and that in my opinion it conforms to acceptable standards of scholarly presentation and is fully adequate, in scope and quality, as a dissertation for the degree of Doctor of Philosophy.

Roger Tran-Son-Tay
Associate Professor of Aerospace Engineering,
Mechanics and Engineering Science

I certify that I have read this study and that in my opinion it conforms to acceptable standards of scholarly presentation and is fully adequate, in scope and quality, as a dissertation for the degree of Doctor of Philosophy.

James F. Klausner

James F. Klausner
Associate Professor of Mechanical Engineering

This dissertation was submitted to the Graduate Faculty of the College of Engineering and to the Graduate School and was accepted as partial fulfillment of the requirements for the degree of Doctor of Philosophy.

May, 1998

Winfred M. Phillips
Dean, College of Engineering

Karen A. Holbrook
Dean, Graduate School